

MO-R184 810

TURBULENCE GENERATION IN COMBUSTION(U) CORNELL UNIV

1/1

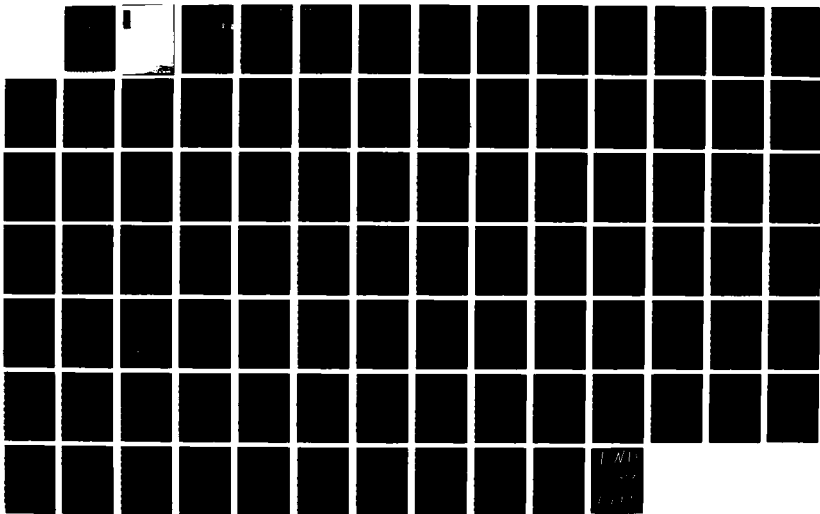
ITHACA NY F C GOULDIN 22 JUL 87 ARO-18738 6-EG

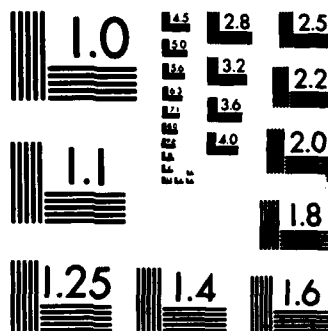
DAAG29-82-K-0187

UNCLASSIFIED

F/G 21/2

NL





MICROCOPY RESOLUTION TEST CHART  
NATIONAL BUREAU OF STANDARDS-1963-A

(2)

DTIC  
ELECTE  
SEP 17 1987  
S D  
D  
Cg

THE VIEW, OPINIONS, AND/OR FINDINGS CONTAINED IN THIS REPORT ARE  
THOSE OF THE AUTHOR (S) AND SHOULD NOT BE CONSTRUED AS AN  
OFFICIAL DEPARTMENT OF THE ARMY POSITION, POLICY, OR DECISION,  
UNLESS SO DESIGNATED BY OTHER DOCUMENTATION.

DISTRIBUTION STATEMENT A

Approved for public release  
Distribution Unlimited

87 9 9 235

UNCLASSIFIED

MASTER COPY

ADAT84870 PURPOSES

SECURITY CLASSIFICATION OF THIS PAGE

## REPORT DOCUMENTATION PAGE

1a. REPORT SECURITY CLASSIFICATION Unclassified		1b. RESTRICTIVE MARKINGS	
2a. SECURITY CLASSIFICATION AUTHORITY		3. DISTRIBUTION/AVAILABILITY OF REPORT Approved for public release; distribution unlimited.	
2b. DECLASSIFICATION/DOWNGRADING SCHEDULE		5. MONITORING ORGANIZATION REPORT NUMBER(S) ARO 18738.6-EG	
4. PERFORMING ORGANIZATION REPORT NUMBER(S)	7a. NAME OF MONITORING ORGANIZATION U. S. Army Research Office		
6a. NAME OF PERFORMING ORGANIZATION Cornell University	6b. OFFICE SYMBOL (if applicable)	7b. ADDRESS (City, State, and ZIP Code) P. O. Box 12211 Research Triangle Park, NC 27709-2211	
6c. ADDRESS (City, State, and ZIP Code) Ithaca, NY 14853	9. PROCUREMENT INSTRUMENT IDENTIFICATION NUMBER		
8a. NAME OF FUNDING/SPONSORING ORGANIZATION U. S. Army Research Office	8b. OFFICE SYMBOL (if applicable)	10. SOURCE OF FUNDING NUMBERS	
8c. ADDRESS (City, State, and ZIP Code) P. O. Box 12211 Research Triangle Park, NC 27709-2211	PROGRAM ELEMENT NO.	PROJECT NO.	TASK NO.
11. TITLE (Include Security Classification) Turbulence Generation in Combustion (Unclassified)		WORK UNIT ACCESSION NO.	
12. PERSONAL AUTHOR(S) F. C. Gouldin			
13a. TYPE OF REPORT Final	13b. TIME COVERED FROM 82-9-15 TO 87-3-31	14. DATE OF REPORT (Year, Month, Day) 87-7-22	15. PAGE COUNT 87
16. SUPPLEMENTARY NOTATION The view, opinions and/or findings contained in this report are those of the author(s) and should not be construed as an official Department of the Army position, policy, or decision, unless so designated by other documentation.			
17. COSATI CODES		18. SUBJECT TERMS (Continue on reverse if necessary and identify by block number)	
FIELD	GROUP	Premixed turbulent combustion, laser doppler velocimetry	
		Rayleigh scattering, fractals, laser tomography, flamelets	
19. ABSTRACT (Continue on reverse if necessary and identify by block number)			
<p>Several tasks of research on turbulent flames have been pursued. The focus has been on low to moderate Reynolds number, premixed flames which are dominated by flamelet structures, i. e., the major heat releasing chemical reactions occur in thin sheets. Large density changes occur across flamelets and therefore it is expected that these structures have an important influence on turbulence generation. The focus of the research has thus been on flamelet characteristics.</p>			
20. DISTRIBUTION/AVAILABILITY OF ABSTRACT <input type="checkbox"/> UNCLASSIFIED/UNLIMITED <input type="checkbox"/> SAME AS RPT. <input type="checkbox"/> OTIC USERS		21. ABSTRACT SECURITY CLASSIFICATION Unclassified	
22a. NAME OF RESPONSIBLE INDIVIDUAL		22b. TELEPHONE (Include Area Code)	22c. OFFICE SYMBOL

continued

UNCLASSIFIED

SECURITY CLASSIFICATION OF THIS PAGE

19. Abstract (continued)

A fractal representation of surfaces in turbulent flows is found to be a very useful tool for modeling purposes. Experiments support the hypothesis that flamelet surfaces can be represented by fractal surfaces, but more experiments are needed before the evidence can be considered conclusive. Passage time pdf's which reflect the dynamic character of flamelets are also useful in combustion modeling. Such distributions were measured and found to be reasonably well represented by one of two proposed functional forms for the pdf's. If a very exact representation is required neither function seems ideal. Flamelet position and conditioned velocity measurements were performed. The pdf of flamelet position is nearly gaussian and the standard deviation of the distribution is a measure of flame brush thickness. The velocity measurements reveal the flamelet to be a source of flow acceleration. But experimental problems have hindered the gathering of quantitative data on the magnitude of this acceleration.

Accession For	
NTIS CRA&I	<input checked="checked" type="checkbox"/>
DTIC TAB	<input type="checkbox"/>
Unannounced	<input type="checkbox"/>
Justification	
By	
Distribution /	
Availability Codes	
Date	Avail and/or Special
A-1	



UNCLASSIFIED

SECURITY CLASSIFICATION OF THIS PAGE

## TABLE OF CONTENTS

	<u>Page</u>
REPORT DOCUMENTATION PAGE/ABSTRACT	
I. INTRODUCTION	1
II. MODEL DEVELOPMENT	2
II. 1 Model for Turbulent Burning Velocity	2
II. 2 Chemical Closure Model	4
II. 3 Modeling of Jets and Jet Flames	5
III. EXPERIMENTAL RESEARCH	8
III. 1 Passage Time Measurements	8
III. 2 Conditional Velocity Measurements	9
III. 3 Evaluation of the Fractal Character of Flamelets	10
IV. TURBULENCE GENERATION	12
V. SUMMARY	13
REFERENCES	14
TABLE 1	16
FIGURE CAPTIONS	17
APPENDIX A: Chemical Closure Model For Fractal Flamelets	A1
APPENDIX B: An Interpretation of Jet Mixing Using Fractals	B1
APPENDIX C: Simultaneous Measurements of Flamelet Position and Gas Velocity in Premixed Turbulent Flames	C1
APPENDIX D: Personnel Working on Project	D1
APPENDIX E: Publications, Reports and Meeting Presentations	D1

## I. INTRODUCTION

The original objective of this work was to employ laser velocimetry (LV), laser induced Rayleigh scattering (RS) and pressure probe techniques to measure velocity, gas density profiles and pressure in premixed turbulent flames for determining the influence of combustion and density fluctuations on turbulence. The purpose was to study the generation of turbulence and the enhancement of turbulent transport in the reaction zone of turbulent flames in order to improve our understanding of these processes and to improve turbulent combustion models. A primary focus of the experiments was to measure terms appearing in the turbulence energy balance equation. Two terms were of particular interest -- the term representing work by the turbulent shear stresses against the mean flow and the term giving turbulence generation by the mean pressure gradient.

The experiments were to be carried out on a laboratory v-flame burner which had been studied previously at Cornell [1,2]. The burner supports flames held by rods in grid turbulence. With this burner, low turbulence Reynolds numbers are obtained [3], and reaction is confined to thin sheets for the conditions studied [2]. The burner is described in more detail below.

As the research progressed there were changes in the objectives as a result of new findings both at Cornell and elsewhere, new capabilities, and of new ideas.

During the period of funding the following research was accomplished, funded solely or partially by ARO: 1) development of models for premixed turbulent flames based on a fractal description of reaction sheets, 2) extension of fractal based modeling concepts to jet mixing and turbulent jet diffusion flames, 3) measurement of passage times in premixed turbulent flames using Rayleigh scattering with results compared to the model proposed by Bray, Libby & Moss [4], 4) conditional LV velocity measurements in v-flames, and 5) preliminary studies of the fractal character of v-flames. Much of this work has been reported previously in journal articles [3,5] or Cornell University reports [6,7]. In this report our research findings will be summarized and discussed. Emphasis will be placed on results not previously reported. It should be noted that work on conditional velocity measurements continues and the student working on the project expects to complete his degree work by August 1987. Modeling work also continues and a manuscript for journal submittal is in draft stage.

## II. MODEL DEVELOPMENT

Models for predicting the turbulent burning velocity and the mean fuel consumption rate per unit volume of premixed, turbulent flames have been proposed. Fractal ideas have been applied to the modeling of jet mixing and of jet flame length. This work is summarized in this section.

### II.1 Model for Turbulent Burning Velocity

For a range of turbulence conditions including conditions of practical interest, reaction in premixed turbulent flames occurs in thin reaction sheets referred to as flamelets. For modest levels of turbulence the structure of these sheets approaches that of steady laminar flames. For this condition Damkohler has suggested that

$$u_t = u_0 \frac{A_T}{A_L} \quad (1)$$

where  $u_t$  and  $u_0$  are the turbulent and laminar burning velocities,  $A_L$  is the flamelet surface area for laminar flow, and  $A_T$  is the ensemble average flamelet area in turbulent flow. Thus, in this model the sole effect of turbulence is to generate flamelet surface area.

Damkohler's model can be extended to higher levels of turbulence by allowing for perturbations of the flamelet structure by the turbulence, i.e., allowing for flamelet stretch. Then

$$u_t = \langle u_L \rangle \frac{A_T}{A_L}, \quad (2)$$

where  $\langle u_L \rangle$  is the mean, stretched-flamelet burning velocity.

Early attempts to use Damkohler's model suggestion were not successful. A major reason for this lack of success appears to be the failure of area ratio estimates to account for the multiple length scale wrinkling of flamelet surfaces by turbulence [5]. Rough surfaces with multiple, self-similar scales of wrinkling can be characterized with the mathematics of fractals [8]. In our research we have used this characterization to estimate the area ratio in (1) and (2).

Consider an isotropic, homogeneous fractal surface filling a volume  $L^3$  in space. One aspect of the surface's fractal character is that if one measures the surface area,  $A$ , in  $L^3$  with a measurement scale  $\epsilon$  which is commensurate with the scales of surface wrinkling he finds for varying  $\epsilon$  that

$$A / L^3 \sim |\epsilon / L|^{-D} \epsilon^2 / L^3. \quad (3)$$

See also Fig. 1 and [5, 8].  $D$  is the fractal dimension and is defined by (3). Fractal character is reflected in the power law dependency of  $A$  versus  $\epsilon$ .

Mandelbrot [9] has suggested that constant property surfaces in isotropic, homogeneous turbulence are fractal. This hypothesis is supported by experiment [10,11]

and by analysis of cloud dispersion [12]. These surfaces are expected to exhibit fractal character for a limited range of measurement scales corresponding to the range of scales of wrinkling. The experimental results of [11] indicate that the limits to fractal behavior are associated with an inner cutoff, which is the Kolmogorov ( $\eta$ ) scale of turbulence, and an outer cutoff, which is the integral ( $l$ ) scale. This finding suggests that the inertial subrange turbulence eddies are the agents of self-similar fractal wrinkling. A simple model of how an eddy could wrinkle a surface is also suggestive of this conclusion. An eddy of length scale  $l_n$  and velocity scale  $u_n$  causes a sinusoidal like wrinkle of wavelength  $l_n$  and amplitude  $u_n \Delta t$ , where  $\Delta t$  is the eddy life time. Typical scaling gives  $\Delta t \sim l_n / u_n$  and the aspect ratio of the wrinkles is seen to be one, independent of the wrinkle amplitude and wavelength, i.e., the wrinkling is similar at all scales.

In our research [5] it is assumed that flamelet surfaces can be represented as fractal surfaces and the assumption is used to estimate the area ratio in (2). It is assumed that there are inner ( $\epsilon_i$ ) and outer ( $\epsilon_o$ ) cutoffs to the fractal behavior for flamelets and that the ensemble average of measured flamelet area will vary with measurement scale as shown in Fig. 1b. Further it is argued that  $A_i$ , the area at the inner cutoff, is the ensemble average flamelet area in  $L^3$ , while  $A_o$ , the area at the outer cutoff, would be the flamelet area in the absence of turbulence. Thus

$$u_t = \langle u_L \rangle \frac{A_i}{A_o} = \langle u_L \rangle \left( \frac{\epsilon_o}{\epsilon_i} \right)^D. \quad (4)$$

One sees that in this model the area ratio is given in terms of three parameters - two length scales and the fractal dimension.

To complete the burning velocity model expressions for these length scales, a value for  $D$  and an expression for  $\langle u_L \rangle$  are required. In [5] it is argued that

$$\epsilon_o = l, \text{ and} \quad (5)$$

$$\epsilon_i = \eta \left( 1 - (1 - A_t^{-1/4} R_l^{-3/4}) \exp(-A_t^{1/4} R_l^{-1/4} u' / \langle u_L \rangle) \right). \quad (6)$$

$A_t$  is an empirical constant obtained from data on noncombusting turbulent flow.  $u'$  is the root mean square of velocity fluctuations; and  $R_l$  is the turbulence Reynolds number ( $R_l = u' l / \nu$ ). Also presented in [5] is an expression for  $\langle u_L \rangle$  based on an analytical expression for flamelet stretch effects developed by Law [5]. For brevity this expression is not repeated here. From the above expressions and an expression for the ratio  $\eta / l$  good for grid turbulence one finds

$$u_t = \langle u_L \rangle \{ [1 - (1 - A_t^{-1/4} R_l^{-3/4}) \exp(-(A_t / R_l)^{1/4} u' / \langle u_L \rangle)] A_t^{1/4} R_l^{3/4} \}^{D-2}. \quad (7)$$

In [5] model predictions for burning velocity are compared to data obtained at Leeds University [13, 14]. A value for  $D$  of 2.37 is used based on the results of [10-12]. The comparison shows good agreement for a wide range of  $R_l$  (1,000 - 40,000) and of

$u'/u_0$  ( $u'/u_0 \leq 40$ ) for various fuels.

## II.2. Chemical Closure Model

In a complementary research program a model for premixed turbulent flames has been developed based upon conditional statistics and a second order transport closure model developed by Professor Lumley of Cornell and his students. Model equations for conditional second order statistics are proposed and solved. Conditioning is on being either in reactants or products and the model approach assumes combustion to occur in flamelets. A paper describing this model will appear soon [15].

We have extended this modeling effort as part of our ARO supported research by proposing a chemical closure model based on the assumption of fractal flamelets. This work was started at Cambridge University (during the visit of F C G) and is a joint effort with Professor K N C Bray of Cambridge and Dr. J-Y Chen of Sandia National Laboratories, Livermore. A closure model has been proposed for the mean fuel consumption rate, and it has been evaluated in numerical and analytical calculations.

The proposed closure model expression can be written as

$$\langle \omega_f \rangle = C_R \rho_0 \langle \Delta Y_f u_L \rangle_f (l f / \eta)^{D-2} l_F^{-1} \langle c \rangle (1 - \langle c \rangle), \quad (8)$$

with  $f$  given by

$$f = [1 - (1 - A_t^{-1/4} R_t^{-3/4}) \exp(-A_t^{1/4} R_t^{-1/4} u' / \langle u_L \rangle)].$$

$C_R$  is a model constant;  $\rho_0$  is the reactant gas density;  $\Delta Y_f$  is the change in fuel mass fraction across the flamelet;  $l_F$  is the local flame brush thickness; and  $c$  is the reaction progress variable which is defined as the ratio of the fuel mass fraction less the initial fuel mass fraction and  $\Delta Y_f$ . The  $f$  subscript on the angle bracket denotes a conditional average with conditioning on the flamelet.

Details of the model development and the analyses are presented in Appendix A. Here we present a summary of the findings. The model is used in simplified analyses of normal and oblique flames.

For a normal flame, we assume high Reynolds number, one-dimensional flow in the mean, and constant  $\Delta Y_f$ ,  $\langle u_L \rangle$ ,  $\eta$ ,  $f$  and  $l$ . Integration of the equation for  $\langle c \rangle$  across the flame brush gives

$$u_t / \langle u_L \rangle = (l f / \eta)^{D-2}$$

(which is identical to our burning velocity model prediction) provided that

$$C_R = l_F / \int_{-\infty}^{\infty} \langle c \rangle (1 - \langle c \rangle) dx, \quad (9)$$

which is reasonable. Thus the closure model for normal flames is consistent with the burning velocity model.

The above analysis can be extended to the oblique flame case provided several additional assumption are made. The assumptions to be made include constant density, parabolic flow ( the flame brush lies almost parallel to the flow direction ), and flow similarity. A major point of interest in this analysis is to see if a turbulent burning velocity could be defined for the oblique flame case. A definable burning velocity is obtained with  $u_t / \langle u_L \rangle = (l f / \eta)^{D-2}$  provided (9) is valid and either the flames brush thickness is constant or grows linearly with distance in the flow direction.

Numerical calculations using the transport closure of [15] were performed for oblique flames with constant density in decaying grid turbulence. Calculated unconditional normal stresses and other turbulence properties compared well with the grid turbulence data of [16] which is for nonreacting flow.

Flame results were obtained for a range of conditions with a single value for  $C_R$ ;  $C_R = 4.0$ . Calculated burning velocities compare favorably with values obtained from the burning velocity model as would be expected from the results of the normal and oblique flames analyses discussed above. However flame brush thickness did not grow linearly and there were slight but noticeable variances between the burning velocity calculated and that obtained from the  $u_t$  model. These differences are attributed to a departure from similarity in the flows obtained by numerical calculations. In turn the departure from similarity is attributed to turbulence decay.

As part of the numerical calculations we obtained results using the new chemical closure model with a two-equation, gradient transport model in the equation for  $\langle c \rangle$ ; A  $k$ - $\epsilon$  model was used with  $k$  and  $\epsilon$  obtained from the second order model results. The differences between the two transport models are striking. The gradient model under predicts the turbulent fluxes, and consequently the flame brush thickness is also under predicted. On the other hand the burning velocities predicted using the new chemical closure model and either of the two transport models are quite similar.

Overall we are very pleased with the model results. The representation of flamelet surface geometry by fractals appears to be a very promising approach which we intend to continue to pursue.

### II.3 Modeling of Jets and Jet Flames

The flamelet concept may also be applied to nonpremixed flames [17]. In this case reaction still is assumed to occur in thin sheet like regions which are centered on the stoichiometric mixture fraction surface,  $Z = Z_s$ . (  $Z$  is the mass weighted mixture fraction. ) We have developed modeling ideas applicable to jet mixing and reacting jets based on the assumption that constant mixture fraction surfaces can be represented as fractal surfaces. A paper applying these ideas to jet mixing has been submitted for journal publication [18], Appendix B. This work is now summarized.

An axisymmetric jet is modeled, and the jet structure is viewed as a set of constant concentration surfaces. Stationary turbulence and uniform density are assumed, and a balance equation for the ensemble mean flux of jet fluid across a  $Z$  constant surface is developed which states that this flux must equal the mean flow supplying the jet. Terms in this balance equation are modeled 1) by assuming that the geometry of constant concentration surfaces can be represented by fractal surfaces and 2) by estimating the mean jet fluid mass flux per unit area of a constant concentration surface in terms of the Kolmogorov velocity. To complete the analysis similarity in the jet structure is assumed.

Consider a slice of the jet defined by  $x$  to  $x + dx$ , where  $x$  is axial distance. The average  $Z$  surface area in this slice is modeled as

$$dA_Z = 2\pi r_{<Z>} (A_i^{1/4} R_i^{3/4})^{D-2} dx. \quad (10)$$

$r_{<Z>}$  is the local radius of the  $<Z>$  contour with  $<Z> = Z$ ; the area of the  $<Z>$  constant surface is identified as  $A_0$ . The average flux of jet fluid per unit area of a  $Z$  constant surface is modeled as  $C_d \rho Z v$  with  $v$  being the Kolmogorov velocity,  $\rho$  the density, and  $C_d$  a model constant. The average flux of jet fluid across a  $Z$  surface between  $x$  and  $x + dx$  is obtained by multiplying (10) by  $C_d \rho Z v$ . The resulting expression is integrated over  $x$  using a standard similarity form for  $r_{<Z>}$ . The result is

$$L/d = C C_d R_i^{[3/(4-\mu)][D-2] + [1/2-3/(4-\mu)]} Z_0. \quad (11)$$

$L$  is the axial distance at which  $<Z>$  on the jet axis falls to  $Z_0$ , and  $d$  is the initial jet diameter.  $C$  is an empirical constant [18], and  $\mu$  is the intermittency exponent --  $0.25 \leq \mu \leq 0.5$ . The form of (11) is that expected from similarity provided there is no Reynolds number dependency which in turn requires

$$D = 2 + \frac{(\mu + 2)}{6}. \quad (12)$$

Thus the jet mixing analysis gives an expression for the fractal dimension. The expression is identical to the one obtained by others [12, 19] from an analysis of cloud dispersion in homogeneous, isotropic turbulence. For the expected range of  $\mu$  values, (12) gives  $2.33 \leq D \leq 2.42$  which is consistent with experiment and the value used in our burning velocity model. All of these results support the idea of a universal expression for  $D$  valid for high Reynolds number.

Some preliminary work has been performed to extend our fractal modeling ideas to the reacting jet case. Variable density effects have been added in an approximation, and an expression for the length of jet flames has been developed. The flame length expression with  $D$  satisfying (12) is

$$L_f/d = C(1/Z_s) \sqrt{(\rho_j/\rho_f)}. \quad (13)$$

$Z_s$  is the stoichiometric jet fluid mixture fraction, while  $\rho_j$  and  $\rho_f$  are the initial jet fluid density and an average flame gas density, respectively. This work has been presented and

a report is available [19].

As in the case of premixed flames our initial application of fractal concepts to modeling of jet mixing and combustion has proved useful and encouraging. Further work with fractals on nonpremixed flames is planned and will be supported by ARO in a new program of research [20].

### III. EXPERIMENTAL RESEARCH

Our experimental research may be divided into three distinct tasks: measurement of passage times in turbulent v-flames, conditional velocity measurements in v-flames and preliminary studies of the fractal character of flamelets in low Reynolds number turbulent premixed flames. The results of each of these efforts are reported separately.

#### III.1 Passage time measurements

Bray, Libby and Moss (BLM) have proposed a model for premixed turbulent flames which makes use of the probability distribution function (pdf) of passage times -- the time duration between the passage of a flamelet at a point in the turbulent flame brush. In their work BLM distinguish between times in reactants and times in products. In their initial work [4] the pdf was assumed to take the form

$$P(t_i) = \frac{1}{\langle t_i \rangle} \exp\left(-\frac{t_i}{\langle t_i \rangle}\right), \quad i = r \text{ or } p. \quad (14)$$

r and p refer to reactant and products respectively, while  $\langle t_i \rangle$  is the local mean passage time.

This form is not satisfactory at small  $t_i$  since it does not approach zero as  $t_i$  approaches zero. Recently Bray and Libby (BL) have proposed another form for  $P(t_i)$  [21], the gamma two distribution.

$$P(t_i) = \frac{4 t_i}{\langle t_i \rangle^2} \exp\left(-\frac{2 t_i}{\langle t_i \rangle}\right), \quad i = r, p. \quad (15)$$

This distribution approaches zero at small  $t_i$  as expected.

We have made Rayleigh scattering measurements to determine  $P(t_i)$  and test the hypotheses of BLM and of BL. In premixed flames Rayleigh scattering is proportional to the gas density, and where flamelets are present, the temporal signal from Rayleigh scattering will be, apart from noise, a random series of changes from high to low and back again. The changes in signal level correspond to a flamelet passage event and therefore passage time data can be obtained from Rayleigh scattering time series records stored on computer.

Passage time measurements were performed on low Reynolds number v-flames. A schematic of the burner used is shown in Figure 1. An unconfined v-flame is stabilized in grid turbulence on a rod (1.5mm dia.) mounted across the exit of a cylindrical burner (50mm dia.). Turbulence is generated by woven-wire screens mounted 30mm below the rod. Fuel (commercial grade methane) and air are mixed in a plenum chamber and flow into the burner. For details see [2, 3].

Rayleigh scattering is induced by a 1 watt argon-ion laser operating in the green. Scattered photons are detected by a photomultiplier and the signal is stored on computer. The spatial resolution of the measurements is approximately 0.1mm and the temporal resolution is 200μs. Minimum resolution is set by signal-to-noise considerations [3].

Scattering measurements were performed for three different flame conditions and at

several different spatial locations in each flame. The initial results for the three flames, which are reported in [3], are in rough agreement with the hypothesis of BLM at least for large  $t_f$ . There are discrepancies in the comparisons at small  $t_f$  where the gamma two distribution suggested by BL is expected to give a better result. Comparison of experimental data with a gamma two distribution does show better agreement for the lower Reynolds number flames at smaller  $t_f$ . But comparisons at larger  $t_f$  and for the higher Reynolds number flame are not as good as given by (14). Sample pdfs are shown in Fig. 2. On the basis of these data one concludes that there is room for further improvement in the representation of  $P(t_f)$ .

### III.2 Conditional Velocity Measurements

For low Reynolds number turbulence, as noted above, the flamelet structure is expected to approach that of an unperturbed laminar flame. Assuming an unperturbed, quasi-steady structure there is a jump in fluid velocity normal to the flamelet surface across this surface which is equal to the laminar burning velocity times the density ratio across the flamelet minus one. For small  $u'$  relative to  $u_0$  this acceleration could be important to turbulence generation. We undertook conditional velocity measurements in order to detect flow acceleration across flamelets. These measurements entailed the simultaneous measurement of flamelet position and gas velocity. Laser induced scattering techniques were employed in these measurements. Some of the results have been read at a ASME-JSME meeting and are available in report form [7] and Appendix C.

These measurements were made on v-flames. Gas velocity is measured with a commercial LV system composed of an argon-ion laser, counter-type signal processor, and associated optical components. The spatial resolution of the velocity measurements is a few tenths of a millimeter.

Flamelet position along a line in space is measured with a light scattering technique. The reactant flow is seeded with an oil mist which evaporates in the flamelet and thus marks reactants but not products. Scattering from a He-Ne laser is detected with a photomultiplier tube which sees scattering from a one centimeter portion of the laser beam. Thus the detected signal strength depends on the amount of reactant gas along the portion of the laser beam viewed, i. e., the position of the flamelet along the laser beam. The He-Ne laser beam is aligned in the horizontal; see Fig. 1.

For measurements, the LV measurement volume is located at different points along the He-Ne laser beam. Position and velocity data are recorded simultaneously on a computer. The oil mist used for the position measurements is excellent for LV measurements. However, since the oil evaporates in the flamelet, a second refractory particle seed must be added to the flow for velocity measurements in the products. The refractory seed levels are low enough so that the position measurement is not affected by the addition of refractory scattering particles. Vertical and horizontal (perpendicular to the vertical plane containing the stabilizer rod) velocities are measured.

The position and velocity data are analyzed to give the pdf of flamelet position along the He-Ne laser beam and conditioned velocities. Conditioning is by being either in products or reactants and by distance from the flamelet. We expect that conditioning by distance will provide evidence regarding flow acceleration across flamelets.

Measurements in reactants (without refractory seed) have been performed and results reported [7]. Measurements with refractory seed are in progress. They are the thesis research of Paul Miles; he is expected to complete his thesis in August 1987. Results

to date of note are summarized in the following.

The pdf of flamelet position is nearly Gaussian and the its standard deviation is a useful measure of the flame brush thickness. The standard deviation grows approximately as a linear function of downstream distance. The derivative of the flamelet position signal is determined and viewed as a measure of the flamelet velocity [7]. Surprisingly high values of the derivative are observed. Power spectra of the derivative signal are compared to spectra of the horizontal velocity (the V component). The two spectra are nearly coincidence in the frequency range from approximately 500 to about 1500 Hz. Mean velocities measured in reactants are consistent with those measured by others in a similar v-flame. Velocity statistics conditioned by distance from the flamelet in reactants do not contain surprises. In particular rms levels do not vary significantly with distance -- see Fig. 10, Appendix C.

Measurements with refractory seed are in progress. The persistence due to slow evaporation of large oil drops through the flamelet have caused problems in these measurements. Refractory seed concentrations are orders of magnitude below that of the oil mist. As a consequence a small percentage of large oil drops which do not influence the position measurement or the reactant velocity measurement, appear to bias the product gas velocity measurements. We are currently working to resolve this problem.

### III.3 Evaluation of the fractal character of flamelets

While it is not obvious how to assess surface fractal character directly, inferences can be draw from the application of laser tomography and point, scalar measurements; see for example [11]. Preliminary experiments on v-flames have been performed using tomography and point scattering measurements [24, 25].

The intersection of a flamelet surface with a plane can be visualized with laser tomography [23]. For these experiments the reactant flow is seeded with an oil mist as for the velocity measurements. The output of a high energy, pulsed Nd:Yag laser is frequency doubled into the green (300 mj per pulse in the green), and lenses used to form the laser beam into a sheet of light approximately 0.5mm in thickness. The flame brush is illuminated by the laser, and the reactant gas in the plane of illumination is made visible by scattering of light from the oil mist. Photographs of the flame brush are taken with a 35mm camera synchronized with the laser pulse. Because the oil evaporates in the flamelet there is no scattering from the products, and consequently the curve defined by the boundary between regions of scattering and of no scattering observed in the photographs --called tomograms -- is the intersection of the plane defined by the laser and the flamelet surface.

Curves formed by the intersection of a plane with a fractal surface are fractal, and for isotropic fractal surfaces the fractal dimension of the curve is one less than that of the surface from which it is formed. We assume that the curve fractal dimensions which we measure are also one less than that of the fractal flamelet. For curves, fractal dimension can be defined in terms of measured length,  $L$ , in a manner analogous to that for surfaces. Thus

$$L / L^2 \sim |\epsilon / L|^{-D} \epsilon / L^2. \quad (16)$$

Here  $D$  is the fractal dimension of the curve;  $L$  is the scale of the surface area over which  $L$  is measured; and  $\epsilon$  is the measurement scale.

In our studies tomograms for several different flame conditions -- see Table 1 -- are

digitized and their fractal dimension determined by application of (16). Plots of  $L$  versus  $\epsilon$  were made and slopes taken. A sample plot is given in Fig. 3. Since there are limits to the length scales of wrinkling we expect a curve similar in shape to that in Fig. 1b, two horizontal lines connected by a straight line with slope  $1 - D$ . Furthermore for a surface fractal dimension of 2.37 we expect a curve dimension of 1.37. In Fig. 3 we see that the shape is in general what we expect. However the maximum  $\epsilon$  is not large enough to unambiguously show behavior above the outer cutoff. Also the fractal dimension taken from the curve is well below the expected value. Low fractal dimensions are observed for all the flame conditions studied, Table 1. From measured length curves, inner and outer cutoffs are also estimated and found to be several times larger than the Kolmogorov and integral scales respectively.

We attribute the low fractal dimension obtained in these measurements to two factors, low turbulence Reynolds number and low  $u'/u_0$ . Fractal wrinkling is most likely caused by the inertial subrange turbulent eddies. For low Reynolds number turbulence these eddies are not fully developed which may influence the character of surface wrinkling. In section II.1 a simple model for surface wrinkling by turbulent eddies was presented. For this model, the amplitude of wrinkling depends on a time scale,  $\Delta t$ , which is the time a surface is exposed to an eddy and was taken as the eddy life time. Since a flamelet propagates relative to the reactant mixture, exposure time may be less than an eddy life time. An alternate exposure time is given by  $l_n / u_0$ . For  $u_0 > u_n$  this latter time is the exposure time and the amplitude of corrugation by our model is  $l_n (u_n/u_0)$ . Thus the condition  $u_n = u_0$  marks a transition in behavior. The  $l_n$  for  $u_n = u_0$  is defined as the Gibson scale --  $l_G$  -- and by standard scaling arguments  $l_G = l (u_0 / u')^3$ . For our conditions  $l_G > l$ . By our simple, wrinkling model all wrinkle amplitudes scale as  $l_n (u_n/u_0)$  rather than  $l_n$  and it is reasonable to expect a variation in fractal behavior. By the above argument one expects  $D$  would approach 1.37 for large  $R_l$  and large  $u'/u_0$ .

The set of points formed by the intersection of a line with a fractal surface also exhibits fractal character, and for an isotropic fractal surface the fractal dimension of the set of points is two less than the fractal dimension of the surface. A fractal set of points is known as a fractal dust [8]. For points along a line the fractal dimension is determined by the variation in the measure of the set with measurement scale. Divide the line into segments of length  $\epsilon$ . The number of segments in which there is one or more members of the set is  $N$ . Then for a fractal set

$$N \sim \epsilon^{-D} \quad (17)$$

$D$  is again the fractal dimension, and its value falls between 0 and 1.

Time-series, point-scattering measurements were performed to study the fractal character of the distribution of flamelet crossing events in time. As before the reactants are seeded with an oil mist and scattering is excited by a He-Ne laser. Scattered photons from a small volume are detected and used to drive a logic circuit which generates a short duration, logic pulse at each flamelet crossing event. These pulse control a computer clock which counts the time between crossing events, and these times are stored in computer. The spatial resolution of these measurements is a few tenths of a millimeter and the temporal resolution is 50  $\mu\text{sec}$ .

From recorded data the measure of a set of crossing events along the time axis can be determined as a function of  $\epsilon$ . Plots of  $N$  versus  $\epsilon$  are then generated; see Fig. 4. Fractal behavior is not obvious in the data shown in Fig. 4. These data may be represented by several straight line segments and a physical interpretation can be given to each of the segments. The horizontal line to the left is for the case where  $\epsilon$  is below the inner cutoff and all members of the set are resolved. The right most line has a slope of -1 which indicates  $\epsilon$  values above an outer cutoff. In each segment there are set members for all  $\epsilon$  in this range, and none of the time intervals between crossing events are resolved for these large  $\epsilon$ 's. In between these two regions of limiting behavior are two regions of fractal behavior; one having a fractal dimension of approximately 0.1 and the other a dimension of approximately 0.5. The tomographic results imply a fractal dimension for the dust of approximately 0.1, and therefore we associate this segment of the curve with the fractal wrinkling of the flamelet surface.

To understand the portion of the curve where  $D \sim 0.5$  consider a coin toss game in which the winner of each toss receives the coin. The coins are identical and fair. A plot of cumulative winnings for one of the players versus trial number is a random walk, while the distribution of zero winnings versus trial number is a fractal set with dimension 1/2 [8]. This observation suggests that the  $D \sim 0.5$  segment may be the result of large scale flapping of the flamelet. In other words, a smooth, flapping flamelet would give fractal behavior with  $D \sim 0.5$ , while the fractal wrinkling of the flamelet contributes a region in our  $N$  versus  $\epsilon$  plot with  $D \sim 0.1$ . With regard to the proposed burning velocity and chemical closure models the fractal character and fractal dimension of the surface wrinkling are the critical features to be tested by the experiments. Therefore we conclude tentatively that the experiments support the concept of fractal wrinkling and for the conditions studied a fractal dimension of approximately 2.1. We speculate, based on experiments [10, 11] and analyses for nonreacting flows [12, 18, 19] that as  $u'/u_0$  and  $R_f$  increase  $D$  will approach the limiting value given by (12).

Our investigations of fractal behavior are a preliminary, first step, and our interpretation of results is also preliminary. More work is required, especially at higher Reynolds number.

#### IV. TURBULENCE GENERATION

For the flames we have studied reaction occurs in thin sheets separating low and high temperature regions of uniform density. From a mechanistic point of view turbulence generation associated with density change in these flames must be associated with the flamelet. In unconditioned moment closure models density fluctuation effects appear in many terms which require modeling. However these terms do not explicitly account for the fact that density fluctuations effects are found only in the flamelet. We believe that this is a serious short coming of these models because a more detailed, mechanistic picture of density change effects when obtained from experiment ( or other sources ) cannot be incorporated explicitly in the model. On the otherhand such mechanistic information can be incorporated in other model approaches such as the conditional approach developed at Cornell [15].

Similar comments apply to the modeling of chemical species transport effects in premixed flames dominated by flamelets. Temperature and composition are nearly uniform

in reactants and products. Molecular transport of heat and species occurs in the flamelet. Unconditioned moment closures cannot reflect these facts directly while other model approaches can.

The conditioned velocity measurements were undertaken primarily to investigate flow acceleration across the flamelet. Unfortunately the persistence of oil droplets across the flamelet hinders a quantitative evaluation of such acceleration. We continue to work on this problem.

## V. SUMMARY

Several tasks of research on turbulent flames have been pursued. The focus has been on low to moderate Reynolds number premixed flames. A fractal representation of surfaces in turbulent flows is found to be a very useful tool for modeling purposes. Experiments support the hypothesis that flamelet surfaces can be represented by fractal surfaces, but more experiments are needed before the evidence can be considered conclusive. Passage time pdf's are also useful in combustion modeling. Such distributions were measured and found to be reasonably well represented by one of two proposed functional forms for the pdf's. If a very exact representation is required neither function seems ideal. Flame position and conditioned velocity measurements were performed. The pdf of flamelet position is nearly gaussian and the standard deviation of the distribution is a measure of flame brush thickness. The velocity measurements reveal the flamelet to be a source of flow acceleration. But experimental problems have hindered the gathering of quantitative data on the magnitude of this acceleration.

## REFERENCES

1. Dandekar, K V & Gouldin, F C: *AIAA J.* 20, 652-663, 1982.
2. Gouldin, F C & Dandekar, K V: *AIAA J.* 22, 655-663, 1984.
3. Gouldin, F C & Halthore, R: *Exp. in Fluids* 4, 269-278, 1986.
4. Bray, K N C, Libby, P A, & Moss, J B: *Comb. Sci. Tech.* 41, 143-171, 1984.
5. Gouldin, F C: *Comb. Flame* 68, 249-266, 1987.
6. Gouldin, F C: "An Interpretation of jet mixing and jet flame length data using fractals, College of Engineering, Energy Report E-86-02, Cornell University, Ithaca, NY, 1986. Results presented at the Fall Technical Meeting of the Eastern Section: The Combustion Institute, San Juan, Puerto Rico, Dec. 1986.
7. Miles, P & Gouldin, F C: College of Engineering, Energy Report E-86-03, Cornell University, Ithaca, NY, 1986. Presented at the 2nd ASME-JSME Thermal Engineering Conference, Honolulu, Hawaii, March 1987.
8. Mandelbrot, B. B.: *The Fractal Geometry of Nature*, Freeman, New York, 1983.
9. Mandelbrot, B B: *J. Fluid Mech.* 72, 401-416, 1975.
10. Lovejoy, S: *Science* 216, 185, 1982.
11. Sreenivasan, K R & Meneveau, C: *J Fluid Mech.* 173, 356-386, 1986.
12. Hentschel, H G E & Procaccia, I: *Physical Review A - General Physics* 29, 1461-1470, 1984.
13. Abdel-Gayed, R G, Al-Khishali, K J, & Bradley, D: *Proc. Roy. Soc. Lond.* A391, 393-414, 1984.
14. Abdel-Gayed, R G, Bradley, D, Hamid, M N, & Lawes, M: *20th Symposium (International) on Combustion*, The Combustion Inst., 505-512, 1984.
15. Chen, J-Y, Lumley, J L, & Gouldin, F C: to appear in the *21st Symposium (International) on Combustion*, The Combustion Inst., 1987.
16. Warhaft, Z: *J. Fluid Mech.* 144, 363 - 387, 1984.
17. Williams, F A: pp. 189-208, in *Turbulent Mixing in Non-reactive and Reactive Flows*, Plenum Press, 1975.
18. Gouldin, F C: An interpretation of jet mixing using fractals, submitted to *AIAA J.*
19. Kingdon, R D & Ball, R C: The fractal dimension of clouds, submitted to *J.*

**Phys. A, 1987.**

20. Gouldin, F C: "An experimental study of flamelet surfaces in turbulent combustion" proposal submitted to the Army Research Office by Cornell University, August 1986.
21. Bray, K N C & Libby, P A: **Comb. Sci. Tech. 47, 253, 1986.**
22. Cheng, R K: **Comb. Sci. Tech. 41, 109, 1984.**
23. Boyer, L: **Comb. Flame 39, 321-323, 1980.**
24. Hilton, S M: Measurements to Determine the Fractal Character of Premixed Turbulent Flames, Master of Engineering (Engineering Physics) Report, Cornell University, Ithaca, NY, May 1987.
25. Lamb, T: Point In Time Measurements of the Fractal Dimension of Premixed Turbulent Flames, Master of Engineering (Engineering Physics) Report, Cornell University, Ithaca, NY, June 1987.

**Table 1. Tomographic Fractal Analysis Results**

CH<sub>4</sub> - Air flames.  
8 mesh screen turbulence generator

$\phi$	mean axial <u>velocity (m/s)</u>	<u>R<sub>t</sub></u>	number of curves <u>analyzed</u>	mean fractal <u>dimension</u>	standard <u>deviation</u>
0.8	4.1	25	18	1.09	0.03
1.0	4.2	25	16	1.11	0.03
0.8	3.8	23.5	16	1.11	0.04

## FIGURE CAPTIONS

1. Schematic of burner showing location of wire mesh turbulence generator, stabilizer rod, and laser beam for flamelet position measurement. The inner jet diameter is 5 cm, and the outer, annular jet diameter is 7.6 cm. The fuel is methane.
2. Distribution of passage times in the 10 mesh,  $\langle U \rangle = 3.8$  m/s flame. Squares denote times in products and pluses denote times in reactants at a point 5.5 cm downstream from the wire mesh. Triangles denote times in products and X's times in reactants at 7.0 cm.  $\langle c \rangle = 0.46$ . The straight line indicates the exponential pdf form while the curved line is the gamma 2 distribution. See Ref. 3 for details.
3. Typical length plot for fractal analysis of tomograms [24].
4. Typical plot for fractal dust analysis of the time series measurements of flamelet crossing events [25].

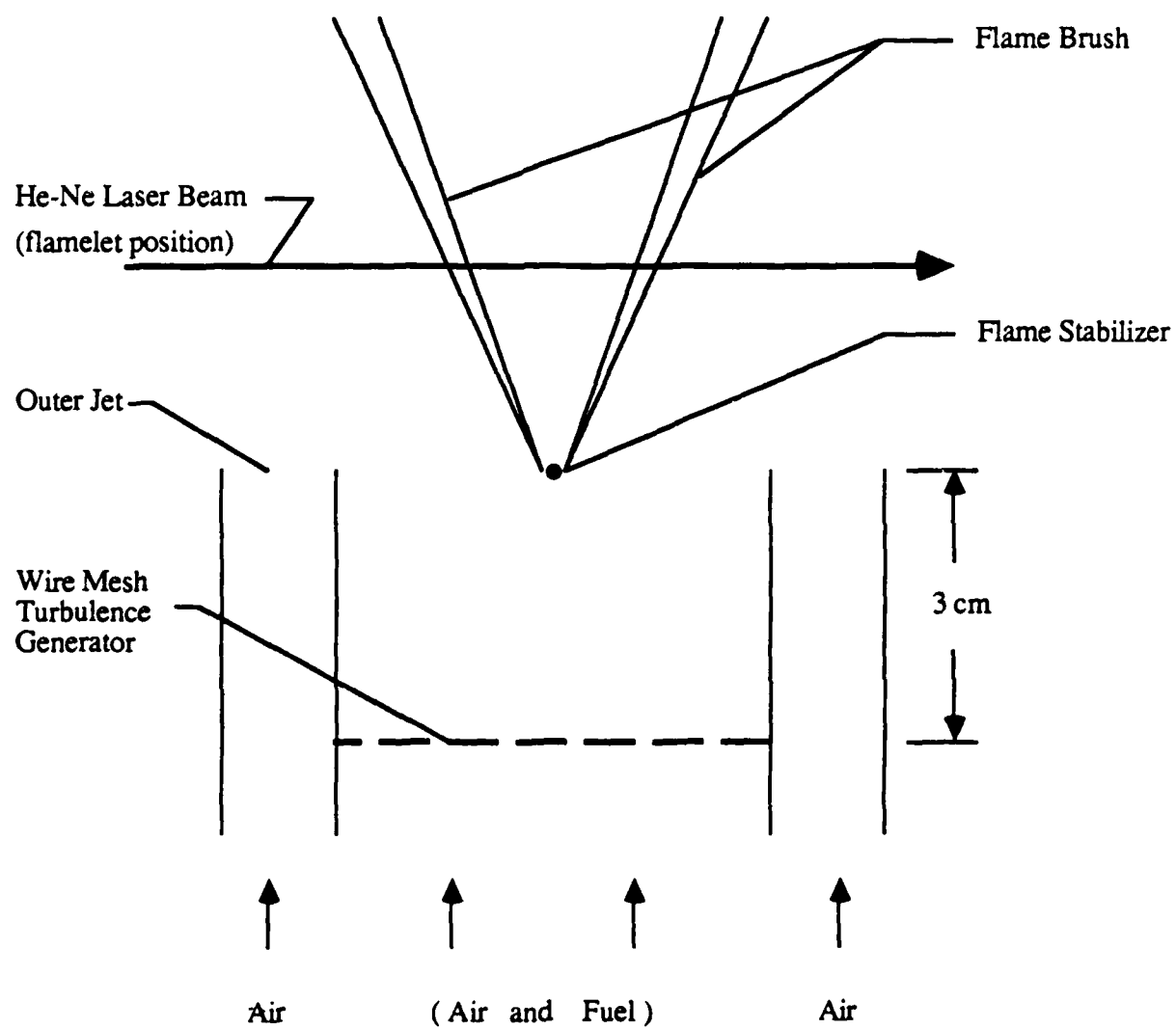


Fig. 1.

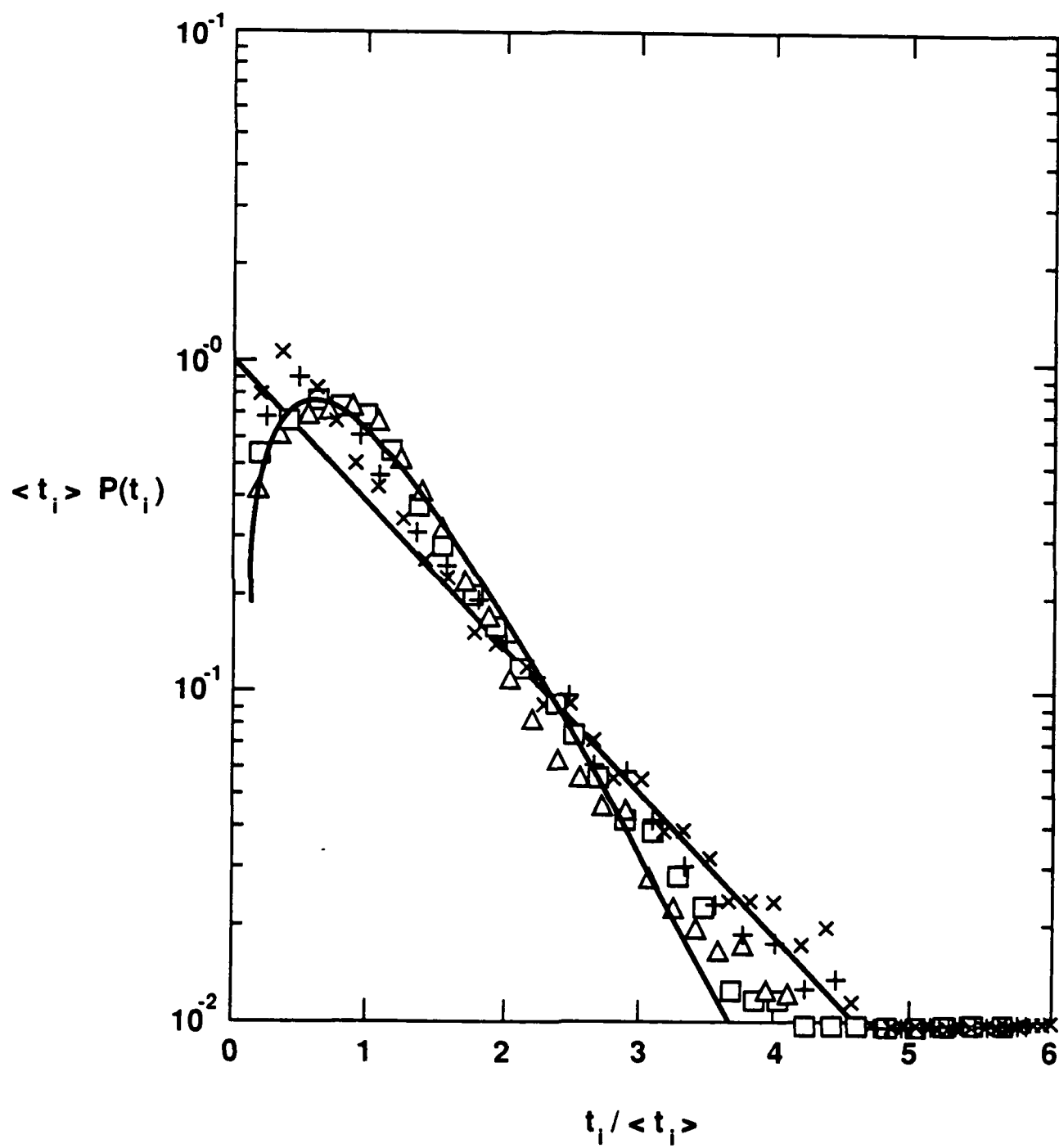


Fig 2

Methane-Air V-flame  
 $\phi = 0.8$ ,  $\bar{U} = 4.1$  m/s,  $Re \cong 25$ ,  $l = 2.70$  mm  
Fractal Dimension = 1.14018

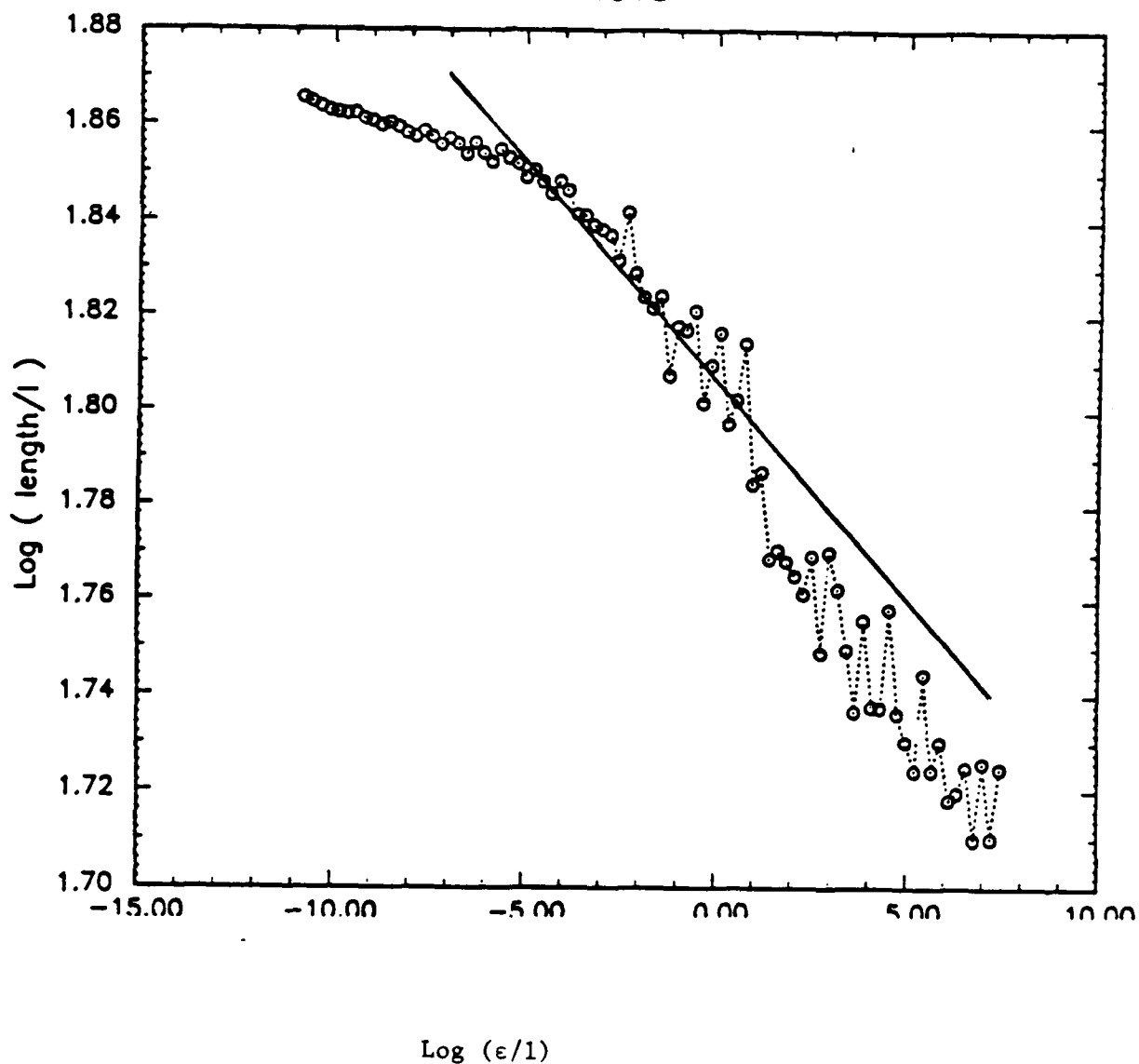


Fig 3

## 11\_7 Fractal Plot

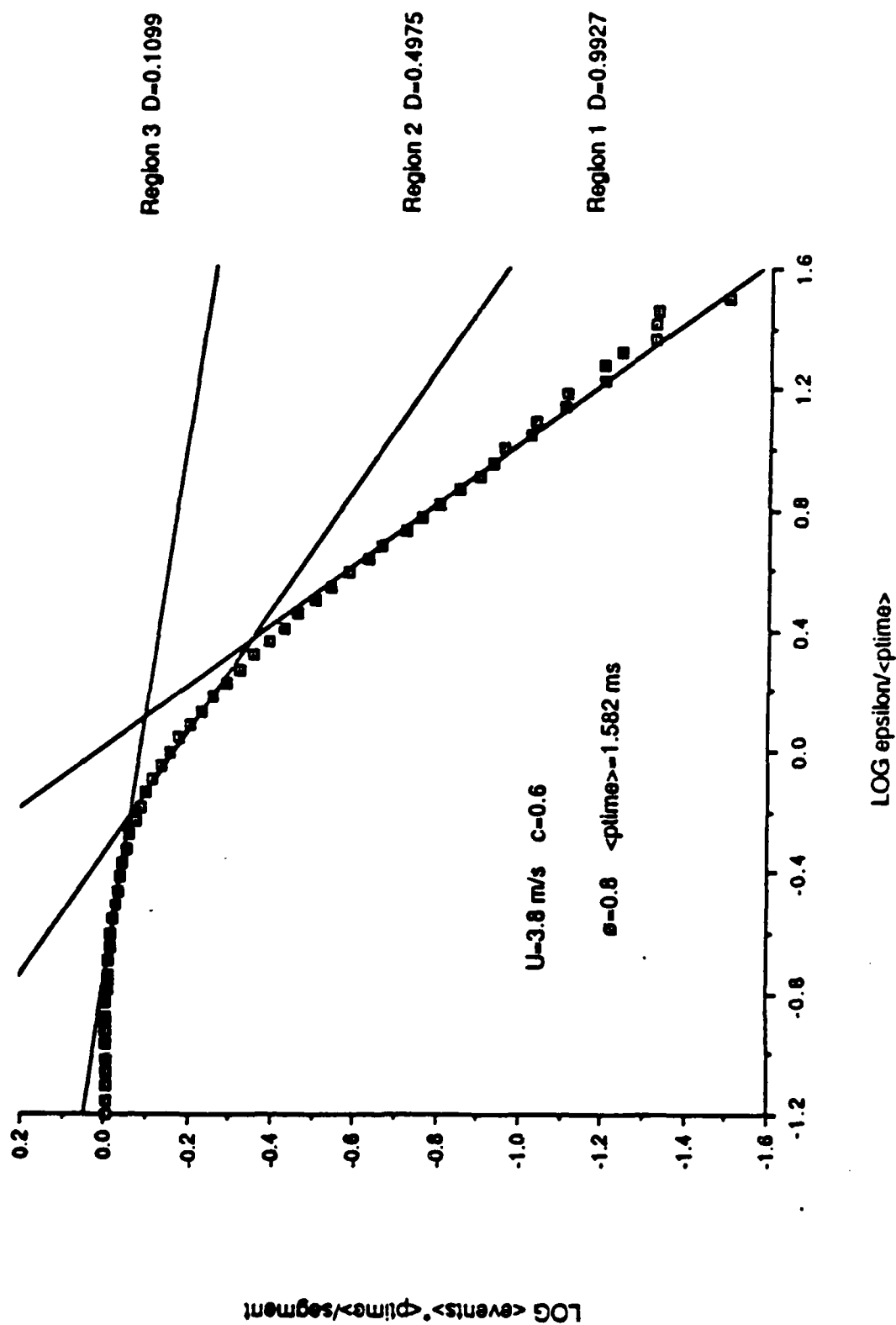
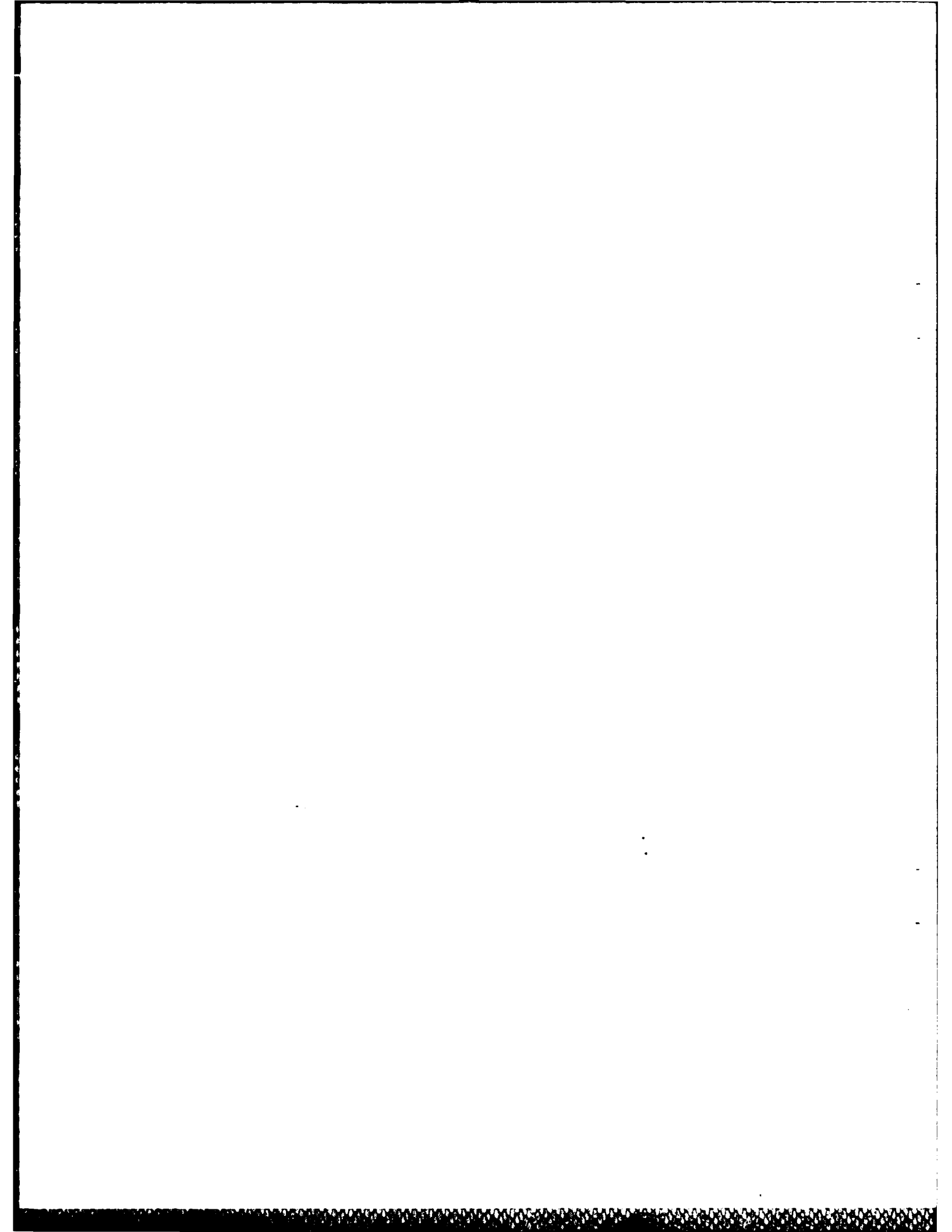


Fig 4



## APPENDIX A

CHEMICAL CLOSURE MODEL FOR  
FRACTAL FLAMELETS

F. C. Gouldin  
Cornell University  
Ithaca, N. Y. 14850

K. N. C. Bray  
Cambridge University  
Cambridge, England

J.-Y. Chen  
Sandia National Laboratories  
Livermore, CA 94550

## Abstract

A chemical closure model for premixed turbulent flames is proposed and tested by analysis and numerical computation for flames with vanishingly small density change. The model is based on the assumption that reaction zones can be modeled as thin sheets -- flamelets -- and that the geometry of these sheets can be represented by fractal surfaces. The model expression for mean fuel consumption rate is

$$\langle \omega_f \rangle = C_R \rho_0 \langle \Delta Y_f u_L \rangle_f (l / \eta)^{D-2} l_f^{-1} \langle c \rangle (1 - \langle c \rangle),$$

with  $f$  given by

$$f = [1 - (1 - A_t^{-1/4} R_t^{-3/4}) \exp(-A_t^{1/4} R_t^{-1/4} u' / \langle u_L \rangle_f)],$$

and

$$l / \eta = A_t^{1/4} R_t^{3/4},$$

where  $D$  is the fractal dimension of the flamelet surface and is the new parameter introduced by the fractal geometry assumption.

This model is tested in simplified analyses of normal and oblique flames with good results. The oblique flame analysis provides new insight into the definition of the turbulent burning velocity. Numerical computations are performed with a conditioned second order closure scheme, and the chemical closure model performance is found to be good. Computed results with a gradient transport model for species diffusion show that turbulent fluxes are significantly under predicted in comparison with the second order closure results.

## I. Introduction

In [1] a model for turbulent burning velocity is proposed based on the assumption that chemical reaction and heat release rates can be modeled as occurring in thin sheets -- flamelets -- and that the geometry of these sheets can be represented as fractal. It is argued that flamelet surfaces are extremely rough with multiple scales of wrinkling and that mathematical relationships true for fractal surfaces can be used to advantage in characterizing flamelet surface area.

Fractal surfaces are rough and a significant feature of this roughness is the regular variation of measured surface area with measurement scale [1,2,3]. For an isotropic fractal surface in a volume  $L^3$ ,

$$A / L^3 \sim \epsilon^{2-D} / L^3. \quad (1)$$

$A$  is the measured area, and  $\epsilon$  is the measurement scale.  $D$  is the fractal dimension of the surface and is bounded such that  $2 \leq D < 3$ . Fractal surfaces are extremely wrinkled, and according to Mandelbrot [3] they appear to be space filling. The larger  $D$  the more space filling a fractal surface will appear.

For flamelets as for constant property surfaces in turbulent flow, there is a limit to the range of length scales over which fractal behavior is observed. The variation of  $A$  with  $\epsilon$  will not follow (1) for  $\epsilon$  outside the fractal range, and for surfaces with a limited range of fractal behavior Gouldin [1] hypothesizes a simple behavior for  $A$  versus  $\epsilon$ , which is depicted in Fig. 1. At this point two new parameters enter the fractal description, the inner and outer cutoffs --  $\epsilon_i$  and  $\epsilon_o$  [3]. Flamelet surface area is finite and thus  $A$  must approach a limit,  $A_i$ , as  $\epsilon \rightarrow 0$ . For large  $\epsilon$  and anchored flames such as a bunsen flame, we expect that on large measurement scales the surface will appear smooth and  $A \rightarrow A_o$  as  $\epsilon \rightarrow \infty$ .

This limiting behavior at both large and small  $\epsilon$  is represented by horizontal line segments with  $\epsilon_i$  and  $\epsilon_o$  defined such that  $A_o / L^3 \sim \epsilon_o^{2-D} / L^3$  and  $A_i / L^3 \sim \epsilon_i^{2-D} / L^3$ .

Mean flamelet surface area is estimated in [1] using the results displayed in Fig. 1. Here we use similar reasoning to that in [1] to obtain a model for the local mean rate of fuel consumption. Then normal and oblique flames are analyzed with the proposed rate model under the assumption that density change is negligible, and a burning velocity expression is obtained which is identical to that of [1]. A numerical analysis of anchored flames in grid turbulence is performed with the new closure model and with a conditioned, second order transport model developed by Chen, Lumley and Gouldin [4]. The calculation results are realistic and consistent with those of [1]. Finally, flame calculation results with a gradient transport model for turbulent species flux are compared to results from the second order model. The gradient model predictions are not in agreement with those of the second order model.

## II. Chemical Closure Model

The proposed rate expression for fuel consumption is of the form

$$\langle \omega_f \rangle = C_R \rho_0 \langle \Delta Y_f u_L \rangle_f (\epsilon_i / \epsilon_0)^{2-D} l_c^{-1} \langle c \rangle (1 - \langle c \rangle) l_c / l_F, \quad (2)$$

where  $C_R$  is a model "constant",  $u_L$  is the local laminar burning velocity of the flamelet and  $\Delta Y_f$  is the change in fuel mass fraction across the flamelet. The notation  $\langle \rangle_f$  represents an average over the flamelet surface,  $l_F$  is the local, turbulent flame brush thickness, while  $l_c$  will be defined below. Finally,  $\rho_0$  is the cold gas density, and  $\langle c \rangle$  is the mean degree of reaction where  $c = (Y_f - Y_f^0) / \Delta Y_f$  and  $Y_f^0$  is the initial fuel mass fraction. This expression is justified using the following arguments.

Consider a cubic volume centered in space on a point  $x$  with side  $l_c$  which is small enough that the ensemble mean conditions inside the volume can be assumed to be uniform with a mean degree of reaction  $\langle c \rangle$ . Assume that the flamelet geometry can be represented by a fractal surface of fractal dimension  $D$ , inner cutoff  $\epsilon_i$ , and outer cutoff  $\epsilon_0$ . Here,  $\epsilon_0$  is representative of the larger scales of wrinkling of the flamelet surface and for the flamelet surface to be distributed on average in a uniform manner over  $l_c^3$  we require that  $l_c \geq \epsilon_0$ . Let  $P_C$  be the probability that a flamelet is present in the volume  $l_c^3$ .

According to Mandelbrot [1,3] a constant property surface ( e.g., a constant temperature surface) in homogenous, isotropic turbulence is fractal. In a cube of volume  $L^3$ , the mean surface area per unit volume of a fractal surface measured at a length scale  $\epsilon$  is

$$A/L^3 = C |\epsilon/L|^{-D} \epsilon^2 / L^3.$$

$C$  is a constant termed by Mandelbrot the lacunarity [2]. As noted, Gouldin [1] has argued that if there is a characteristic minimum length scale of wrinkling, which is defined as the inner cutoff, the actual mean surface area per unit volume is finite and can be written a

$$A/L^3 = C |\epsilon_i/L|^{-D} \epsilon_i^2 / L^3.$$

Mandelbrot considered homogeneous, isotropic turbulence. Then  $L^3$  is a volume embedded in turbulent fluid and the surface is dispersed throughout this volume in a statistically uniform manner. Flamelets are not expected to fill space in the same manner as Mandelbrot's constant property surfaces. To adapt Mandelbrot's fractal surface concepts to the present problem it is assumed that, when there is flamelet present in  $l_c^3$ , it fills  $l_c^3$  in the same manner as a constant property surface in isotropic, homogeneous turbulence fills  $L^3$ . Thus the average flamelet surface area in  $l_c^3$  can be expressed as

$$A_c = C |\epsilon_i / l_c|^{-D} \epsilon_i^2 P_c, \quad (3)$$

where  $P_c$ , as noted, is the probability of finding a flamelet in the volume  $l_c^3$ .

For modeling we propose that the mean rate of fuel consumption can be written as a product of  $A_c$  and the mean rate of fuel consumption per unit flamelet area  $-\rho_o \langle \Delta Y_f u_L \rangle_f$ . Flamelet surface wrinkling and other effects of turbulence will perturb the flamelet structure and therefore alter fuel consumption rates.  $\rho_o \Delta Y_f u_L$  represents the local instantaneous consumption rate in terms of the reactant density, the change in fuel mass fraction across the flamelet and the laminar burning velocity. This expression may be interpreted as a definition for the laminar burning velocity. It is implicit in our modeling approach that good estimates of  $\rho_o \langle \Delta Y_f u_L \rangle_f$  can be obtained and our focus is on the modeling of  $A_c$ . A fuller discussion of possible modeling for  $\rho_o \langle \Delta Y_f u_L \rangle_f$  is given in [1].

With our expression for mean fuel consumption per unit area, the mean consumption rate in  $l_c^3$  is just  $\rho_o \langle \Delta Y_f u_L \rangle_f A_c$  and

$$\langle \omega_f \rangle \sim \rho_o \langle \Delta Y_f u_L \rangle_f \epsilon_i^{2-D} l_c^{D-3} P_c,$$

with  $P_c$ ,  $\epsilon_i$  and  $l_c$  yet to be determined.

There is experimental evidence for v-flames [5] that the probability density function describing flamelet location on a line which is normal to the flame brush is Gaussian. If flamelet motion is the result of many random impulses the central limit theorem also suggests that this probability will be Gaussian. For thin flamelets a reasonable approximation [5] to the value of the Gaussian function at a point  $x$  is given by

$C_n \langle c(x) \rangle (1 - \langle c(x) \rangle)$  where  $C_n$  is a normalization constant. For clarity the functional dependency of  $\langle c \rangle$  on position,  $x$ , is shown explicitly. The probability of finding the flamelet along a segment of the normal which is  $l_c$  is just  $C_n \langle c \rangle (1 - \langle c \rangle) l_c$ . The integrated probability over the flame brush thickness,  $l_F$ , should be one and therefore  $C_n \sim 1/l_F$ . For  $P_c$  it follows that

$$P_c \sim \langle c \rangle (1 - \langle c \rangle) l_c / l_F. \quad (4)$$

The inner cutoff is a measure of the smallest scales of wrinkling. For unit Schmidt number we expect that the smallest possible scale of wrinkling due to turbulent velocity fluctuations is related to the Kolmogorov microscale. Gouldin [1] has hypothesized that for flamelets the inner cutoff is equal to or greater than the Kolmogorov scale and that it depends on the ratio  $u'/\langle u_L \rangle_f$ . He suggests an expression for  $\epsilon_i$  [1] -

$$\epsilon_i = \eta/f = \eta/[1 - (1 - A_t^{-1/4} R_t^{-3/4}) \exp(-A_t^{1/4} R_t^{-1/4} u'/\langle u_L \rangle_f)], \quad (5)$$

where  $\eta$  is the Kolmogorov microscale,  $R_t$  the turbulent Reynolds number and  $u'$  is the root mean square of velocity fluctuations.  $\eta$  represents the minimum possible scale of surface wrinkling, while  $f$  accounts for smoothing at the smallest scales of wrinkling due to flamelet propagation relative to the reactant flow. While this relationship for  $f$  is speculative and future research may well lead to an alternate expression for  $\epsilon_i$ , the above form is adopted here.

The arguments in [1] suggest that  $l_c$  should be a multiple of  $l$ , the turbulence integral scale, if not equal to  $l$ . Implicit in the arguments leading to (3) is the assumption that when present the wrinkled flamelet surface is assumed to fill  $l_c^3$  as Mandelbrot's fractal, constant property surface fills  $L^3$ . In order for this to be true we expect  $l_c \sim l$ , where  $l$  is taken as the outer cutoff ( $l = \epsilon_0$ ). Our argument here is based on the assumption that, while the flamelet can extend over large distances in two directions, its extent in the third direction is limited. At any instant flamelet sheets can be bounded by two smooth surfaces with a local separation distance which is proportional to the outer cutoff which in turn is assumed to be  $l$ . If flamelet wrinkling is such that flamelets double back on

themselves many times the separation distance of these two bounding surfaces would be larger and  $l_c$  could be larger than the outer cutoff. We assume that such doubling back on large scales is not important. Doubling back on scales up to the order of the outer cutoff is expected and accounted for by the fractal description of flamelets

At this point a digression on the length scales introduced in this work may be helpful.  $\eta$  and  $l$  are traditional turbulence length scales and are widely used for characterizing turbulence.  $\epsilon_i$  and  $\epsilon_0$  are scales introduced with the fractal description of rough surfaces, and they are related by hypothesis (which is supported by experiment) to the turbulence length scales,  $\eta$  and  $l$ .  $l_c$  is introduced for purposes of exposition.

A major difficulty in adapting Mandelbrot's results [3] for surfaces in turbulent flow to the present problem arises because Mandelbrot assumes isotropic surface distributions while our flamelet distributions are highly anisotropic. To overcome this problem we focus attention on a small volume,  $l_c^3$ . When the flamelet is in this volume its distribution in the volume is nearly isotropic, and an ensemble of such occurrences should have an even more isotropic distribution. Clearly, for the arguments leading to Eq. (4) to hold  $l_c$  must be larger than the scales of surface wrinkling or the surface contained in  $l_c^3$  will not be representative of all scales of wrinkling. At the same time  $l_c$  cannot be too large or the isotropic character will be lost. Thus  $l_c = l = \epsilon_0$  appears to be the obvious choice. This choice for  $l_c$  implies that  $l_F > l$  which may surprise some people. Instantaneously the flamelet is not wrinkled sufficiently to occupy a volume comparable to the entire turbulent flame brush. Instead it occupies at any instant a smaller volume, and it occupies the entire flame brush only in an average sense.

An alternative line of argument can be developed which leads to the same closure expression as above. In this case  $l_c/l_F$  is set equal to a constant. Thus the probability of the flamelet being in  $l_c^3$  for a given  $\langle c \rangle$  but different  $l_F$  is fixed.  $l_c$  varies with  $l_F$  and the

flamelet does not fill  $l_c^3$ . Following arguments similar to those of [1] one concludes that the conditional mean flamelet area in  $l_c^3$  is given as

$$A_i = (\epsilon_0/\epsilon_i)^{D-2} A_0$$

where  $\epsilon_i = \eta/f$ ,  $\epsilon_0 = l$ , and  $A_0$  is defined in Fig. 1. (Conditioning is on the presence of the flamelet in the volume defined by  $l_c^3$ .) Furthermore  $A_0 \sim l_c^2$  so that

$$A \sim (l f/\eta)^{D-2} l_c^2 \text{ and}$$

$$A/l_c^3 \sim (l f/\eta)^{D-2} l_c^{-1}$$

which leads to the same result for  $\langle \omega_f \rangle$  as above when the probability  $P_c$  is incorporated. In this case  $P_c \sim \langle c \rangle (1 - \langle c \rangle) l_c/l_f$ .

The new step in this argument relative to the reasoning of [1] is the scaling  $A_0 \sim l_c^2$ .  $A_0$ , the area measured for  $\epsilon \geq \epsilon_0$ , is the mean area that the flamelet would have while in  $l_c^3$  if the flamelet was viewed at large  $\epsilon$  and appeared smooth, i. e., without wrinkles. In this case the flamelet would be planar and its area in  $l_c^3$  scales as  $l_c^2$ .

In summary, the final expression for  $\langle \omega_f \rangle$  is

$$\langle \omega_f \rangle = C_R \rho_0 \langle \Delta Y_f u_L \rangle_f (l f/\eta)^{D-2} l_f^{-1} \langle c \rangle (1 - \langle c \rangle). \quad (2')$$

$f$  is given by

$$f = [1 - (1 - A_t^{-1/4} R_t^{-3/4}) \exp(-A_t^{1/4} R_t^{-1/4} u' / \langle u_L \rangle_f)].$$

Also note that for homogeneous, isotropic turbulence  $l/\eta = A_t^{1/4} R_t^{3/4}$  [1].

### III. Analyses of Normal and Oblique Flames

Normal and oblique flames are analyzed using the proposed rate model as presented in (9). Results for the burning velocity are compared to the burning velocity model of [1].

For a normal flame assuming high Reynolds number, one-dimensional flow in the mean and  $\Delta Y_f$  constant (for convenience), one can develop an equation for  $\langle c \rangle$ :

$$\rho_0 u_t d\langle c \rangle/dx +$$

$$\begin{aligned} d/dx (<\rho><c'u> + <c><\rho'u> + <U><c'\rho> + <\rho'c'u>) \\ &= <\omega_f>/\Delta Y_f. \end{aligned} \quad (6)$$

$u_t$  is the mean reactant flow velocity approaching the flame brush or time mean reaction zone and is the turbulent burning velocity. Primes denote fluctuations in  $c$  and  $\rho$ , while  $U$  and  $u$  are the instantaneous and fluctuating velocities respectively. If this equation is integrated from  $-\infty$  to  $+\infty$  with  $<c> = 0$  at  $x = -\infty$  and  $<c> = 1$  at  $+\infty$ , one obtains

$$\rho_o u_t = \int_{-\infty}^{\infty} <\omega_f>/\Delta Y_f dx,$$

and substituting for  $<\omega_f>$

$$\rho_o u_t = \rho_o \int_{-\infty}^{\infty} C_R <u_L>_f (l_c f/\eta)^{D-2} <c>(1-<c>) l_F^{-1} dx.$$

It is implicit in the formulation presented in the previous section that most of the spatial variation in  $<\omega_f>$  is due to  $<c>(1-<c>)$ , i.e., it is in the probability of finding a flamelet in  $l_c^3$  at  $x$ .

Assume that  $<u_L>_f$ ,  $\eta$ ,  $f$  and  $l_c$  are uniform in space and dependent on conditions in the reactants. Also note that the fractal modeling in [1] gives  $u_t/<u_L>_f = (l f/\eta)^{D-2}$ . It follows that

$$\left(\frac{l f}{\eta}\right)^{D-2} = C_R \left(\frac{l_c f}{\eta}\right)^{D-2} l_F^{-1} \int_{-\infty}^{\infty} <c>(1-<c>) dx \quad (7)$$

For this relationship to be valid  $l_c = l$ , as suggested in the previous section, and

$$C_R = l_F / \int_{-\infty}^{\infty} <c>(1-<c>) dx. \quad (8)$$

Clearly,

$$\int_{-\infty}^{\infty} \langle c \rangle (1 - \langle c \rangle) dx$$

is a measure of the turbulent flame brush thickness. Thus

$$l_F / \int_{-\infty}^{\infty} \langle c \rangle (1 - \langle c \rangle) dx$$

is a constant for a given geometry and initial conditions. The application of the present model to the normal flame geometry is thus seen to be self-consistent with previous work [1].

The above analysis for normal flames can be extended to oblique flames without great difficulty and it is interesting to see if the notion of a turbulent burning velocity may be applied to oblique flames.

As above, assume constant density and, hence, straight streamlines. We are interested in cases where the flame brush thickness increases in the streamwise direction as is observed experimentally, and we assume a priori that the mean flame brush structure follows similarity at least locally. We assume that  $\langle c \rangle$  constant surfaces can be approximated locally by plane surfaces and, to first order, that the flame brush thickness grows linearly with distance along the flame brush. Finally we assume slow growth in flame thickness and parabolic flow.

The geometry to be studied is shown in Fig 2. Note that by definition the  $\zeta$  axis lies along  $\langle c \rangle = 0.5$ , and  $\eta$  is perpendicular to  $\zeta$ , while the  $x$  and  $y$  axes lie along and perpendicular to the approach flow, respectively.

A control volume analysis is pursued and the net mean flux of products out of the control volume is set equal to the mean rate of production in the volume. For a rectangular volume of unit depth the rate of product formation can be written as

$$\dot{P} = \int_{\zeta_1}^{\zeta_2} \int_{\eta_P}^{\eta_R} p \langle \omega_f \rangle d\eta d\zeta,$$

$\eta_R$  and  $\eta_P$  define the edges of the flame brush, and  $p$  is the ratio of the amount of product mass formed per unit mass of fuel reacted. By referring to the above model for  $\langle \omega_f \rangle$  one notes that, if  $\langle c \rangle$  satisfies similarity, that is,  $\langle c \rangle$  is a function only of  $\eta / (\zeta + \zeta_0)$  where  $\zeta_0$  is a suitably chosen constant, and  $\epsilon_0/\epsilon_1$  is constant, the integral of  $\langle \omega_f \rangle$  over  $\eta$  is a constant and production can be written as

$$\dot{P} = \delta p I_{\omega},$$

where

$$I_{\omega} = \int_{\eta_P}^{\eta_R} \langle \omega_f \rangle d\eta$$

which is constant, ie., independent of  $\zeta$ .

For the product fluxes into and out of the control volume only convection is considered for faces 1 and 2, and turbulent fluxes across the other two faces are zero since conditions are uniform in the vicinity of both faces. Thus only convective fluxes need be estimated and no turbulence modeling is needed at this point. The neglect of turbulent fluxes of product across 1 and 2 implies a boundary layer approximation, ie., parabolic flow and small  $dI_P/d\zeta$ . Product flux into the control volume is

$M_{in} = \rho \langle U \rangle \cos \theta [l_F(1) I_c + \tan(\theta + \theta_p) \delta]$ , where similarity has been used and

$$I_c = \int_{\eta_P}^{\eta_R} \langle c \rangle d\eta / l_F.$$

The angles  $\theta$  and  $\theta_p$  are defined in Fig. 2 and  $l_F(1)$  denotes the flame brush thickness at 1.

For the flux out one obtains

$$M_{out} = \rho \langle U \rangle \cos \theta [l_F(2) I_c + \tan \theta \delta].$$

The second term in this expression is the flux across the control volume face which is totally in products.

Equating the difference of  $M_{out}$  and  $M_{in}$  to production one obtains

$$\delta p I_\omega = \cos \theta \rho \langle U \rangle [ (l_F(2) - l_F(1)) I_c + (\tan \theta - \tan(\theta + \theta_p)) \delta ].$$

For unit Schmidt number and  $\langle \omega_f \rangle$  an even function of  $\eta$ , by symmetry  $\theta_R - \theta = \theta + \theta_p = \Delta\theta$ . Then

$$p I_\omega = \sin \theta \rho \langle U \rangle [ 1 + (2I_c - 1) \tan \Delta\theta / \tan \theta ], \quad (9)$$

where we have made use of the relationship  $(l_F(2) - l_F(1)) = 2 \delta \tan \Delta\theta$ . Without chemical reaction, symmetry requires that  $\theta = 0$  and  $I_c = 1/2$ . Here we look for a solution which gives a meaningful definition for the turbulent burning velocity. One can obtain such a result in two ways: assuming either  $I_c = 1/2$  or  $\Delta\theta = 0$ . In either case the same expression for  $u_t$  is obtained.

$$\rho u_t = \sin \theta \rho u = p I_\omega, \quad (10)$$

Thus a meaningful burning velocity, defined as the component of the mean approach flow velocity perpendicular to  $\zeta$  is obtained and is the integral of the mean product production rate across the flame brush.

The control volume width,  $\delta$ , does not appear in the final expression for  $u_t$  as would be expected. However, implicit in the analysis is the assumption that similarity is valid for a control volume with finite  $\delta$ .

Using the closure model presented above one can evaluate  $I_\omega$  and finds by substitution

$$u_t = C_R \langle u_L \rangle_f (fl / \eta)^{D-2} p I_R, \quad (11)$$

where

$$I_R = \int_{\eta_P}^{\eta_R} \langle c \rangle (1 - \langle c \rangle) d\eta / l_F.$$

From the analysis of normal flames  $C_R = 1/I_R$ , and one sees that  $u_t$  as defined here for oblique flames is equal to that for normal flames and that  $u_t$  is independent of  $\zeta$  provided similarity holds which implies nondecaying turbulence.

The major assumption used to obtain this result is that of similarity. This assumption plays a major role in our evaluation of  $M_{in}$  and  $M_{out}$ . It should be noted, on the other hand, that the constancy of  $I_\omega$  is inherent in the modeling of  $\langle \omega_f \rangle$ , provided  $\epsilon_0/\epsilon_i$  is constant across the flame brush, and does not require an additional assumption. The quantity  $\langle c \rangle (1 - \langle c \rangle) / l_F$  is proportional to the probability of finding the flamelet at a point where the mean degree of reaction is  $\langle c \rangle$ , and thus the integral  $I_R$  is constant because the probability of finding the flamelet somewhere across the flame brush is unity.

The condition  $\Delta\theta = 0$  corresponds to a constant flame brush thickness which is contrary to observations, while with  $I_c = 1/2$  the thickness continues to increase with increasing  $\zeta$ . If  $\langle \omega_f \rangle$  is an even function of  $\eta$ , by symmetry, we expect  $I_c$ , which is the mean value of  $\langle c \rangle$  when averaged across the flame brush, to be approximately a half. (N.B.: our numerical calculations give  $I_c \approx 1/2$ .) A continually growing flame brush might be thought to imply an increasing combustion rate because of an increase in flamelet area. However, as noted, our rate model scales  $\langle \omega_f \rangle$  by  $l_F$ , and  $I_\omega$  is independent of  $\zeta$ . This scaling arises via Eq. (4) according to which the probability  $P_c$  of finding a flamelet in a volume  $l_c^3$  decreases as  $\zeta$  increases. A physical interpretation of this behavior is that the flame brush thickness grows with increasing  $\zeta$  due to the cumulative effects of the many,

random upstream displacements of the flamelet surface(s) in a process which may have some likeness to a random walk. These displacements cause the flame brush to grow but they do not increase flamelet area and thereby combustion rate. Flamelet area is increased by the fractal wrinkling of flamelet surfaces due to the reactant flow turbulence. This area generation is dependent on  $l f/\eta$  and not the flame brush thickness.

#### IV. Numerical Analysis

Results of calculations using the proposed rate model of Eq. (2') and the second order transport model with conditional statistics of Chen, Lumley and Gouldin [4] are now presented and discussed. The transport model is based on model equations for conditioned moments, where conditioning is for being either in reactants,  $c=0$ , or in products,  $c=1$ . The instantaneous progress variable acts as the indicator function.

An equation for the mean progress variable, for negligible density change and high Reynolds number, can be written [4] as

$$\partial \langle c \rangle / \partial t + \langle U \rangle \cdot \nabla \langle c \rangle = \nabla \cdot \{ (\langle U \rangle - \langle U \rangle^{(1)}) \langle c \rangle \} - \langle \omega_f \rangle.$$

$\langle U \rangle^{(1)}$  is the conditioned velocity in the products, and the first term on the right hand side of the equation is the turbulent flux of products. This term would be given by  $-\nabla \cdot D_t \nabla \langle c \rangle$  if a gradient transport model were used;  $D_t$  is the turbulent diffusivity. Instead we solve a model equation for  $\langle U \rangle^{(1)}$  as well as finding  $\langle U \rangle$ , and consequently, gradient transport modeling is avoided.

These model equations (consult [4] for more detail of the model) are combined with the new rate model, and calculations are performed for an oblique flame in decaying grid turbulence. The flow and flame configuration are shown schematically in Fig. 3. This is the same configuration as considered in [4] and comparison of the present results with those in [4] can be made by the reader to see the influence of changing rate models. For calculations the flow is assumed to be parabolic. Upstream boundary conditions and model constants for the calculations are given in Table I; note that  $D = 2.4$ .

As a test of the turbulence model for nonreacting flow, the decay of grid turbulence was calculated, and the results for  $\langle u^2 \rangle$ ,  $l$  and  $R_l$  compared to the experimental data of Warhaft [6]. Comparisons are made in Fig. 4 where it can be seen that model predictions for  $\langle u^2 \rangle$  and  $R_l$  are very good.

If the assumptions of the analysis of the previous section are valid one would expect that the turbulent burning velocity defined as the component of the mean reactant flow velocity normal to the  $\langle c \rangle = 0.5$  surface would equal that predicted by the fractal model of [1]; see Eq. (11). In Fig. 5 calculation results for  $u_t/u_0$  are compared to those predicted by the burning velocity model. For this comparison  $C_R$  is chosen to give the best overall agreement;  $C_R = 4$ . The comparisons shown in Fig. 5 for a broad range of conditions are quite good both with regard to magnitude and variation of  $u_t/u_0$  with  $x/M$ . We attribute the small observed variations, which are present, between burning velocity model and calculation results to a departure from flow similarity which is assumed in the analysis of the last section.

A lack of similarity can be seen in the variation of lateral  $\langle c \rangle$  profiles with  $x/M$ , and several typical profiles are shown in Fig. 6. By similarity one would expect to see  $l_F$  grow linearly with  $x/M$ . Such behavior is not found in the numerical results. Instead  $l_F$  is found to grow very rapidly at small  $x/M$  and then to grow much more slowly at larger  $x/M$ ; see Fig. 7, which presents  $l_F/x$  versus  $x/M$ .

In performing the calculations for this work some results were also obtained with a gradient transport model for the  $\langle c \rangle$  equation while a full second order model was retained for the turbulent Reynold stresses. For these calculations  $D_t = C_d k^2/\epsilon$ , where  $k$  is the turbulence kinetic energy and  $\epsilon$  is the turbulence energy dissipation rate; the constant  $C_d$  is set equal to 0.09 [7]. We find that results for burning velocity are similar for the two transport models, Fig. 8, but that there is a marked difference in  $l_F$ , Fig. 9. From Fig. 10, it can be seen that gradient transport greatly under predicts turbulent fluxes in comparison with the second order model.

Counter-gradient diffusion is not observed. Libby, et al. [8] have shown that the interaction between the mean pressure gradient and density fluctuations plays a crucial role in causing counter-gradient diffusion. Pressure gradient fluctuations may also contribute to

this phenomenon. Thus it is not surprising that when combustion with negligible density change is considered counter-gradient diffusion is not observed.

That both transport models give essentially the same burning velocity may at first be surprising. The reason for this behavior is as follows. From Eqs. 9 and 10 we see that with similarity  $\rho u_t$  is given by  $\rho I_\omega$  for  $I_c = 1/2$ . As discussed above, with our rate model  $I_\omega$  is dependent only on  $\langle \rho_0 \Delta Y_f u_L \rangle (fl / \eta)^{D-2}$  and hence independent of the species transport model. This result follows from our expression for  $P_c$  and its scaling by  $l_F^{-1}$ . Then since both transport models give  $I_c \approx 1/2$ , they give similar  $u_t$  values.

Conditional and unconditional moments of velocity are presented in Figs. 11 and 12. It can be seen that unconditional mean velocities in the transverse (y) direction remain close to zero. They should equal zero in the absence of density change. Conditional mean velocities ( Fig. 11 ) for the burned and unburned zones are of equal magnitude but opposite sign, and their difference decreases in the flow direction as the turbulence decays. The relative magnitude and sign of the conditional transverse velocities must undergo significant change in the presence of combustion with heat release and density change if counter-gradient diffusion is to be observed. Transverse turbulent normal stress profiles are presented in Fig.12. The unconditioned stresses are nearly uniform as is required in the absence of density change, while conditional stresses vary significantly across the flame brush.

From the above presentation and the figures it is clear that the new rate model gives consistent and plausible results. Predicted burning velocities are in the expected range. However exact correspondence to the burning velocity model of Section III is not achieved. This lack of agreement is most likely the result of the departure from flow similarity in the numerical results which in turn we attribute to the decay of turbulence.

In the model calculations a constant density has been assumed and no counter-gradient diffusion is observed. At present the conditional modeling approach has not been

adapted to account for density changes across the flamelet. Work to allow for density change is needed.

## V. Summary and Closing Comments

A closure model for mean fuel consumption rate in premixed turbulent flames has been proposed and applied to several test problems. The model expresses the mean rate in terms of the product of the mean fuel consumption rate per unit flamelet surface area and of an expression for the mean flamelet area. The latter expression is obtained under the assumption that flamelet surface geometry can be represented by fractal surfaces. In addition the model uses an empirical expression from [5] for the probability of finding the flamelet in a volume  $l_c^3$ .

The new parameter appearing with the model is the fractal dimension. Based on the results reported in [1] and related experimental [9,10] and theoretical results [11,12,13] we recommend that  $D \approx 2.37$ , although for the present calculations we have used a value of 2.4.

Test problem results are mutually consistent and plausible. The rate model is easy to use and gives burning velocity values which are equal to the predictions of a new burning velocity model [1] which also uses fractal concepts.

The oblique flame analysis suggests that a meaningful burning velocity can be defined for oblique flames, and that  $u_t$  values can be related to the traditional definition of the burning velocity of normal flames. However, the oblique flame analysis rests on the assumption of similarity, and the expression for burning velocity requires a supplemental condition -- either  $\Delta\theta = 0$  or  $I_c = 1/2$ . The numerical calculations of Section IV show that departures from similarity can affect the burning velocity variation. In the absence of similarity it may be possible to develop an alternative, useful definition for the burning velocity. Until such a definition has been established, turbulent burning velocity data should be interpreted with caution.

The empirical basis for the relationship  $P_c \sim \langle c \rangle (1 - \langle c \rangle)$  can and should be made more substantial. For example the passage time model of [14] suggests  $P \sim \langle c \rangle (1 - \langle c \rangle)$  but not the normalization by  $l_f^{-1}$ . Furthermore in [5] the turbulence Reynolds number

is low and multiple flamelet crossings of lines parallel to the  $\eta$  axis are rare events. It is reasonable to expect that future work will lead to an improved expression of  $P_c$ . Developments of the passage time analyses of Bray, Libby and Moss [14, 15] may help in this respect. The possible occurrence of large scale doubling as described in Section II needs further study. If such events are important it may be necessary to change our scaling of  $l_c$  and our expression for  $P_c$ . To avoid confusion it should be noted that the neglect of large scale doubling back does not preclude doubling back on scales up to the order of the outer cutoff. Thus along lines parallel to the  $\eta$  axis multiple flamelet crossings at any instant will occur over a length of order of the outer cutoff. The region of these crossings will fluctuate in time and thus form a flame brush which is thicker than the outer cutoff.

The ratio  $\eta/f$  has been used to represent the inner cutoff. There is some question as to the appropriateness of this representation [1,16]. Our expression for  $\eta/f$  has been taken from [1] and the present work provides no test of its validity. Should a better representation of  $\epsilon_i$  be developed it is easily incorporated in the model.

The fractal character of flamelets is open to direct experimental verification by methods such as those described by Sreenivasan and Maneveau [9]. Information on the fractal dimension and the cutoffs can also be obtained. Results available to date are preliminary [16,17], and they are for low turbulence Reynolds numbers. While they show fractal behavior, inferred  $D$  values are low -- between 2.1 and 2.2. These low values may be related to the low turbulence Reynolds number of the flow and to the lack of a developed inertial subrange in the velocity fluctuation power spectrum. Thus measurements at high turbulence Reynolds numbers are required.

## REFERENCES

1. Gouldin, F. C.: An Application of Fractals to Modeling Premixed Turbulent Flames, **Comb. and Flame** in press.
2. Mandelbrot, B. B.: **The fractal geometry of nature**, W. H. Freeman Co., 1983.
3. Mandelbrot, B. B.: **J. Fluid Mech.** 72, 401-416, 1975.
4. Chen, J.-Y., Lumley, J. L. & Gouldin, F. C.: Modeling of Wrinkled Laminar Flames with Intermittency and Conditional Statistics, to appear in the **21st Symposium (International) on Combustion**, The Combustion Institute, Pittsburgh, 1987.
5. Miles, P. & Gouldin, F. C.: Simultaneous measurements of flamelet position and gas velocity in premixed turbulent flames, College of Engineering, Energy Report E-86-03, Cornell University, Ithaca, NY, 1986. Presented at the 2nd ASME-JSME Thermal Engineering Conference, Honolulu, Hawaii, March 1987.
6. Warhaft, Z.: **J. Fluid Mech.** 144, 363-387, 1984.
7. Jones, W P & Launder, B E: **Int. J. Heat Mass Transfer** 15, 301, 1972.
8. Libby, P. A. & Bray, K. N. C.: **AIAA J.** 19, 205-213, 1981.
9. Sreenivasan, K.R. and Meneveau, C.: **J. Fluid Mech.** 173, 356-386, 1986.
10. Lovejoy, S.: **Science** 216 1185 (1982).
11. Hentschel, H G E and Procaccia, I: **Physical Review A - General Physics** 29, 1461-1470, 1984
12. Kingdon, R.D. and Ball, R.C.: **The Fractal Dimension of Clouds**. Physics Department, University of Cambridge, submitted to **J. Phys. A**.
13. Gouldin, F.C.: **An Interpretation of Jet Mixing Using Fractals**, Mechanical and Aerospace Engineering, Energy Program Report E-87-01, Cornell University, Ithaca, N. Y., May 1987.
14. Bray, K.N.C., Libby, P.A. and Moss, J.B.: **Combustion Science and Technology** 41, 143, 1984.
15. Bray, K.N.C. and Libby, P.A.: **Combustion Science and Technology** 47, 253-274, 1986.
16. North, G.L. and Santavicca, D. A.: **"Fractal analysis of premixed turbulent flame structure"**, paper presented at the Fall Technical Meeting of the Eastern Section of the Combustion Institute, San Juan, Puerto Rico, Dec. 15-17, 1986.
17. Peters, N: in the **21st Symposium (International) on Combustion**, The Combustion Institute, 1987.

# FIGURES

- Fig. 1. Variation with measurement scale of measured area in a cubic volume of side  $L$  for a surface exhibiting fractal character. a) No inner or outer cutoffs. b) Inner and outer cutoffs to fractal behavior.
- Fig. 2. Schematic diagram of flame brush showing coordinate systems.
- Fig. 3. Sketch of flow configuration assumed for calculation.
- Fig. 4. Comparisons of model predictions for (a)  $\langle uu \rangle / \langle U^2 \rangle$  and (b)  $R_t$  with Warhaft data [6].
- Fig. 5. Comparisons of burning velocities obtained with new rate model and predictions from model of Reference 1: a) varying  $R_t$  (by varying  $v$ ), b) varying unstrained laminar burning velocities,  $u_0 = 2u_r$ ,  $u_r$ ,  $u_r/2$  and  $u_r = 1$  cm/s, and c) varying initial turbulence integral scale,  $l_r = 7.27$  mm (note  $v$  is adjusted to give constant  $R_t$ ).
- Fig. 6.  $\langle c \rangle$  profiles at three locations for standard conditions.  $x/M = 50, 100$  and  $200$ .
- Fig. 7. Flame brush thickness for different  $R_t$ , see Fig. 5a for burning velocity results.
- Fig. 8. Burning velocity predictions from second-order model and from gradient transport model, standard conditions. Burning velocity model predictions are also shown.
- Fig. 9. Flame brush thickness predictions for second-order model and gradient transport model, standard conditions.
- Fig. 10. Turbulent fluxes for standard conditions a) from conditional statistics and b) from gradient transport.
- Fig. 11. Second order model predictions of transverse mean velocity, both conditioned and unconditioned. Note that  $\langle vc' \rangle = \langle c \rangle (1 - \langle c \rangle) (\langle V \rangle^{(1)} - \langle V \rangle^{(0)})$ .  $x/M = 50.0$ .
- Fig. 12. Second order model predictions of transverse turbulent normal stresses, both conditioned and unconditioned.  $x/M = 50.0$ .

TABLE I

Standard Inlet Conditions:

$$\langle u \rangle = 7 \text{ m/s}$$

$$\dot{u}/\langle U \rangle = 0.07$$

$$\dot{u} = 49 \text{ cm/s}$$

$$l_r = 7.27 \text{ mm}^*$$

$$u_r = 1 \text{ cm/s (laminar flame speed)}^*$$

$$\nu = 1.85 \times 10^{-5} \text{ m}^2/\text{s}$$

$$R_l = 229$$

Model Constants:

$$C_R = 4.0$$

$$D = 2.4$$

$$A_t = 0.37 \text{ [1]}$$

$$C_d = 0.09 \text{ [7]}$$

For other constants see [4]

\* r denotes standard reference value.

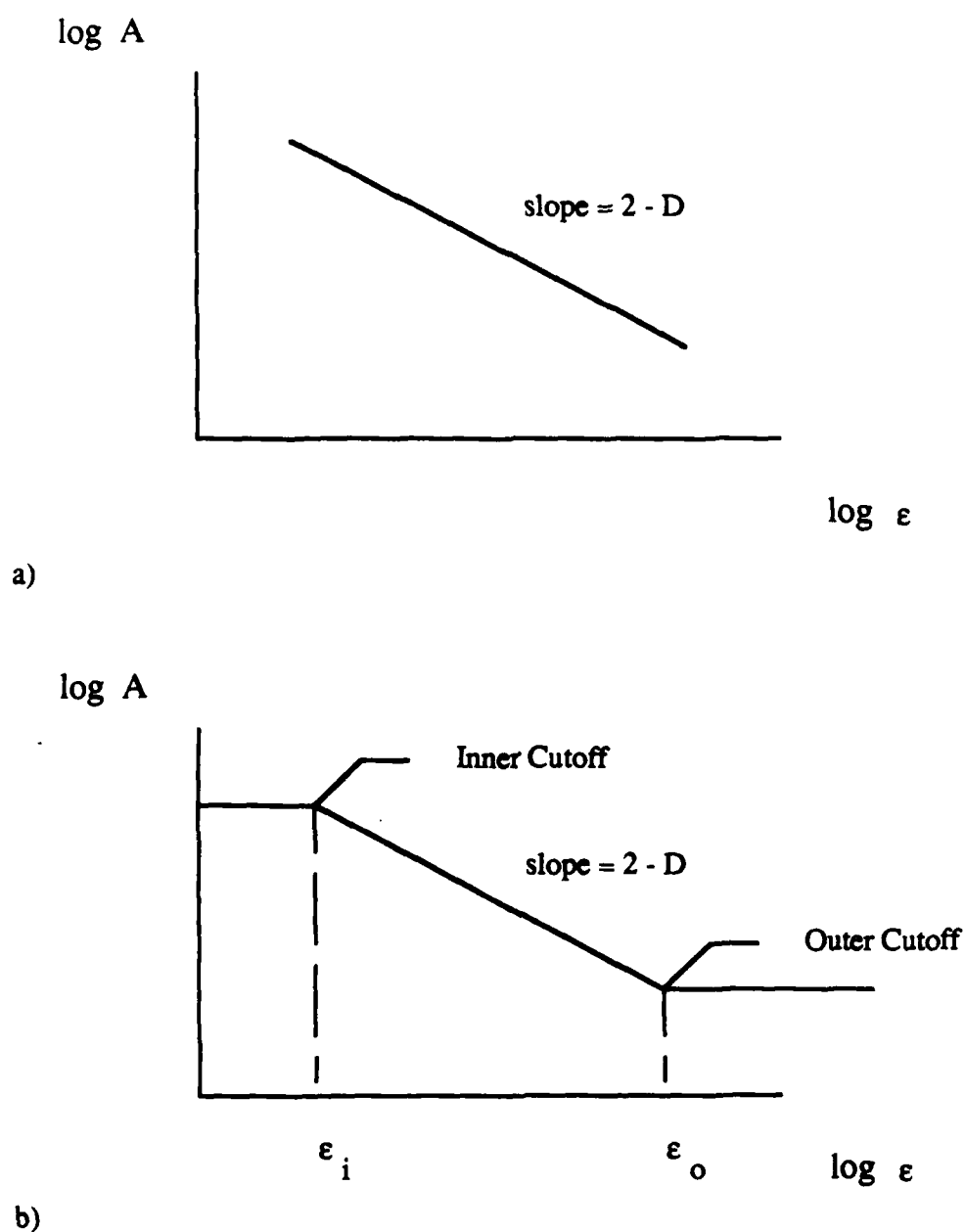


Fig. 1. Variation with measurement scale of measured area in a cubic volume of side  $L$  for a surface exhibiting fractal character. a) No inner or outer cutoff. b) Inner and outer cutoffs to fractal behavior.

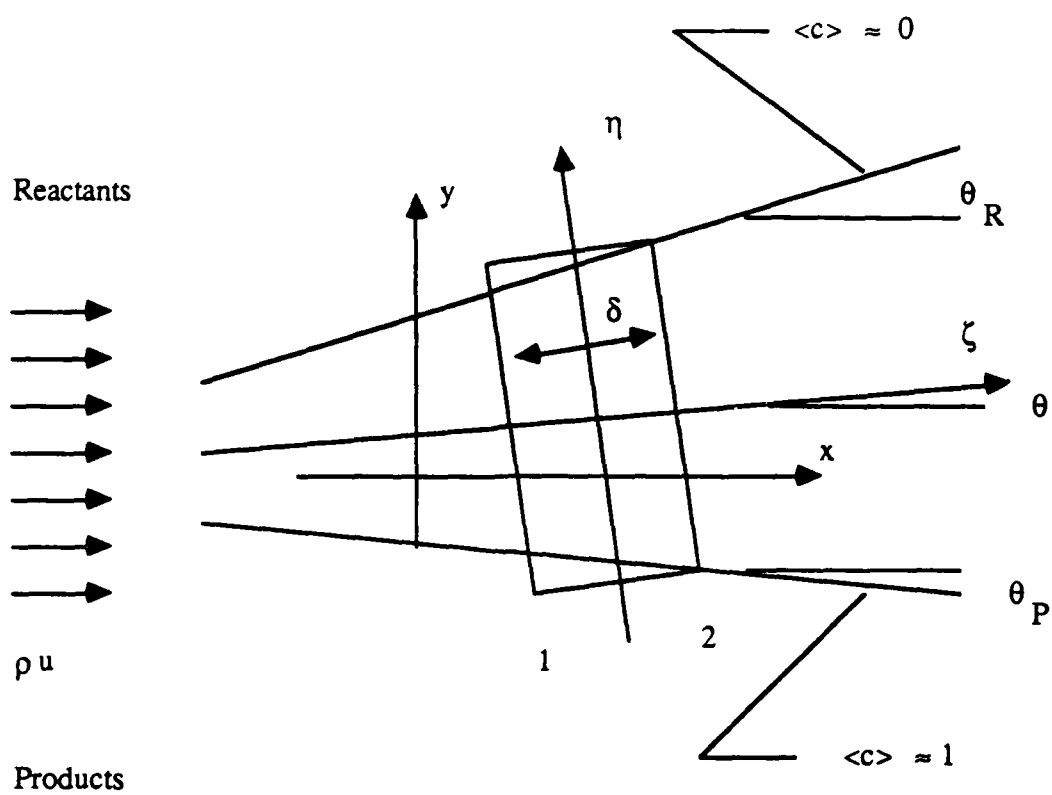


Fig. 2. Schematic diagram of flame brush showing coordinate systems.

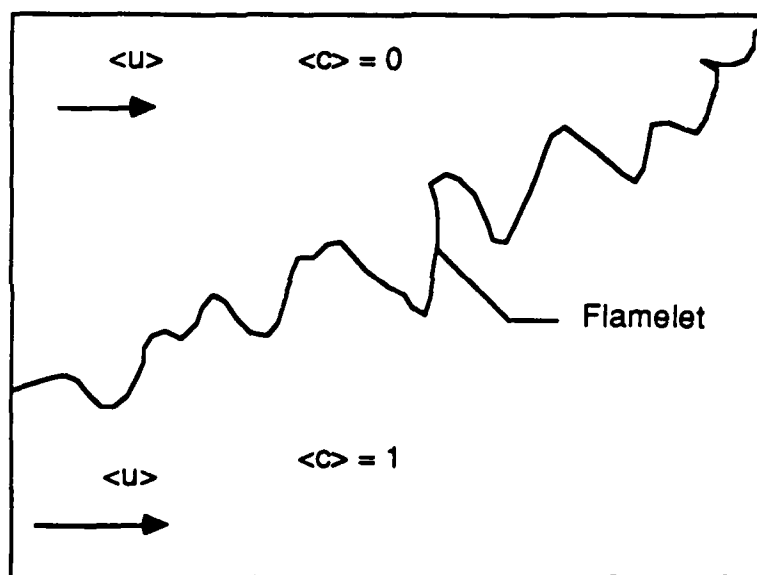


Fig. 3. Sketch of flow configuration for calculations.

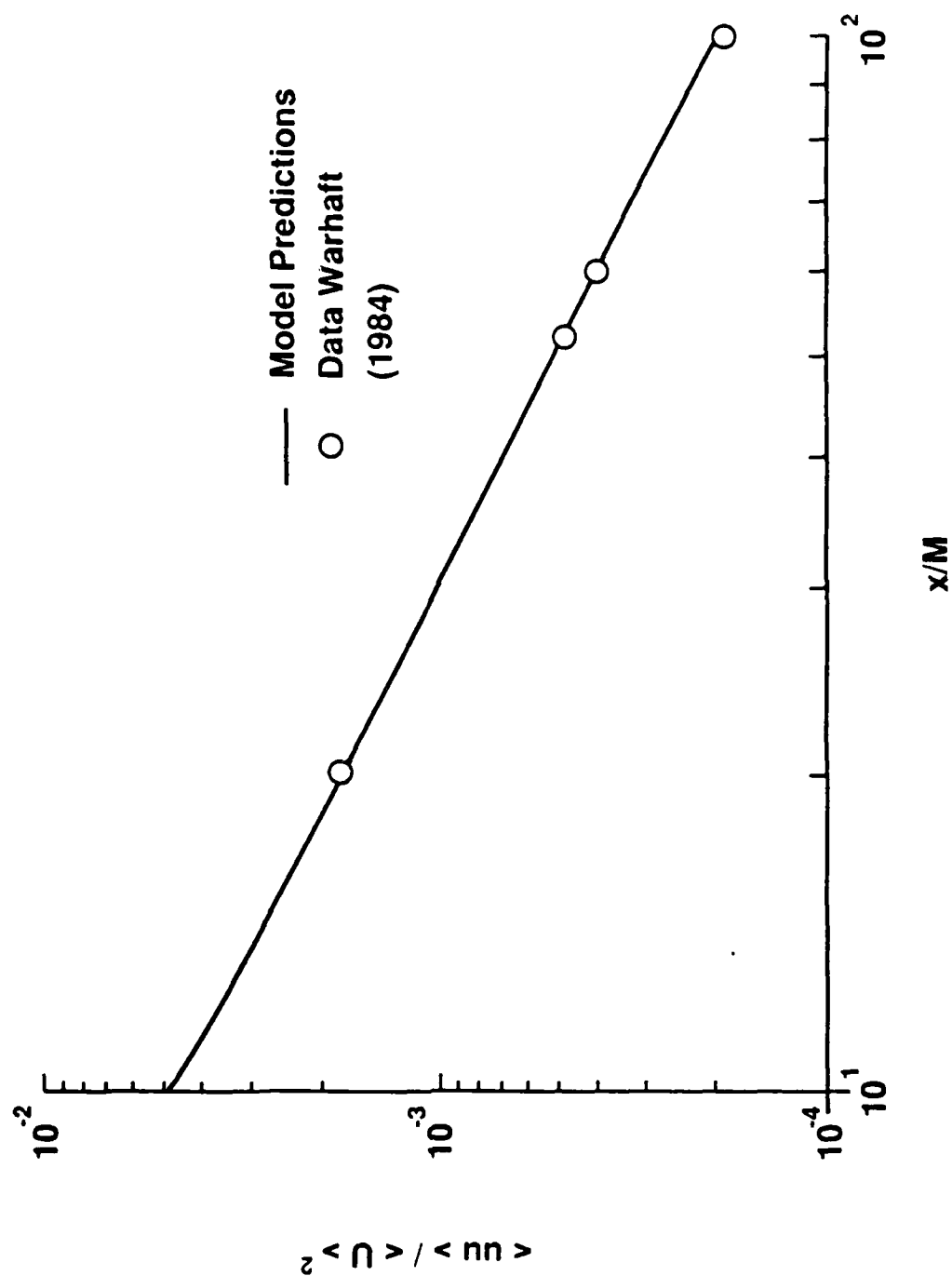


Fig 4a

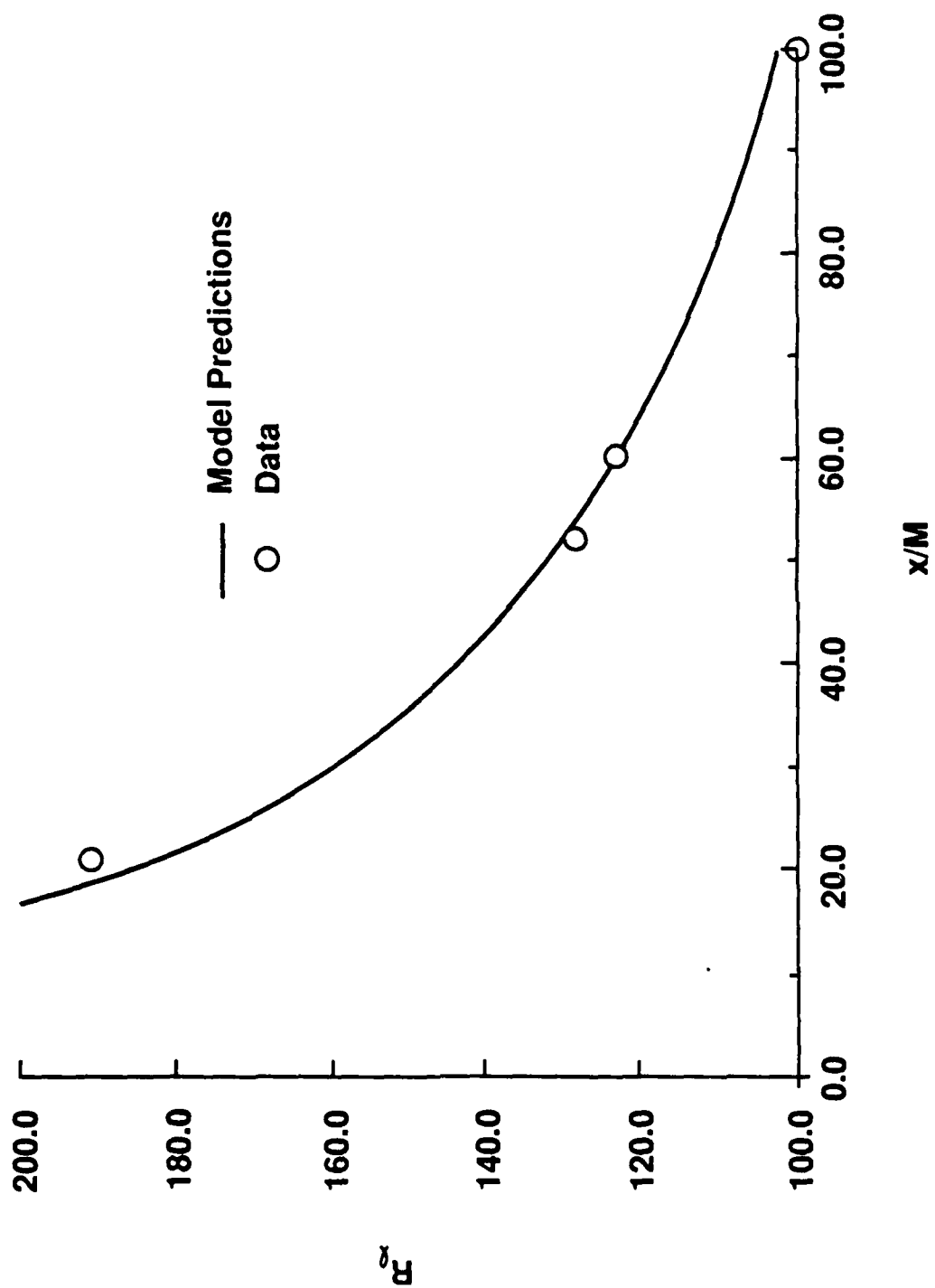


Fig 4b

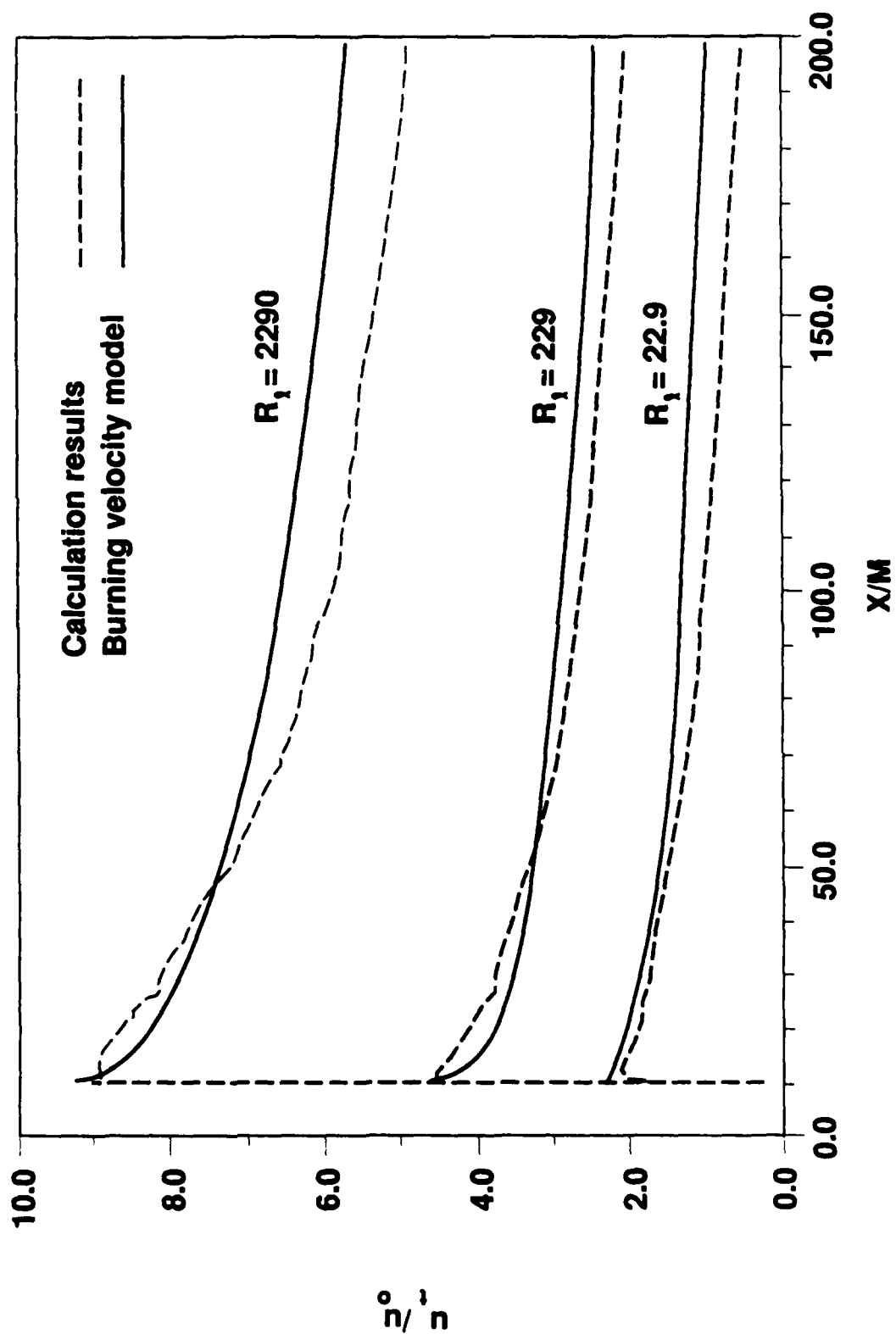


Fig 5a

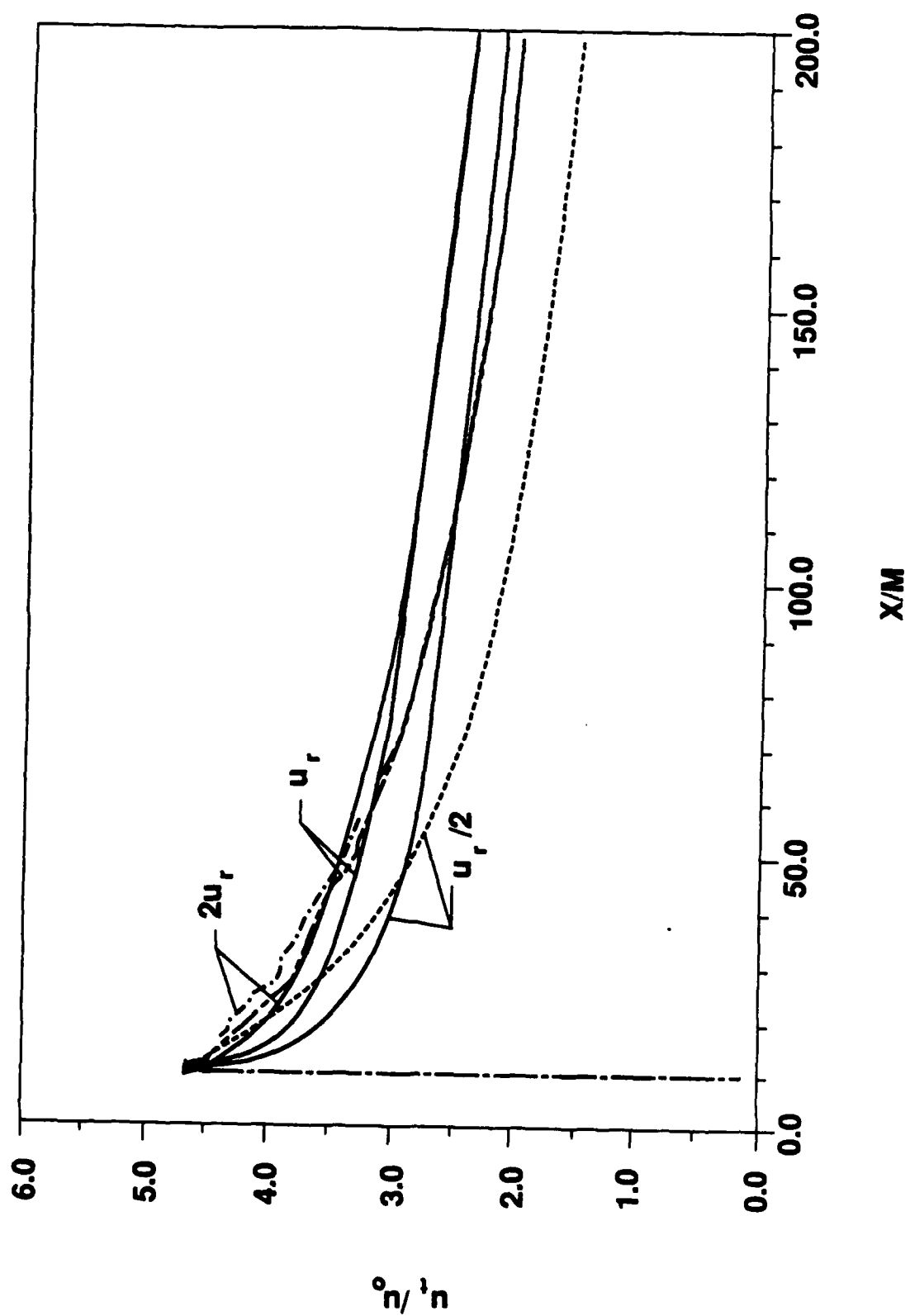


Fig 5b

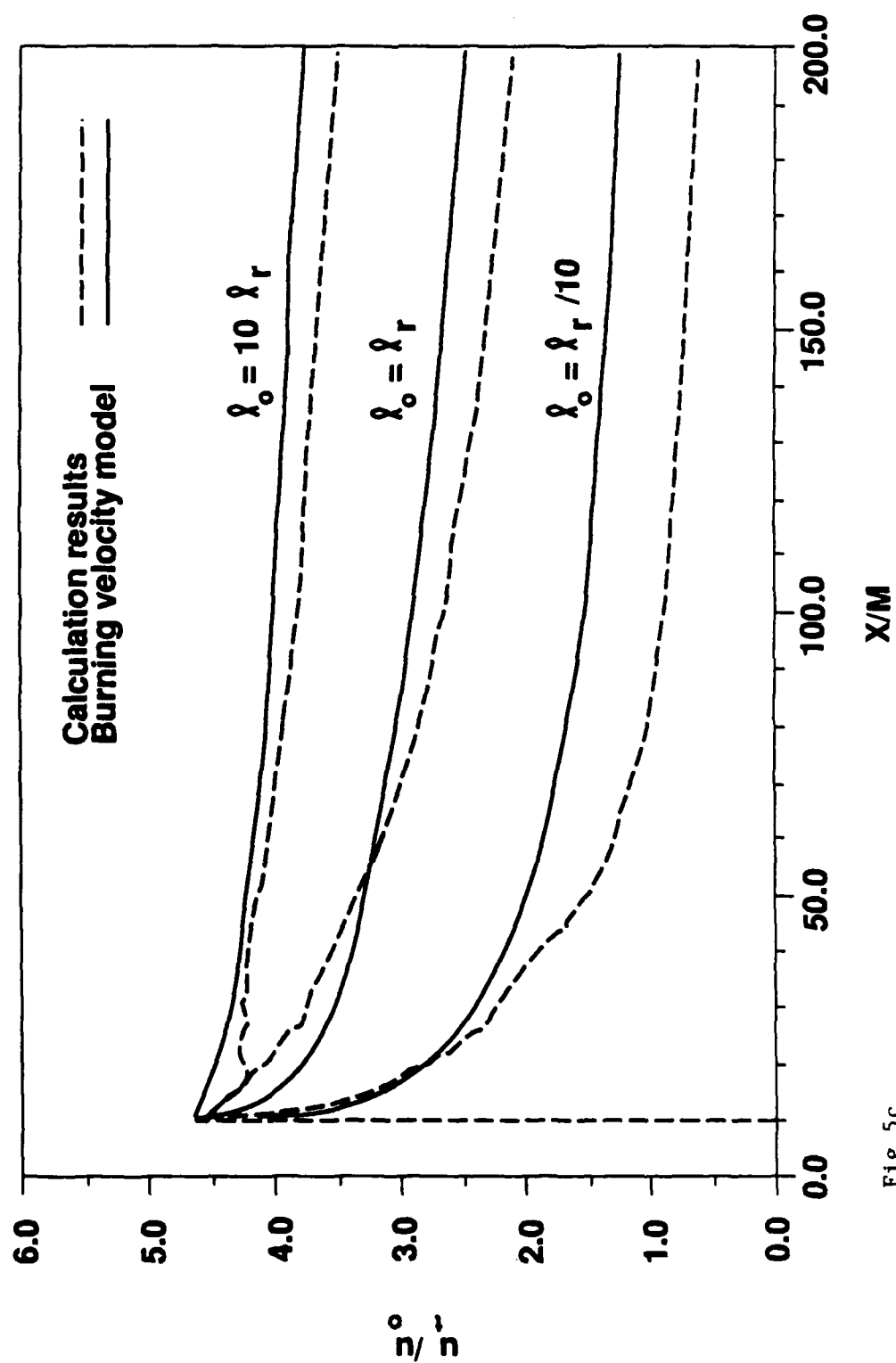


Fig 5c

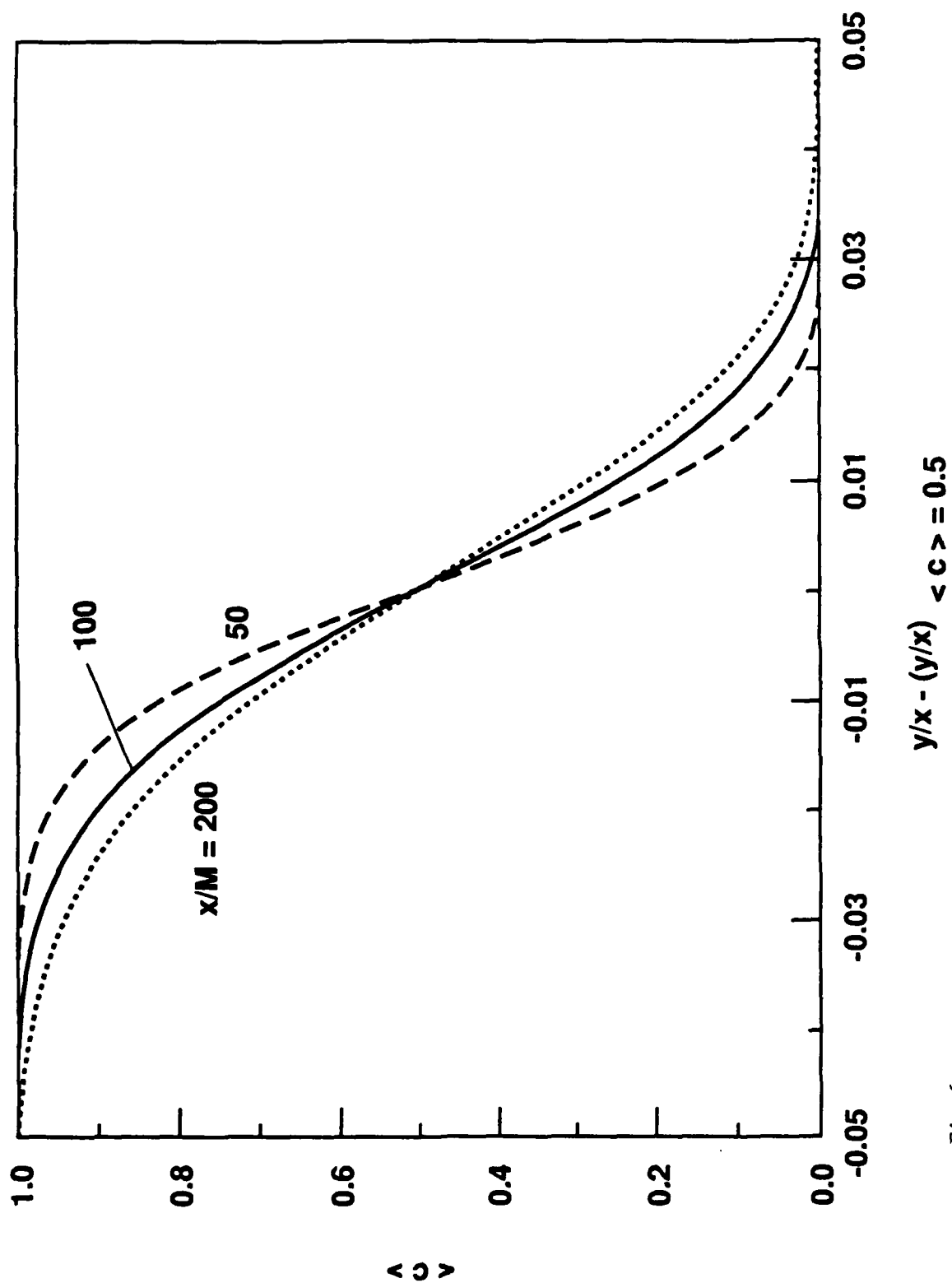


Fig 6

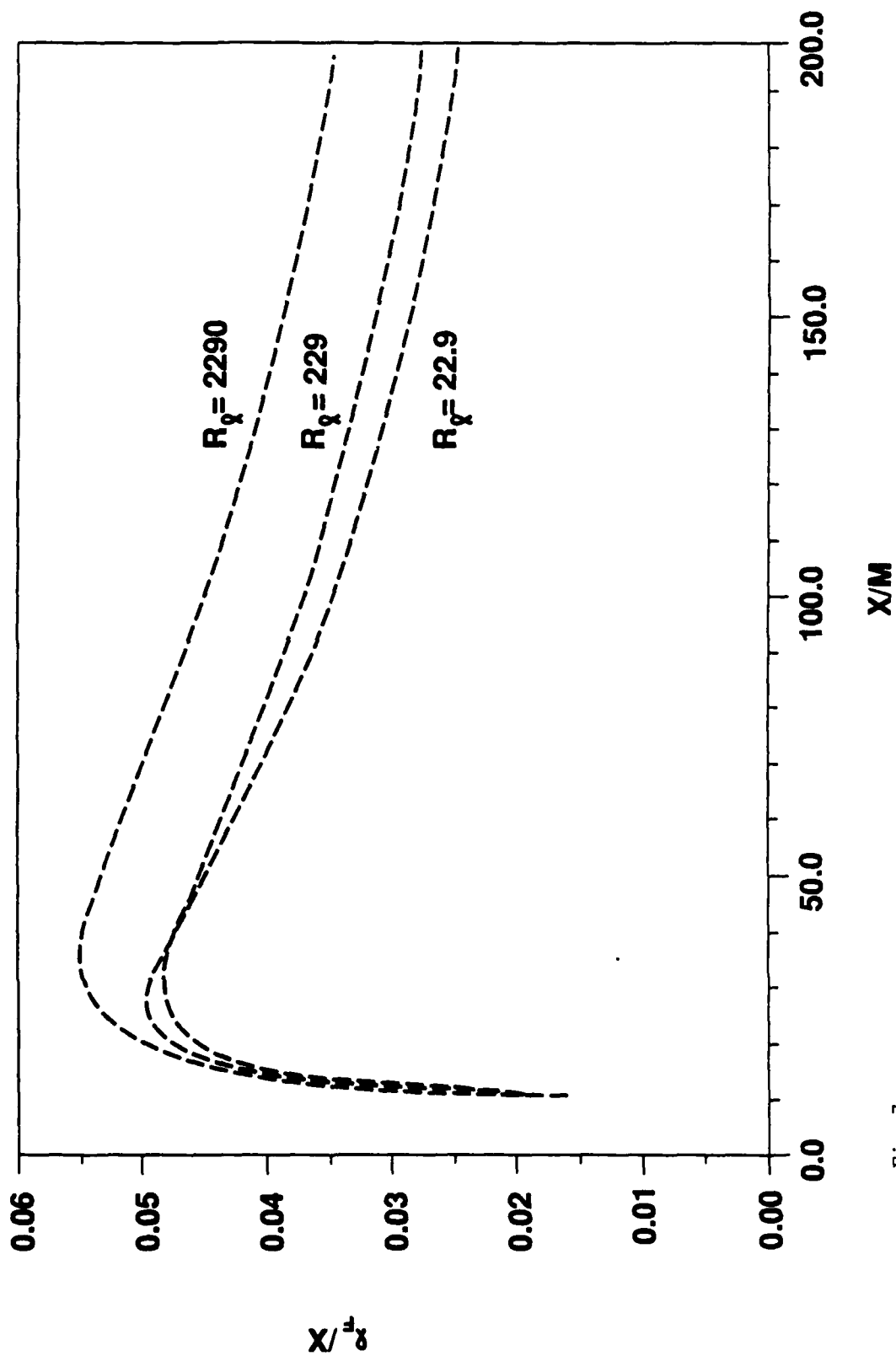


Fig 7

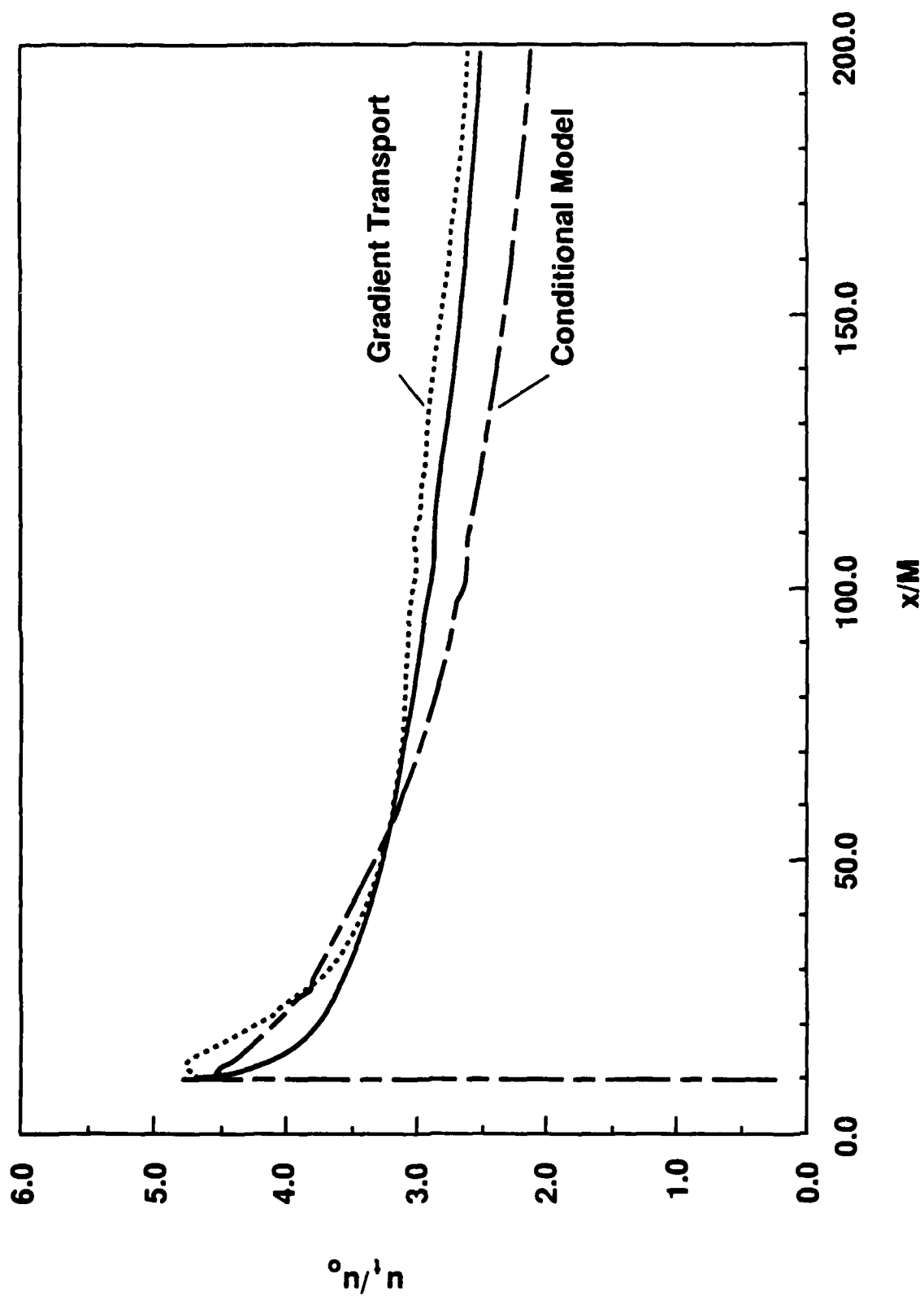


Fig 8

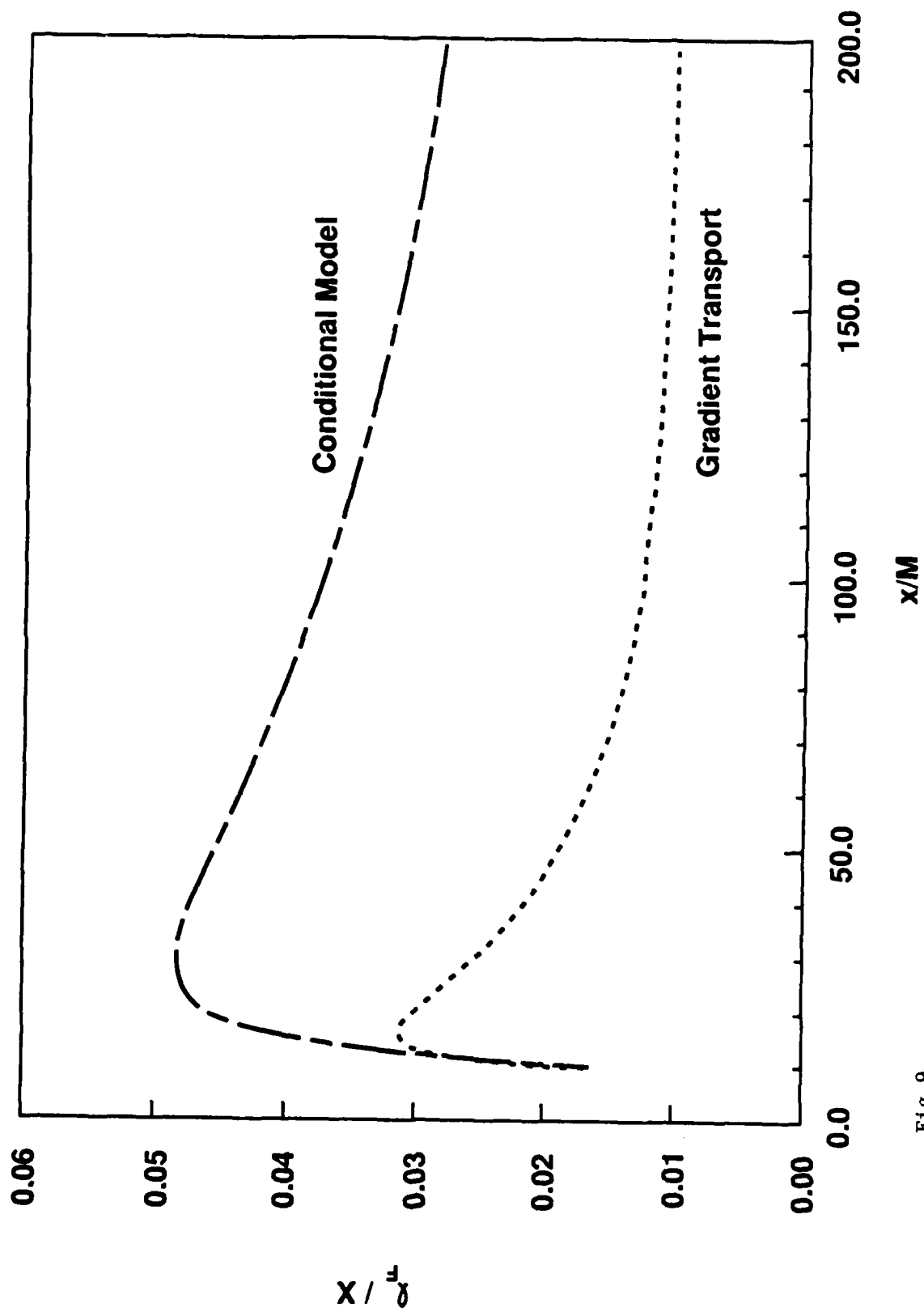


Fig 9

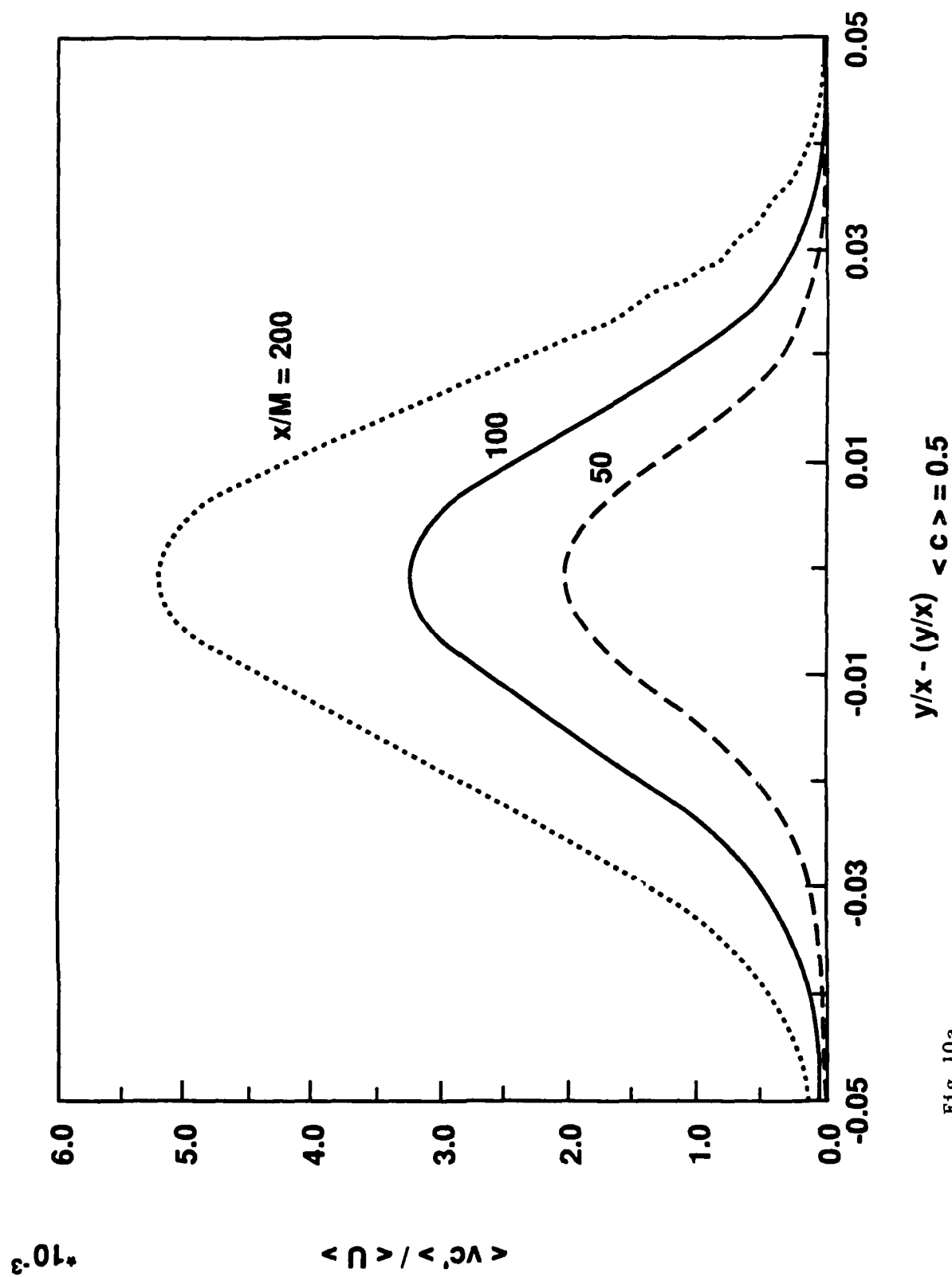


Fig 10a

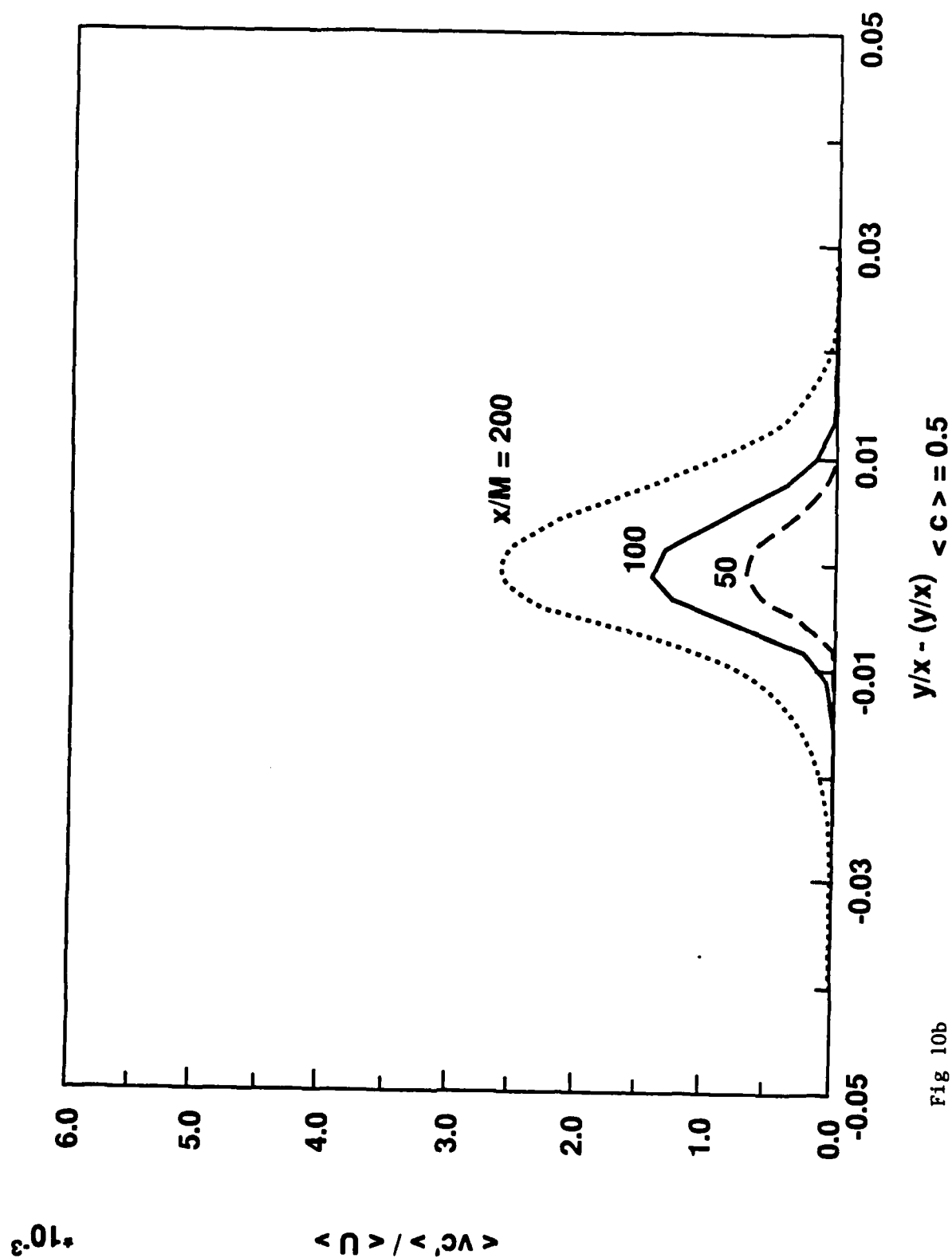


Fig 10b

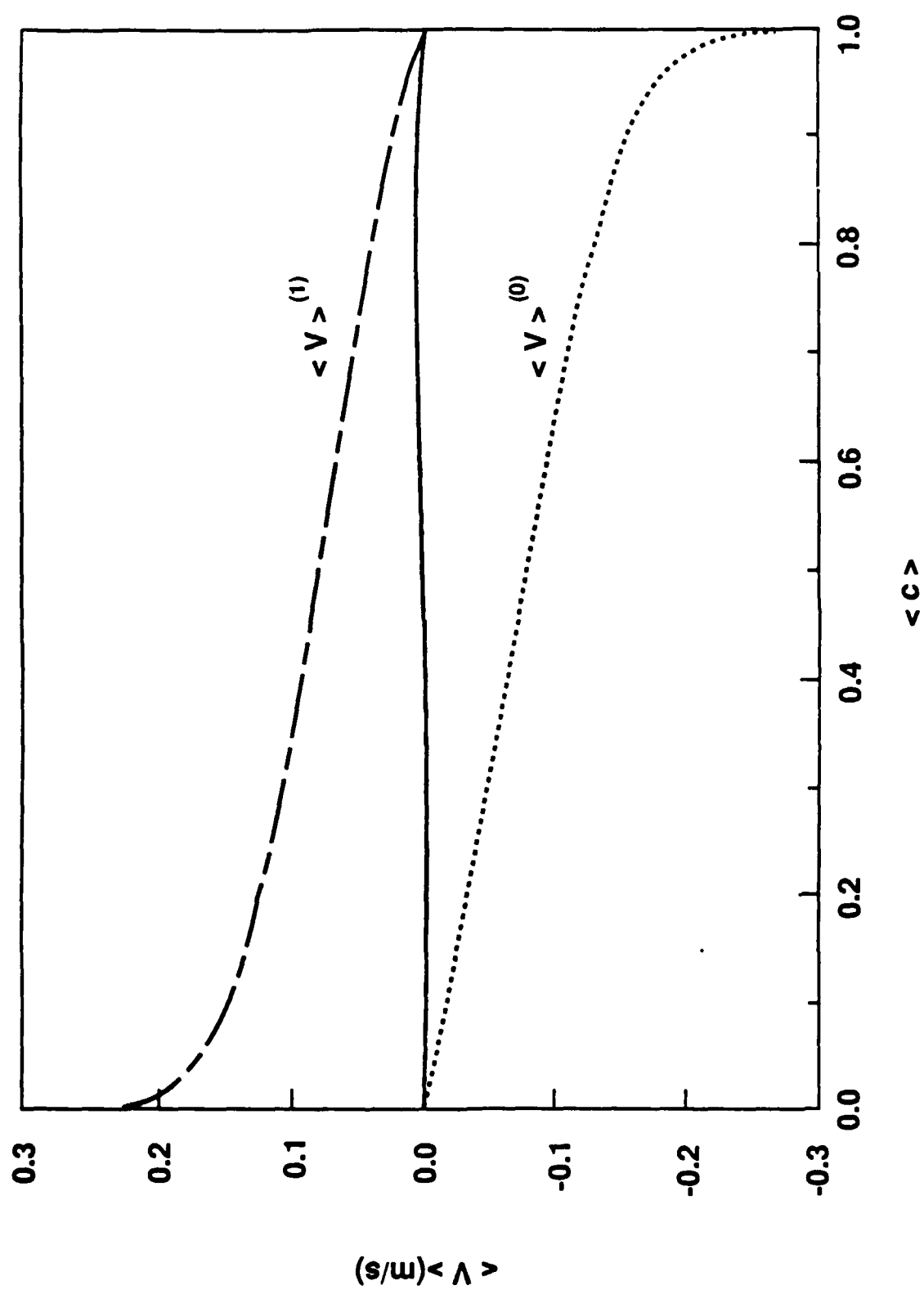


Fig 11

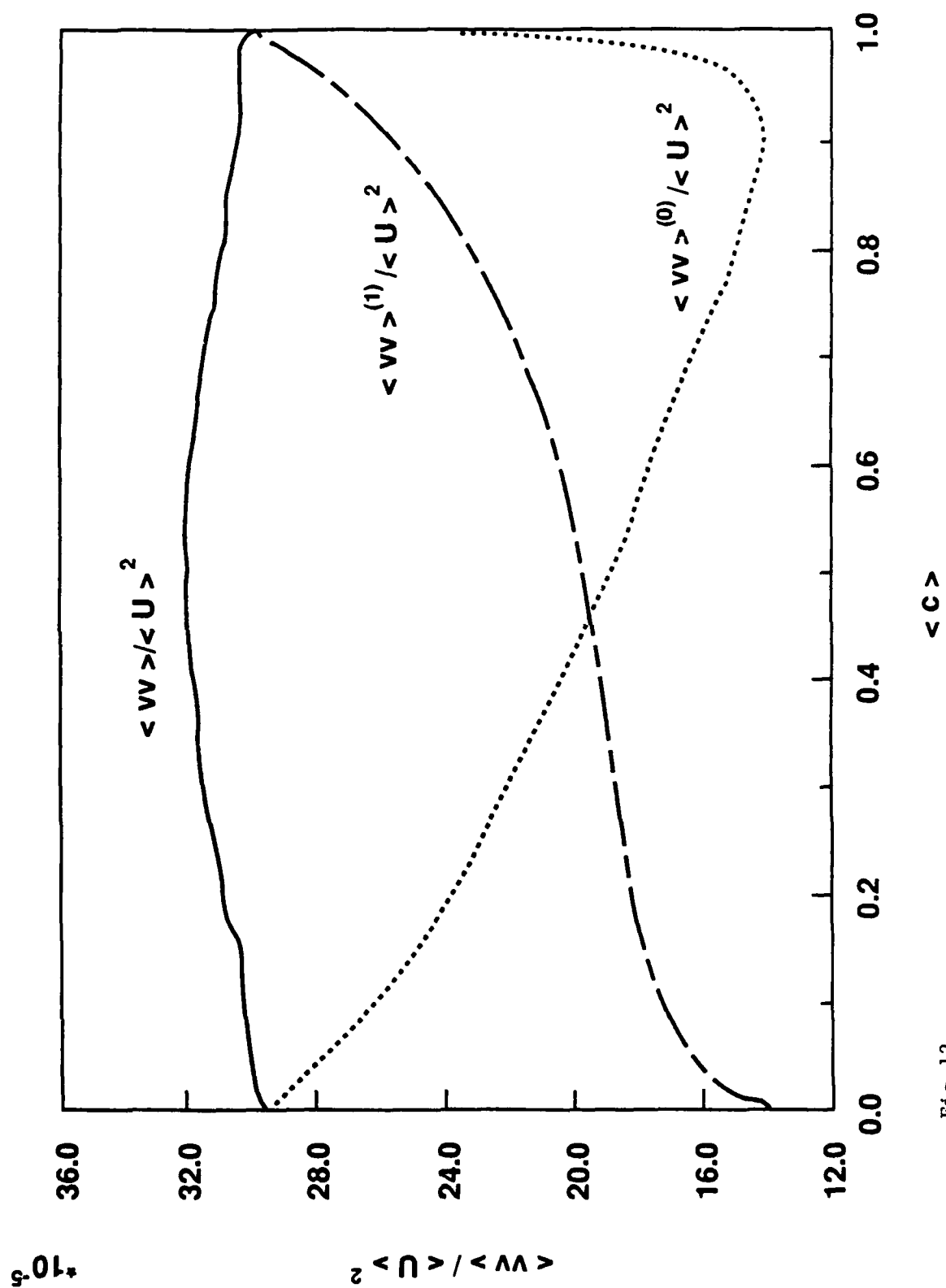


Fig 12

## APPENDIX B

## An Interpretation of Jet Mixing Using Fractals

F. C. Gouldin  
Mechanical and Aerospace Engineering  
Cornell University  
Ithaca, New York 14853

## ABSTRACT

An analysis of axisymmetric jet mixing is reported in which the jet structure is modeled as a set of constant concentration surfaces. Stationary turbulence is assumed, and a balance equation for the ensemble mean flux of jet fluid across constant jet fluid concentration surfaces is developed. Terms in the equation are modeled 1) by assuming that the geometry of constant concentration surfaces can be represented by fractal surfaces and 2) by estimating the mean jet fluid mass flux per unit area of a constant concentration surface as the Kolmogorov velocity. Flow similarity is assumed. It is found that for Reynolds number independence the fractal dimension is given by

$$D = 2 + \frac{\mu + 2}{6}.$$

In addition an expression for the centerline variation of mean jet fluid mass fraction is obtained; the expression is of similarity form as expected.

## Introduction

In [1] Mandelbrot proposes that constant scalar property surfaces in homogeneous, isotropic turbulence are fractal surfaces and suggests two values for the fractal dimension depending on the spatial variance of the scalar field.  $D = 2 \frac{1}{2}$  for Gauss-Burger turbulence and  $2 \frac{2}{3}$  for Gauss-Kolmogorov turbulence. Lovejoy for clouds [2] and Sreenivasan and Maneveau [3] for shear flows obtain data suggesting fractal dimensions between approximately 2.32 and 2.4 for constant property surfaces. These values are noticeably lower than the two suggested by Mandelbrot. Hentschel and Procaccia [4] and more recently Kingdon and Ball [5] present analyses of cloud dispersion in homogeneous, isotropic turbulence. In these analyses molecular transport is ignored, high turbulence Reynolds number is assumed and the dispersion of one species into another is modeled by considering the quantity  $Q(l, t | l', 0)$ , which is the probability that a pair of diffusing particles of fluid separated by  $l'$  at  $t = 0$  will be a vector distance  $l$  apart at  $t$ .  $Q$  in turn is related to the structure function  $S(l, t)$  at a point  $r$  for a scalar  $\theta$ :

$$S(l, t) = \frac{1}{V} \int dr \langle |\theta(r + l, t) - \theta(r, t)|^2 \rangle$$

For small  $|l| = l$ ,  $S(l, t)$  scales as a power of  $l$ , and the exponent gives the fractal dimension.

Both Hentschel and Procaccia and Kingdon and Ball develop models for  $Q$  and suggest a form for  $S(l, t)$  as  $l \rightarrow 0$ .

$$\lim_{l \rightarrow 0} S(l) \sim l^B$$

with  $B$  constant. Both arguments contain heuristic elements. There is a fundamental difference between the two sets of authors in their modeling of  $Q$  and in their expressions for  $\lim_{l \rightarrow 0} S(l)$ . Yet their final expressions for  $D$  are the same:

$$D = 2 + \frac{\mu + 2}{6}.$$

$\mu$  is the intermittency exponent.

In this paper a semi-empirical, physically oriented model of mixing in jet flows is developed which assumes the instantaneous jet structure can be represented by an ensemble of fractal, constant property surfaces. The model gives an expression for mean jet fluid concentration on the jet centerline which contains the jet Reynolds number raised to a power. For there to be no Reynolds number dependency as required for similarity, it is necessary for the exponent to equal zero. As a result, one finds  $D = 2 + ((2+\mu)/6)$  as obtained both by Hentschel and Procaccia and by Kingdon and Ball. This expression for  $D$  is the major finding to be reported. While it is identical to that of others it is obtained by very different reasoning and for a different flow, a free shear flow.

### Jet Mixing Model

For analysis the following major assumptions are made. The flow is an axisymmetric jet into a stagnant fluid with uniform and constant density. The turbulence is assumed to be stationary and jet Reynolds number is large such that the flow is Reynolds number independent. The distributions of mean composition and mean velocity follow similarity. It is further assumed that surfaces of constant jet fluid mass fraction may be represented by fractal surfaces for the purpose of estimating the ensemble mean area of such surfaces.

With similarity the mean jet structure is given by the following expressions [6].

$$\langle U \rangle = u_0 f(r/r_{1/2}). \quad (1)$$

$$U_j / u_0 = C_u x/d. \quad (2)$$

$$\langle Z \rangle = Z_0 g(r/r_{1/2}). \quad (3)$$

$$1/Z_0 = C_z x/d. \quad (4)$$

The quantities in the above equations are defined as follows:  $x$  is axial distance;  $r$  is radial distance.  $U$  is the axial velocity,  $U_j$  its momentum flux weighted average at the jet origin ( $x=0$ ), and  $u_0$  its mean value on the jet axis.  $Z$  is the jet fluid mass fraction and  $Z_0$  its mean value on the axis.  $d$  is the initial jet diameter, and  $r_{1/2}$  is the jet half radius.  $C_u$  and  $C_z$  are empirical constants. Finally  $\langle \rangle$  denotes ensemble mean. (4) gives the centerline decay of the mean jet fluid mass fraction. The modeling presented here will lead to an expression similar to (4) with a term  $R_l^{h(D)}$ , where  $R_l$  is a turbulence Reynolds number based on the integral scale,  $l$ , and the root mean square of velocity fluctuations. For similarity  $h(D) = 0$  and an expression for  $D$  is obtained.

From experiment it is found that  $f$  and  $g$  can be expressed to reasonable accuracy by

$$\exp(-(ar/r_{1/2})^2), \quad (5)$$

where  $a$  is an empirical constant.

The instantaneous jet structure can be viewed as a set of constant  $Z$  surfaces and it is hypothesized that these surfaces exhibit fractal character over a range of length scales associated with the scales of the turbulent velocity fluctuations, namely  $\eta$  ( the Kolmogorov scale ) to  $l$ . In this work a fractal description is assumed to obtain an expression for mean surface area. The success of the resultant model supports the fractal hypothesis and a certain expression for  $D$  but does not prove the fractal hypothesis.

For a surface,  $S$ , enclosing a volume,  $V$ , an integral equation for jet fluid conservation may be written as

$$\frac{d}{dt} \int_V \rho Z \, d\tau = \int_V \frac{\partial \rho Z}{\partial t} \, d\tau + \int_S \rho Z \, \mathbf{q}_b \cdot \mathbf{ds} = - \int_S [\rho Z (\mathbf{q} - \mathbf{q}_b) + \mathbf{j}_Z] \cdot \mathbf{ds}.$$

This is a general equation for a surface moving with an arbitrary local velocity,  $\mathbf{q}_b$ .  $\mathbf{q}$  is the fluid velocity, and  $\mathbf{j}_Z$  is the diffusive flux of jet fluid. Let the surface be defined by a constant value for  $Z$ , and take the ensemble average of this equation. For stationary turbulence the mean of the left hand side must be zero, and one obtains

$$\left\langle \int_S \rho Z (\mathbf{q} - \mathbf{q}_b) \cdot \mathbf{ds} \right\rangle + \left\langle \int_S \mathbf{j}_Z \cdot \mathbf{ds} \right\rangle = 0 \quad (6)$$

For jet flow the surface integrals may be written as the sum of two types of terms - a flux of fluid from the jet and a surface integral.

$$M_j = \pi(d/2)^2 \rho V_j = \left\langle \int_S [\rho Z (\mathbf{q} - \mathbf{q}_b) + \mathbf{j}_Z] \cdot \mathbf{ds} \right\rangle. \quad (7)$$

$V_j$  is the initial volume flux weighted average jet velocity. The areas  $S$  in (6) and (7) differ by the initial cross-sectional area of the jet. It is assumed that  $Z$  constant surfaces are attached to the lip of the jet and that these surfaces are simply connected. The first assumption is valid, and if the second assumption is relaxed it seems reasonable to argue that the average result, (7), is not affected. The right hand side of (7) is now evaluated approximately.

Consider the segment of  $Z$  constant surface between  $x$  and  $x+dx$ . We approximate the contribution from the surface in this region to the right hand side of (7) by a mean flux times a mean surface area. (7) is then estimated by integrating these contributions over  $x$ . The mean surface area is estimated with the help of the fractal hypothesis.

As noted above we assume fractal behavior of  $Z$  surfaces for a range of length scales between an inner cutoff ( $\epsilon_i$ ) and an outer cutoff ( $\epsilon_o$ ). Measurements of area at scales outside the range of fractal behavior are assumed to give one of two constant values corresponding to large or small measurement scale. In [7], it is argued that  $A_i$ , the area of a fractal surface measured at scales below the inner cutoff, is the actual ensemble mean surface area of a constant property surface, i.e.,  $A_Z = A_i$ . Also from [7] one may write for the ratio of the two surface areas measured beyond the cutoffs

$$A_i/A_o = (\epsilon_o/\epsilon_i)^{D-2} = (l/\eta)^{D-2}, \quad (8)$$

where  $l$  and  $\eta$  are used as the outer and inner cutoffs. The choice of  $\eta$  as the inner cutoff implies a unit Schmidt number. For homogeneous, isotopic turbulence  $l/\eta = A_t^{1/4} R_l^{3/4}$  [7] with  $A_t$  a constant, and substitution gives

$$A_i/A_o = (A_t^{1/4} R_l^{3/4})^{D-2}. \quad (9)$$

$A_o$  is the surface area measured for  $\epsilon > l$ . By assumption  $A_o$  for a  $Z$  surface is equated to the area of the  $\langle Z \rangle$  constant surface for which  $\langle Z \rangle$  equals  $Z$ . Sketches of the intersections of a  $\langle Z \rangle$  constant surface and of realizations of a  $Z$  constant surface with a plane containing the jet axis are depicted in Fig. 1. Note in Fig. 1,  $L$  is defined as the axial

location where the  $\langle Z \rangle$  constant surface crosses the  $x$  axis. Eq. 9 is now applied to obtain an expression for  $dA_Z$ , the mean  $Z$  surface area between  $x$  and  $x+dx$ .

The area of the  $\langle Z \rangle$  surface in the region  $x$  to  $x+dx$  is

$$dA_{\langle Z \rangle} = 2\pi r_{\langle Z \rangle} dx,$$

and therefore if  $dA_Z / dA_{\langle Z \rangle} = A_i / A_0$ , one obtains

$$dA_Z = 2\pi r_{\langle Z \rangle} (A_i^{1/4} R_l^{3/4})^{D-2} dx \quad (10)$$

as the ensemble average of the  $Z$  surface area in the region  $x, x + dx$ .  $r_{\langle Z \rangle}$  is the radial location of the  $\langle Z \rangle$  surface at  $x$ .

The arguments leading through (8) to (10) may be made graphically. For a surface exhibiting fractal behavior between length scales  $\epsilon_i$  to  $\epsilon_0$ , the measured surface area is assumed to vary with measurement scale as shown in Fig. 2. Fractal behavior is given by the power law dependency of  $A$  upon  $\epsilon$ . For  $\epsilon \rightarrow 0$ ,  $A$  must approach a constant value, the true value, if the surface has a minimum scale of wrinkling as assumed. For a  $Z$  surface molecular diffusion is expected to limit the minimum scale of wrinkling. This limiting behavior at small  $\epsilon$ , is represented by the horizontal line in Fig. 2 at  $A = A_i$ . We define  $\epsilon_i$  by  $A_i/L^3 \sim (\epsilon_i/L)^{2-D}/L$  and assume on physical grounds that  $\epsilon_i = \eta$ . (N.B.: since the ratio  $A_i/A_0$  is required, the constant of proportionality is unimportant in this application.)

The behavior of  $A$  versus  $\epsilon$  depicted in Fig. 2 for large  $\epsilon$  implies that the surface appears smooth and planar at large length scale. The area of this planar surface is  $A_0$ , and the outer cutoff is defined by  $A_0/L^3 \sim (\epsilon_0/L)^{2-D}/L$ . We assume that  $\epsilon_0 = l$ . For this planar assumption to be valid it is expected that  $\epsilon_0$  must be much less than the radius of curvature of the  $\langle Z \rangle$  surface. This limiting behavior for large  $\epsilon$  is reasonable for shear flows but may not be reasonable for homogeneous, isotopic turbulence.

Physically it is expected that the  $Z$  surface will spend most of its time in the vicinity of the  $\langle Z \rangle$  surface. Hence  $A_0$  is identified with the latter surface.

Finally, it is assumed that (10) refers to the average surface area between  $x$  and  $x+dx$ . The actual surface area should vary from realization to realization, and the surface for each such realization is expected to exhibit fractal character. Thus the identification of (10) with mean values is nontrivial and open to question. A similar assumption is made in [7] with success. A fuller justification of the assumption is left to future work.

The flux of jet fluid across a  $Z$  surface is the result of convection ( $q - q_b$ ) and diffusion ( $j_z$ ). To estimate the mean of these two fluxes we write  $u_d = D/\eta_d$ , where  $\eta_d$  is an effective length scale defined by the above expression, and the total mean mass flux across the surface per unit area is  $\rho Z u_d$ . (N.B.:  $D$  here is the diffusion coefficient. There should be no confusion with the fractal dimension since the latter appears as an exponent.) Gibson [8] has considered the motion of a constant property surface in turbulent flow. From his analysis

$$(q - q_b) = -D(\nabla^2 Z / |\nabla Z|)(\nabla Z / |\nabla Z|)$$

in the present context, while the diffusive flux is given by

$$j_z = -\rho Z D \nabla \ln Z,$$

for Fick's law diffusion. Thus the appropriate length scale for  $u_d$  is related to

$$\langle |(\nabla^2 Z / |\nabla Z|)(\nabla Z / |\nabla Z|) + \nabla \ln Z| \rangle^{-1}.$$

One expects intuitively that the largest contributions to  $\eta_d$  come from regions in the flow where  $Z$  is varying rapidly with distance and hence both  $\nabla^2 Z$  and  $\nabla \ln Z$  are large.

These regions contain the smallest turbulent eddies and thus an appropriate estimate for  $\eta_d$  would seem to be a quantity proportional to  $\eta$  for a unit Schmidt number.

Assuming unit Schmidt number, we replace  $D$  by  $\nu$  and estimate  $\eta_d$  by  $(1/C_d)\eta$ , which gives  $u_d = C_d \nu$ , where  $\nu$  is the Kolmogorov velocity scale and  $C_d$  is a model constant. Furthermore, for homogeneous, isotropic turbulence  $\nu = A_t^{1/4} R_t^{-1/4} u'$ . We will use this expression for  $\nu$  arguing that since the  $Z$  surface is embedded in turbulent fluid and thus  $u'$  is conditioned on being in turbulent fluid the use of an expression for homogeneous, isotropic turbulence is reasonable. Further we assume that  $u'$  can be expressed in terms of  $u_0$ ;  $u' = (u'/u_0)u_0$  with  $u'/u_0$  being constant over the jet. Conditioned velocity measurements in jets show that  $u'/u_0$ , while not constant in a jet, does not vary greatly, and thus the above assumption is reasonable as a first approximation. An expression for  $u_d$  can now be written.

$$u_d = C_d A_t^{1/4} R_t^{-1/4} (u'/u_0) u_0. \quad (11)$$

According to the Gibson expression,  $q - q_b$  is undefined or infinite at critical points, i.e., at points where  $\nabla Z = 0$ . On physical grounds one expects  $q - q_b$  at critical points to be infinite and to be large in the region of a critical point. Thus it seems reasonable to argue that surfaces will move away or through and then away from critical points very rapidly. Hence the contributions of such points to  $\langle q - q_b \rangle$  are expected to be negligible. Alternatively, one can argue that the ensemble average of the integral of  $(q - q_b) \cdot ds$  over the area of a constant property surface must be finite even if  $q - q_b$  at singular points is not. Then  $\langle q - q_b \rangle$  is defined by the ratio of the ensemble average integral and the ensemble average area. The second agreement, which complements the first, is based on the physically reasonable assumption that the average convective flux of fluid across a constant property surface is finite.

By combining (10) and (11), and integrating along the x-axis one obtains an expression for  $M_j$ .

$$M_j = \rho Z \int_0^L C_d A_t^{1/4} R_l^{-1/4} (u'/u_0) u_0 2\pi r_{<Z>} (A_t^{1/4} R_l^{3/4})^{D-2} dx. \quad (12)$$

To proceed further, relationships for  $r_{<Z>}$  and  $u_0$  as functions of  $x$  are required. These functions depend on the spreading rate of the jet, and the basis for a theoretical development to obtain them is not contained in the fractal picture being explored. As an alternative to such a development empirical expressions based on similarity are used for the needed relationships. Having taken such a step one cannot claim that the resulting expression for centerline concentration is a predictive one. The exercise does, however, allow one to determine whether or not the fractal picture as developed gives results consistent with experiment, thereby providing a test of the applicability of fractal concepts to jet mixing. In addition, a value for  $D$  is obtained.

From similarity and experiment  $r_{1/2}/d = (1/2)L_z x/d$  with  $L_z$  a constant [6]. With this expression and (3) and (5) one can write for  $r_{<Z>}$ :

$$r_{<Z>} = (d/2) L_z a^{-1} \sqrt{\ln(L/x)} x/d, \quad (13)$$

where use has been made of the fact that  $Z_0$  falls to  $<Z>$  at  $x = L$ . (2), (12) and (13) can be combined to give

$$V_j = (L_z/C_d a) C_d A_t^{(D-1)/4} R_l^{(3/4(D-2) - 1/4)} (u'/u_0) U_j \cdot Z(L/d) \int_0^1 \sqrt{\ln(1/\xi)} d\xi, \quad (14)$$

where  $\xi = x/L$ . To obtain (14) use has been made of the fact that  $R_l$ , by similarity, is independent of  $x$ . The integral in (14) is  $(\pi/2)^{1/2}$ .

$U_j$  and  $V_j$  are momentum and volume average velocities and their ratio will vary with initial condition; let  $V_j/U_j = b$ .  $L$  is the axial distance at which the mean jet fluid mass fraction on the centerline equals  $Z$ . Therefore (14) and (4) are identical provided

$$h(D) = (3/4(D-2) - 1/4) = 0$$

and

$$(\pi/2)^{1/2} (L_z/C_u ab) C_d A_t^{(D-1)/4} (u'/u_0) = C_z.$$

The second condition is reasonable. (N.B.:  $C_z$  varies with initial conditions as does  $b$  [6].) Substitution with reasonable values [6, 9] into the above gives  $C_d \approx 0.38$ . The first condition is an equation for  $D$ .

The analysis to this point has not considered the intermittency of viscous dissipation. The effect of this intermittency is to alter the scaling of  $u_d$  and of  $\eta/l$ . Adjustments in the analysis are straight forward. With intermittency the dissipative length scale  $l_d$  replaces  $\eta$  as the inner cutoff and from Frisch, et al. [10]  $l_d \sim l R_l^{3/(4-\mu)}$ . (N.B.: Frisch, et al. introduce their own fractal dimension,  $D_\epsilon$ , such that  $D_\epsilon = 3 - \mu$ . Here the more common  $\mu$  is used in part to avoid confusion with  $D$  which is related to but not equal to  $D_\epsilon$ .)  $u_d$  is scaled as  $E_d^{1/2}$  where  $E_d$  is "the kinetic energy per unit mass on scales"  $\sim l_d$  [10]. Again from [10] it can be shown that this scaling gives  $u_d = u' R_l^{1/2 - 3/(4-\mu)}$ . Thus with intermittency the Reynolds dependency in (14) becomes

$$R_l^{[3/(4-\mu)](D-2)} R_l^{1/2 - 3/(4-\mu)},$$

and for Reynolds number independence

$$D = 2 + (\mu + 2)/6. \quad (15)$$

This result is identical to that obtained by Hentschel and Procaccia [4] and by Kingdon and Ball [5]. Our result for  $\mu = 0$  is not equivalent to Mandelbrot's result ( $D = 2 + 2/3$ ) for Kolmogorov turbulence [1] even though in both cases the variance scales as separation distance to the  $2/3$  power. In his development, Mandelbrot assumes a Gaussian random field; no such assumption is made in the present development. It is noted again that the approach taken by Hentschel and Procaccia and by Kingdon and Ball is quite different than the present one. It is especially noteworthy that the present analysis is for a free shear flow rather than homogeneous, isotopic turbulence.

## Conclusions

A fractal picture of constant property surfaces in round jets is used with similarity arguments and empirical data to obtain an expression for the decay of mean jet fluid mixture fraction along the centerline of the jet which is of appropriate form and numerically correct if a reasonable value for  $C_d$ , the only new empirical constant in the modeling, is chosen. The result provides support for the hypothesis that constant property surfaces in free shear flows are fractal surfaces.

For Reynolds number independence, the  $R_l$  term occurring in the surface area expression must cancel the  $R_l$  term appearing in the expression for  $u_d$  which requires that  $D = 2 + (\mu + 2)/6$ . This expression for  $D$  is equivalent to that obtained in [4] and [5]. The observed range of values for  $\mu$  is  $0.25 \leq \mu \leq 0.5$  [4]. The corresponding range for  $D$  is  $2.33 < D < 2.42$ , a result which compares favorably with the recent experiments of Sreenivasan and Meneveau [3] for free shear flows and with the results of Lovejoy [2] for clouds.

The fractal assumption has been used to obtain an expression for mean surface area - (10). To obtain (10) it was necessary to identify an outer cutoff area and to assume this area is equal to the  $\langle Z \rangle$  surface area. A well defined outer cutoff area is reasonable for surfaces which fill a volume that is relatively narrow in one direction as is the case for shear flows but is most likely not the case in general. The assumption relating the outer cutoff area to the  $\langle Z \rangle$  surface is justified a posteriori by the success of the modeling.

Our equation for  $D$  can be obtained without identifying an expression for the outer cutoff area. (15) is contingent on several steps: 1) expressing  $dA_Z$  in terms of  $A_i/A_0$ , 2) equating  $A_i/A_0$  to  $(\epsilon_i/\epsilon_0)^{2-D}$  and then to  $R_i^{[3/(4-\mu)](D-2)}$ , 3) scaling  $u_d$  by  $u'R_i^{1/2-3/(4-\mu)}$  with  $u'$  scaled by  $U_j d/x$ , and 4) requiring Reynolds number independence. 1) and 2) form the essential features of the fractal hypothesis, while 4) is supported by extensive experiment. Of the four steps 3) is perhaps the most questionable. As discussed above convective fluxes are infinite at critical points. However we do not believe these points cause problems in defining average fluxes. As an alternate to the Kolmogorov scale one could choose the Taylor microscale to represent  $\eta_d$ . An analysis similar to the present one - without correction for intermittency -- which uses this scale gives  $D = 2\frac{2}{3}$ . This result is consistent with Mandelbrot's for Gauss-Kolmogorov turbulence [1] but is inconsistent with experiment and other analyses.

For a range of conditions, chemical reaction in turbulent jet diffusion flames occurs in thin sheets referred to as flamelets [11]. These sheets are associated with constant mixture fraction surfaces, i.e., the stoichiometric mixture fraction surface, and it is felt that fractal based estimates of surface area will be very useful in modeling reacting jets. Preliminary work in this direction is under way [12].

It is emphasized that the fractal picture assumed in this paper is open to experimental verification, e.g., [3]. Laser tomography and other two-dimensional imaging and visualization techniques allow one to study the fractal character of curves formed by the

intersection of constant property surfaces and planes of illumination. From these studies the fractal character of the surfaces themselves can be inferred.

### **Acknowledgements**

This work was initiated while the author was a Science and Engineering Research Council Visiting Fellow at the University Engineering Department, Cambridge, England. Support from the SERC and from the US Army Research Office (Contract number DAAG29-82-K 0187) is acknowledged. Many helpful discussions with Professor K. N. C. Bray the author's host while in Cambridge and with Professor S. B. Pope of Cornell University are gratefully acknowledged.

## References

1. Mandelbrot, B. B.: **J. Fluid Mech.** 72, 401-416, 1975.
2. Lovejoy, S.: **Science** 216, 185, 1982.
3. Sreenivasan, K. R. and Meneveau, C: **J. Fluid Mech.** 173, 356-386, 1986.
4. Hentschel, H G E and Procaccia, I: **Physical Review A - General Physics** 29, 1461-1470, 1984.
5. Kingdon, R D and Ball, R C: The fractal dimension of clouds, Physics Department, University of Cambridge, submitted to **J. Phys. A**.
6. Gouldin, F. C., Schefer, R. W., Johnston, S. C., and Kollman, W.: **Prog. Energy and Combust. Sci.** 12, 257-303, 1986.
7. Gouldin, F. C.: An application of fractals to modeling premixed turbulent flames, **Comb Flame** in press.
8. Gibson, C.H.: **Phys. Fluids** 11, 2305-2315, 1968.
9. Pitts, W. M. and Kasawagi, T.: **J. Fluid Mech.** 141, 391-429, 1984.
10. Frisch, U, Sulem, P-L, and Nelkin, M.: **J. Fluid Mech.** 87, 719 - 736, 1978.
11. Williams, F. A.: **Combustion Theory**, 2nd ed., Benjamin/Cummings, Menlo Park, 1985, p. 408.
12. Gouldin, F.C.: "An interpretation of jet mixing and jet flame length data using fractals", College of Engineering Energy Report E-86-02, Cornell University, Ithaca NY, 1986.

### Figure Captions

1. Sketch depicting the intersection of  $\langle Z \rangle$  and  $Z$  constant surfaces with a plane containing the jet axis. The curves need not be continuous. The curves associated with  $Z$  surfaces should have  $D$  values one less than the corresponding surface.
2. Variation with measurement scale of measured area in a cubic volume of side  $L$  for a surface exhibiting fractal behavior: a) no inner or outer cutoff. b) inner and outer cutoffs to fractal behavior. From Mandelbrot's line of argument [1] for measurement scales in the fractal range,  $A/L^3 \sim (\epsilon/L)^{-D} \epsilon^2/L^3$  [7].

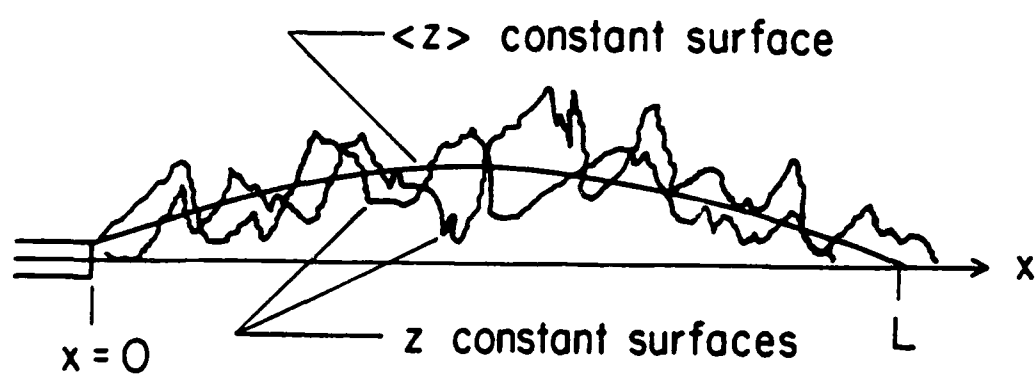


Fig 1

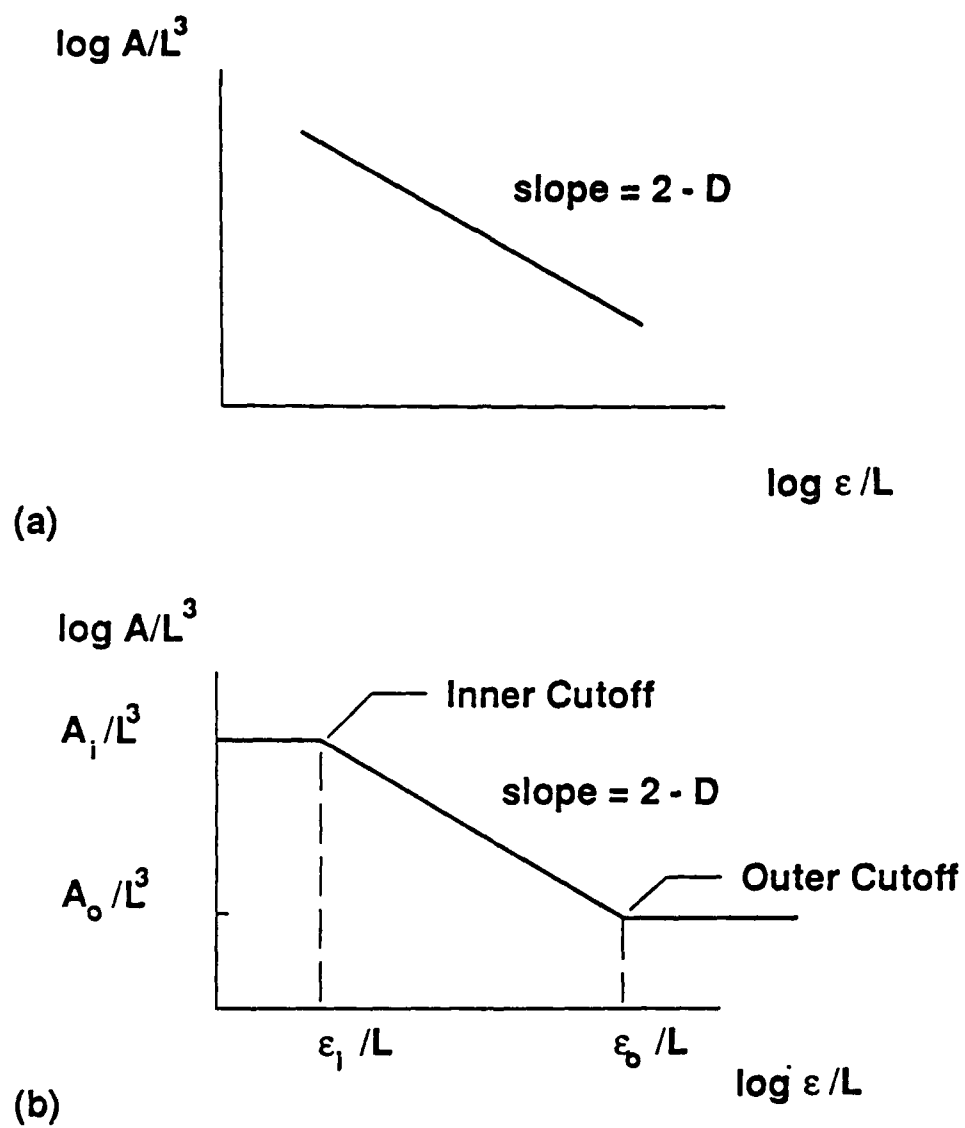


Fig 2

# SIMULTANEOUS MEASUREMENTS OF FLAMELET POSITION AND GAS VELOCITY IN PREMIXED TURBULENT FLAMES

P. Miles and F. C. Gouldin

Sibley School of Mechanical and Aerospace Engineering  
Cornell University  
Ithaca, New York 14853

## ABSTRACT

A technique based on a variation of Laser Tomography and Laser Doppler Velocimetry has been developed and applied to measure simultaneously the flamelet position and reactant gas velocity in premixed, turbulent flames. The reactant flow is seeded with a silicon oil mist which rapidly evaporates and burns in the flamelet. Thus the intensity of scattered light from a laser beam decreases by orders of magnitude across the flamelet, and flamelet position along a line defined by the beam can be monitored continuously. The signal corresponding to flamelet position is differentiated and provides information on flamelet motion.

Reported here are pdf's and moments of flamelet position and its derivative for methane-air flames at two different equivalence ratios. These distributions are found to be essentially Gaussian, and it is observed that the rms fluctuation of flamelet position increases linearly with axial distance. Increasing equivalence ratio increases these rms fluctuations, but spectral analysis shows that the spectral characteristics of flamelet motion are unaffected. Further comparison of the spectra for flamelet motion to reactant velocity spectra indicates that the flamelet motion is controlled by the turbulence field between frequencies of 500 to 1500 Hz.

Conditional analysis of reactant velocity is also performed, and it is found that rms velocity fluctuations remain nearly constant as the flamelet is approached. Higher order moments of the conditioned velocity statistics are also reported.

## NOMENCLATURE

A	Mean reaction rate modelling constant
c	Mean reaction progress variable
d	Instantaneous droplet diameter
$d_0$	Initial droplet diameter
K	Burning constant for oil droplets
$l$	Turbulent integral length scale
n	Oil mist droplet concentration
P	Laser Power
$P(x)$	Flamelet position probability
$Re_t$	Turbulent Reynolds number
s	Space coordinate along laser beam
S	Measured photomultiplier tube signal
U	Streamwise velocity component
V	Cross stream velocity component
$w_r$	Ensemble average volumetric chemical reaction rate

$\langle w(x) \rangle$  Mean rate of chemical reaction per unit volume

$\phi$  Methane-Air Equivalence ratio

$\sigma$  Standard deviation

$\tau_d$  Detector system response

## 1. INTRODUCTION

In premixed turbulent flames, for mixtures characterized by high activation energies, large Damkohler number, and for moderate levels of turbulence, the major heat releasing chemical reactions occur in thin zones which are organized into sheets [1,2]. At very low turbulence levels, these sheets can be represented by unstrained wrinkled-laminar-flames, and the sheets form a more or less contiguous surface in the flame brush. For higher levels of turbulence, the structure of the sheets departs from that of an unstrained laminar flame as the effects of sheet curvature, flame stretch, and unsteady flow become important. Even so, reaction is still distributed in sheets, and the dispersion of chemical reaction into small volumes of highly dispersed fluid occurs only at high turbulence levels. These sheets of chemical reaction are referred to as flamelets and in general the term is used to denote both the high temperature reaction zone, as well as the adjacent convective-diffusive layer (the preheat zone).

To improve our understanding of turbulent flames and to support model development, the geometry of flamelet surfaces, their motion, and the local structure of these sheets must be studied. In this paper we report on a technique for simultaneous measurements of flamelet position and gas velocity developed primarily to measure gas velocities conditioned on distance from the flamelet surface. The approach also allows one to obtain information on the statistics of flamelet position in space and flamelet motion. These measurements, for two different flames, are also reported and discussed.

Still photography, high-speed cinematography, shadow and Schlieren techniques have all been used to obtain information on flamelet surfaces. These techniques have proven useful, but their interpretation is ambiguous primarily because they are all line-of-sight techniques. Hence they provide path integrated information.

Laser tomography and related flow visualization techniques avoid line-of-sight problems and are potentially much more useful for studying flamelet surface characteristics than the above methods. Both still photographs and cine-films can be made, thus allowing flamelet dynamics to be investigated. However, it should be noted that all these methods are subject to the inherent limitation of visualizing a curve generated by the intersection of the flamelet surface and a plane, rather than the flamelet surface itself.

In laser tomography, as applied to premixed flames, the reactant flow is seeded with an oil mist and the flow is illuminated with a sheet of laser light. Since the oil rapidly vaporizes in the reaction zone of the flamelet, scattering from the laser sheet is observed only from the reactants, and the flamelet is marked by the boundary between the scattering and non-scattering regions. This boundary is easily recorded photographically. Several investigators have used tomography for visualization, including its originator, Boyer [3], and Borghi [4].

A variation of laser tomography [5] allows for the measurement of flamelet location along a line in space, defined by the laser sheet illumination and

the image of a slit on this sheet. In this technique, a photomultiplier tube measures the intensity of scattered radiation from the line in space, where the slit is placed in front of the photomultiplier tube, and scattered photons are collected by a lens which in turn makes an image of the laser illumination sheet on this slit.

The integrated intensity of scattered light falling on the detector surface depends on the position of the flamelet along the line, and thus the position can be monitored by recording the photomultiplier output.

Boyer et al. [5] used this position measurement technique along with laser doppler velocimetry (LDV) to study flamelet motions and gas velocities in very weak turbulence. They record for analysis three signals: the flamelet position signal and its derivative, and the LDV signal from the measurement of a single velocity component at a fixed point in space. The data are analyzed for the power spectra of each signal in a frequency range up to 10 Hz. A single flame condition is studied and only spectral data are reported and discussed. The derivative of the flamelet position signal is treated as a component of the flamelet velocity. As discussed below, this treatment of the derivative signal is subject to interpretation.

Suzuki and Mirano [6] have reported measurements of flamelet orientation and speed in a plane, obtained at a point using a triple sensor ion probe. Their analysis of data assumes that the flamelet may be represented by a plane which is parallel to the axis of their probe, and that the spatial orientation of the plane remains constant as it crosses the probe volume. It is claimed that highly curved flamelets, and flamelets which cross at a large angle to the probe axis have characteristic ion current signatures which allow for these events to be recognized and discriminated against. At best this procedure will bias the results. Very high instantaneous flamelet surface speeds are reported, which raises questions about the assumptions made in the data analysis and about Suzuki and Hirano's ability to recognize flamelet crossing events which violate their assumptions.

To date the above work and related references are the only reports in the literature where quantitative measurements of flamelet position, orientation and motion are reported. Boyer et al. [5] record data which could be used to make conditioned velocity measurements, but no results of this type are reported.

In this paper we describe a technique for making flamelet position and gas velocity measurement which is similar to that of Boyer et al. [5]. The method is applied to higher velocity, more turbulent flows than that of Boyer et al. and the objectives are quite different. The laser tomographic technique is used to measure flamelet position along a laser beam; gas velocity at a fixed point on the laser beam is obtained by LDV. The flamelet position signal, its derivative, and the gas velocity signal are recorded. These data records are then analyzed for velocity statistics conditioned on the distance of the velocity measurement point from the flamelet. It is expected that effects of combustion on the turbulence will be evident in such data. The statistics of the flamelet position along the laser beam are also of interest, and have implications for the nature of the flamelet motion. For instance, the distribution will be bi-modal if large amplitude sine waves are causing flamelet motion. Finally, time derivatives of flamelet position are measured and compared with gas velocity data.

## II. EXPERIMENT

### A. Apparatus

1. **Burner Facility.** Figure 1 is a schematic of the burner exit and coordinate system. The turbulent flame is stabilized by a 1.5 mm diameter rod mounted across the exit plane of the 50 mm diameter cylindrical burner. Turbulence is generated by interchangeable woven wire screens (10 mesh and 8 mesh) which are mounted in the central air-fuel jet, 3.0 cm below the exit plane. The fuel is commercial grade methane supplied from high pressure bottles. Air, filtered and dried, is supplied from high pressure tanks which are charged by compressor (both gases are metered by needle valves, and flow rates are monitored with rotameters). The burner is equipped with an annular jet whose velocity may be matched to that of the inner jet in order to shield the flame from the mixing layer formed with room air. Due to the limited air storage capability, and a primary desire to use long averaging times in order to more closely approximate the higher order moments of the measured quantities, this feature was not utilized. All measurements, however, are performed well away from the edge of the jet, and it is felt that the effect of the mixing layer in this region is negligible. This burner has been used in several previous studies at Cornell, e.g. [7] and [8].

2. **LDV System.** Reactant gas velocities are measured using an LDV apparatus consisting of an argon-ion laser (Lexel, Model 95), commercial optics with a Bragg cell frequency shifter (Thermosystems, Inc., 900 series) and a counter type signal processor (Thermosystems, Inc., Model 1980). A dual beam, real fringes optical configuration is employed. The plane containing the two beams is aligned such that the major axis of the ellipsoidal measurement volume lies parallel to the flame stabilizer rod. Scattered light from the seed particles is collected at a 90° angle from the incident radiation, and a 0.25 mm diameter pinhole at the entrance to the photomultiplier tube limits the major axis diameter to about 0.8 mm, while the minor axis diameters are approximately 0.13 mm.

Several checks on the validity of the velocity measurements were performed on both a laminar and turbulent jet in an attempt to maximize the data rate without significantly distorting the measured velocity probability density function (pdf). Laminar jet measurements were made mainly to verify the correct operation of the Bragg cell. In two independent data sets, the measured mean lateral velocity was 0.0 m/sec, but one of the data sets showed secondary peaks in

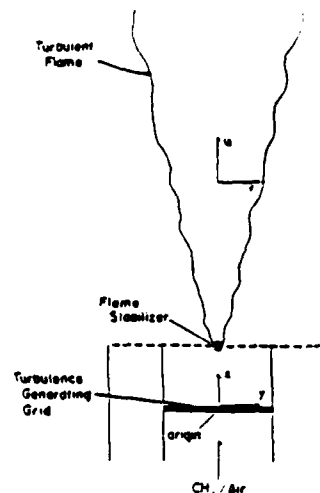


Figure 1. Schematic of Burner and Coordinate System.

the tails of the pdf's, which were present at all data rates. This does not appear in the streamwise velocity component pdf's, nor in all of the lateral component measurements, and has been attributed to intermittent 'leaking' of secondary frequencies in the downmix circuit of the Bragg cell. Tests performed on turbulent jets demonstrated that data rates of about 10 kHz were feasible without significantly broadening or distorting streamwise component velocity pdf's. Above 10 kHz the pdf's begin to broaden and depart significantly from a Gaussian. Cross-stream component pdf's were qualitatively similar, again showing little broadening until data rates were pushed above 10 kHz, although an occasional disconcerting shift in the measured mean velocity was observed. The broadening of the pdf as photomultiplier tube gain and/or amplifier gain is increased is to be expected: with increased gain, marginal particles passing through the edges of the measurement volume are seen. In these regions the fringes are not as parallel and planar as they are near the center of the measurement volume, resulting in an increase in the measured variance. The occasional shift in measured mean velocity is more difficult to explain; again suspicion falls on the downmix circuit. Velocity data was taken at data rates corresponding to 10 kHz when the measurement volume is wholly within the reactants. The preliminary results presented in this paper are reported with the understanding that, though qualitatively correct, more checks of cross-stream velocity measurement validity are required, and are being performed in the on-going work.

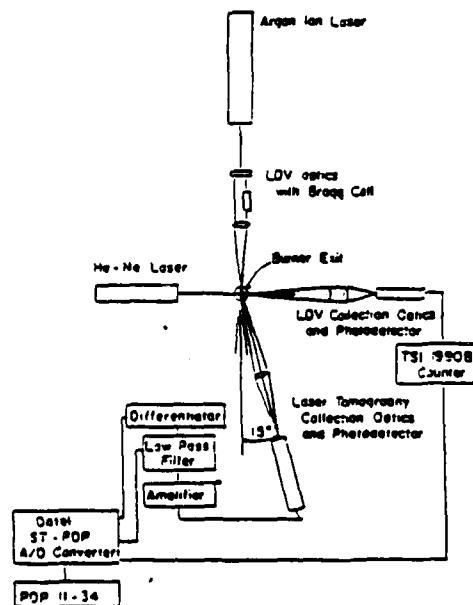


Figure 2. Schematic of Experimental and Data Acquisition System.

3. **Laser Tomographic System.** A sketch of the laser tomographic system, as well as the relative position of the LDV system, is shown in figure 2. A 6 mW, He-Ne laser beam is passed over the center of the burner exit, normal to the vertical plane containing the flame stabilizer rod. A plano-convex lens ( $f = 1000$  m,  $\phi = 30$  mm) is used to reduce the  $1/e^2$  diameter of the beam to about 0.55

mm where it passes over the burner exit. A portion of this beam is imaged by a symmetric, biconvex lens ( $f = 127$  mm,  $\phi = 50$  mm) onto the entrance slit of the photomultiplier tube with a magnification equal to 1.0. The entrance slit has a vertical dimension of 0.5 mm and a length of 9.66 mm; thus, accounting for the angle between the axis of the collection optics and the laser beam, 1.0 cm of the beam is imaged onto the entrance slit.

The signal out of the photomultiplier tube is amplified, low-pass filtered at 5 kHz, and differentiated. The analog differentiating circuit [9] was constructed with a high slew rate op-amp and precision components. The component values result in cut-off frequencies of 26 kHz, to which point the circuit differentiates, and 33 kHz, after which the circuit integrates to avoid 'ringing' caused by high frequency signal components. The circuit was calibrated, and found to follow the theoretical, first order gain curve very closely up to about 3 kHz, where the gain begins to roll off gradually. The response of the circuit to a pure sine wave at 5 kHz was about 8.5% below the calculated time derivative. Data analysis was performed using the theoretical, linear gain curve.

Seeding of the reactants for both laser tomography and LDV measurements is accomplished using atomizing nebulizers similar to those used by Cheng [10] and described by Durst, Melling and Whitelaw [11], who state that with careful design a mean seed particle diameter of near 1.0 micron can be achieved. Relatively clean Doppler bursts from the LDV scattering volume indicate that the majority of seed particles are less than about 3 microns in diameter, though, as noted below, particles as large as 100 microns are present as well. Dow Corning 50 centistoke silicon oil is used. The seed is introduced in the mixing chamber in the base of the burner, where it is thoroughly mixed with the reactants. The mixture then passes through several fine wire mesh screens, which serve to dampen any large scale velocity fluctuations in the flow and disperse the seed uniformly before it passes to the exit section of the burner. The particle number density at the exit plane of the burner is estimated to be about 1000 particles per  $\text{mm}^3$ .

All three signals: gas velocity, flamelet position and its derivative are converted to digital format (Datel, ST-PDP Series) and stored for analysis on a DEC PDP 11-34 computer.

#### B. Details of Flamelet Position Measurement

The integrated intensity of scattered light from a centimeter of the laser beam is measured by a photomultiplier tube. As outlined above, scattered light is observed only from the reactants, and, subject to the following conditions, the photomultiplier tube output is proposed to be linearly related to the position of the flamelet along the laser beam: (1) the seed distribution in the reactants is uniform, (2) overall scattering is not sufficient to significantly attenuate the laser intensity, (3) the detector sensitivity is uniform along the beam, (4) the beam has a negligibly small diameter, and (5) the evaporation/combustion time of the oil droplets is small as compared to their passage time through the flamelet. These conditions will now be discussed.

The photomultiplier output may be written as the integral of the product of the laser beam intensity, the oil mist concentration ( $n$ ), an average scattering cross-section for the mist ( $\sigma$ ), and the local detector system response ( $\tau_d$ ), which in general is a function of position. The limits of integration are the volume formed by the laser beam and the slit image on the laser beam. Since scattering in the products is negligibly small, integration may be limited to those portions of the measurement volume containing reactants. The integral is evaluated first by integrating over the laser beam cross-section leading to an expression in terms of quantities averaged over the cross-section;

$$S = \int n \sigma \tau_d P ds.$$

where  $S$  is the measured signal,  $s$  is the distance along the laser beam, and  $P$  is the laser power. Integration is along portions of the beam containing reactants. For uniform seed distribution in the reactants,  $n\sigma$  is constant; from above,  $\tau_d$  and  $P$  are assumed constant. Therefore  $S$  is proportional to the length of the laser beam subtending the reactants, and if the flamelet crosses the beam only once in the field of view,  $S$  is proportional to the position of the flamelet along the beam.

So far, the angle of intersection between the laser beam and the flamelet has been ignored. For a planar flamelet and a cylindrical laser beam it is easily seen that variations in the angle of intersection do not influence the measurement until the beam and surface approach a parallel state. Except for this extreme, the measurement gives the point of intersection of the flamelet and the axis of the laser beam. Flamelet curvature will affect this relationship and therefore it is best to keep the beam diameter to a minimum, thereby minimizing curvature effects.

The position measurement system is calibrated by removing the turbulence generating grid and holding a laminar flame,  $\phi = 0.8$ , on the burner. The flame is then traversed along the laser beam, while recording the output of the photomultiplier tube as a function of flame position. A least squares linear curve fit is applied, resulting in an expression for flamelet position as a function of photomultiplier tube output. This expression is accurate to within  $\pm 0.3$  mm, and to within approximately  $\pm 0.15$  mm within the central 8 mm of the measurement volume. System response was found to be quite linear, substantiating the assumptions of uniform  $n\sigma$  and constant  $\tau_d$  (Figure 3).

An estimate of droplet evaporation/combustion time of approximately  $10^{-3}$  seconds has been reported by Boyer [3]; our analysis using the so-called "d<sup>2</sup> law" of droplet combustion [11] confirms this report for droplets up to approximately

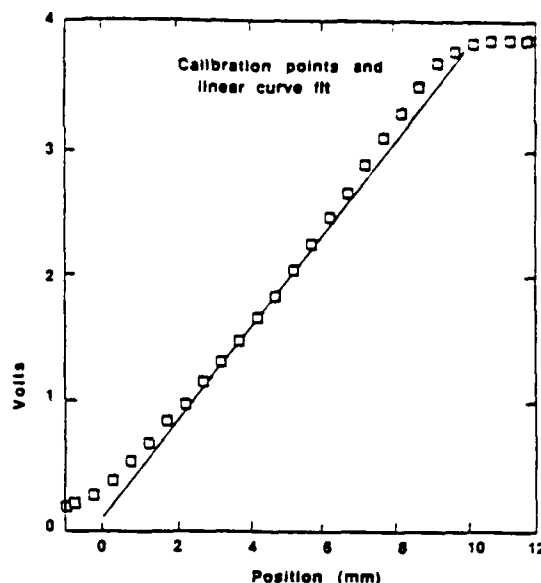


Figure 3. Position Signal Calibration Curve.

10  $\mu\text{m}$  in diameter. For a typical velocity component normal to the flame front of 0.30 m/s, and a flamelet thickness of about 1.0 mm, the residence time of the droplet within the flamelet is about  $3.3 \times 10^{-3}$  seconds. Experimental data, however, obtained from point measurements of scattered light (spatial resolution of about 0.15 mm) near the flamelet, indicate that some droplets persist after passing through the flamelet. Only after a distance of about 1.5 mm from the flamelet have they completely disappeared. This would indicate that some very large droplets are present in the seeded reactants, perhaps as large as 100  $\mu\text{m}$  in diameter. These particles are rare, and, due to the calibration procedure described above, their existence in no way biases our measurements.

An additional concern related to droplet evaporation time is the effect of increased equivalence ratio, resulting in increased flame temperature, on the flamelet position measurements. Since the burning constant,  $K_b$ , in the  $d^2$  law,  $d^2 = d_0^2 - K_b t$ , depends logarithmically on the flame temperature, this effect is slight. Our estimates indicate that the change in measured flamelet position due to increased equivalence ratio ( $\phi = 0.8$  to  $\phi = 1.0$ ) is about  $10^{-3}$  mm. Finally, the heat release due to oil droplet combustion, less the energy required to completely vaporize the droplet, has been compared to the heat release of the methane/air combustion. A ratio of 1 to 200 indicates that this effect is negligible.

Spatial resolution of the position measurement is limited by noise in the signal. Possible significant sources of noise are photon shot noise, large scale, low frequency fluctuations in seed concentration, and marker shot noise (i.e., random fluctuations in seed concentration [13]; the latter being by far the most significant problem. Scattering signals from single particles are quite high, and photon shot noise is not a problem. Two point, time correlation measurements with the points lying on a streamline show zero correlation between signals from pairs of points except for a very small value at a lag time corresponding to the flow time between the points (Figure 4). Thus large scale fluctuations in seed flow are negligible compared to other noise sources, namely marker shot noise.

For identical particles, marker shot noise would be expected to follow Poisson statistics. Variations in particle scattering cross-section at low particle arrival rates might cause non-Poisson behavior. However, measurements of noise pdfs show Gaussian distributions as would be expected for Poisson processes and large samples. Marker shot noise can be reduced by increasing the number of particles in the measurement volume and by reducing the band width of the detector.

To increase particle loadings, four atomizing nebulizers are connected in parallel, and a large fraction of the air flow passes through them. Higher particle concentration levels are possible with condensation type seeders (which give smaller particles as well); this type of device should be explored. An increase in measurement volume will reduce marker shot noise with a concomitant loss in spatial resolution. Limiting band width reduces temporal resolution as well as noise. Taylor's hypothesis may be used to express temporal resolution in spatial terms. For  $U = 3.8$  m/sec and a temporal resolution of 0.1 ms (the minimum time between successive samples of the data channels), the equivalent spatial resolution is 0.38 mm, which is of the same order as the nominal diameter of the laser beam. Thus the two are consistent with each other. In the measurements reported, the position signal is low pass filtered at 5 kHz before storage. With this filter setting, a 1.0 cm long scattering volume, and the 0.55 mm laser beam diameter, the measured signal-to-noise ratio is 45 at full intensity (the measurement volume being entirely in the reactants) and 37 at half intensity. For a Gaussian distribution of noise, these noise figures correspond to spatial uncertainties at a 95% confidence level of  $\pm 0.4$  mm and  $\pm 0.3$  mm for full scale

and half scale measurements, respectively. These numbers compare favorably with the spatial and temporal resolutions of the measurement system, which confirms our choice of these two quantities.

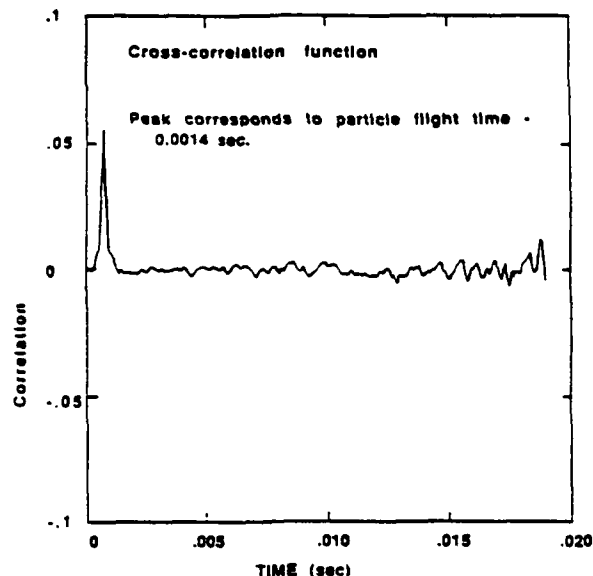


Figure 4. Two-Point, Time Correlation of Scattering Signal.

### C. Data Analysis

The three data signals—flamelet position, its derivative, and the reactant velocity—are analyzed in several different ways: for pdfs, power spectra, and certain conditioned statistics. Standard computer subroutines are used for most of these analyses. However, some comments are in order regarding data analysis and interpretation.

It is tempting to interpret the derivative of the position signal as the flamelet velocity, and for those cases when the flamelet is perpendicular to the laser beam this is a valid, unambiguous interpretation. In general, however, this view must be scrutinized. It is quite clear that the derivative, in general, does not give the velocity of a fixed point on the flamelet, while it does give the rate at which the flamelet position along a line changes in time. Only velocity components normal to the flamelet surface will cause it to move. Tangential velocity components move fluid along the surface but do not move the surface itself, while gradients in the normal velocity cause wrinkling and rotation of the surface. Thus surface points where the surface lies perpendicular to the laser beam move parallel to the beam. Otherwise, they move at an angle to the beam and the motion of the surface along the laser beam does not correspond to the motion of a fixed surface point. In general, when one refers to the velocity of a surface, it is in regard to a fixed point on the surface. We do not measure a component of this velocity here. However, the derivative quantity we do measure does given information on the flamelet motion in space and therefore is of interest.

A major objective of this work is to detect effects of the flamelet on the turbulence field. This may be done in part by conditioned velocity measurements. In the past velocity measurements conditioned on being either in reactants or products have been reported [14,15]. As is seen below, such measurements do not fully reveal the turbulence effects. What is needed is a conditioning of the velocity by distance away from the instantaneous flamelet position. The measurements reported here are a first step in that direction.

Using the flamelet position signal, velocity data are segregated by the distance along the laser beam from the flamelet to the measurement point. For this segregation, the distance is divided into 1 mm segments, i.e., 0 to 1 mm away, 1 to 2 mm away, etc. Once segregated, the velocity data are used to determine means, variance, skewness and kurtosis of the conditioned velocity distributions.

## III. RESULTS AND DISCUSSION

Data was taken for methane-air flames at equivalence ratios of 0.8 and 1.0. For each flame, measurements were performed at four different axial locations: 5.5, 6.0, 6.5 and 7.0 cm above the turbulence generating grid. Two sets of data were taken at each location, one 'slow' set at a sampling rate equal to twice the integral time scale (based on Taylor's hypothesis and measured integral length scales) from which averages and moments are computed, and one 'fast' set which is used for spectral analysis. Each slow data set consists of 40,960 points. These points, by virtue of the slow sampling rate, are independent [16] and, assuming a Gaussian pdf, result in convergence of the calculated variance to within 0.7% of the true measured variance. Skewness and kurtosis converge to

within 1.8 and 2.9%, respectively. The fast data sets consist of 102,400 points sampled at 10 kHz, in blocks of duration 0.1 sec. As the flamelet position signal is filtered at 5 kHz, this should result in alias-free power spectra.

Table 1 shows the turbulence properties and scaling of the approach flow as determined by previous measurements using hot-wire anemometry [17], and is presented here for reference.

In Table 2 are shown the first four moments of the flamelet position signal. These clearly indicate both the effect of equivalence ratio on the magnitude of the flamelet fluctuations and the Gaussian nature of these fluctuations. The increase in the rms fluctuations, which may be taken as a measure of the turbulent flame brush thickness, as the equivalence ratio is increased is similar to the results recently reported by Shephard et al. [18], who have attributed it to increased heat release in the reaction zone. The very nearly linear increase of these fluctuations with axial distance should also be noted. The Gaussian nature again is similar to recently reported results [18,19], and further substantiates the assumption of a Gaussian pdf in the model developed by Namazian, et al. [20] to determine mean density profiles across the flame brush. Figure 5 shows a representative of the measured pdfs.

Table 1  
Turbulence Properties and Scaling

	$U = 3.8$ m/sec		8 mesh grid	
$x$ (cm)	5.5	6.0	6.5	7.0
$u'/U$ (%)	3.5	3.3	3.2	3.1
$\ell$ (mm)	2.48	2.53	2.64	2.70
$R_\ell (u'\ell/\nu)$	24.4	23.5	23.9	23.5

Table 2  
Moments of Flamelet Position Signal

	$y$ (mm)	rms (mm)	skew	kurtosis
$\phi = 0.8$ :				
$x = 5.5$ cm	4.02	0.77	-0.08	2.82
$x = 6.0$ cm	4.40	0.85	-0.09	2.84
$x = 6.5$ cm	4.95	0.93	-0.12	2.80
$x = 7.0$ cm	5.49	1.00	-0.12	2.81
$\phi = 1.0$ :				
$x = 5.5$ cm	6.55	0.74	0.05	3.07
$x = 6.0$ cm	7.85	0.95	0.10	2.83
$x = 6.5$ cm	8.87	1.06	0.08	2.87
$x = 7.0$ cm	10.50	1.39	0.07	2.68

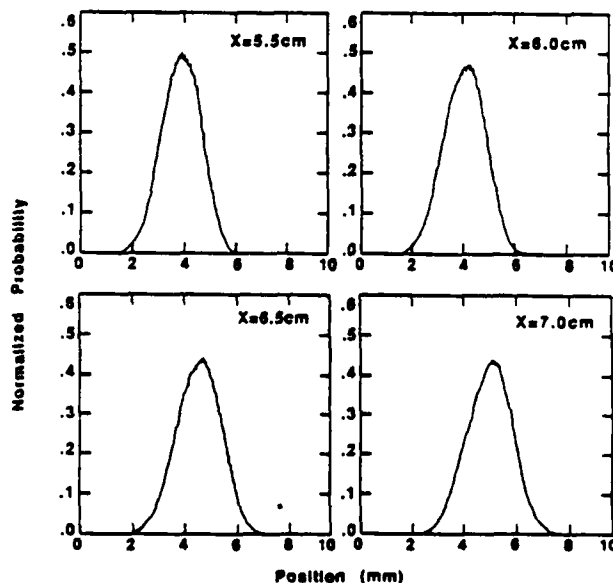


Figure 5. Flamelet Position PDFs for  $\phi = 0.8$ . Axial Positions of 5.5, 6.0, 6.5 and 7.0 cm.

It is also interesting to consider the relationship of the pdf of flamelet position,  $P(x)$ , to the chemical closure problem. If  $\langle \omega(x) \rangle$  is the mean rate of chemical reaction per unit volume at a given  $x$ , and  $\omega_p$  is the ensemble average volumetric chemical reaction rate per flamelet crossing, then

$$\langle \omega(x) \rangle = \omega_p P(x) \quad (a)$$

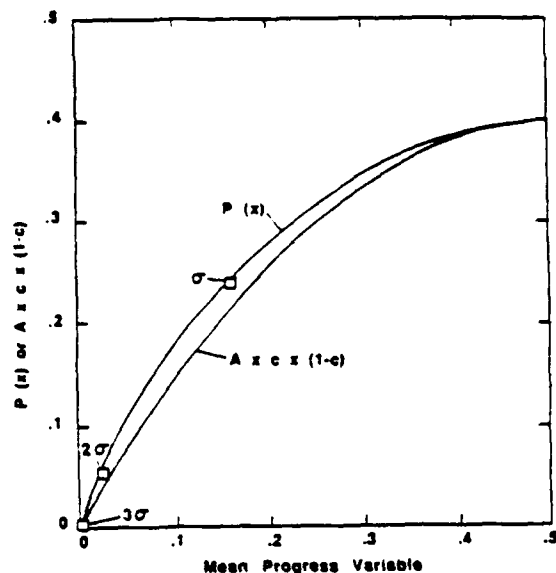


Figure 6. Comparison of  $P(x)$  and  $Ac(1-c)$ .

Frequently (Bray et al. [21]),  $\langle \omega \rangle$  is modelled as a function of  $c(x)$ , the mean reaction progress variable:  $\langle \omega \rangle \propto c(1-c)$ . It is easily shown that for thin flamelets,

$$c(x) = \int_{-\infty}^x P(x') dx' \quad (b)$$

Using this relationship, one can compare the spatial variation of  $\langle \omega \rangle$  predicted by  $c(1-c)$  and that given by  $P(x)$ . To do so,  $P(x)$ ,  $c(x)$  and  $c(1-c)$  can be obtained as a function of  $x$  using the above relationships and the measured  $P(x)$ . We have made such a comparison using a normal distribution to represent the measured  $P(x)$ , primarily for convenience. The results are shown in Figure 6, where  $P$  and  $Ac(1-c)$  are plotted against  $c$ .  $A$  is chosen to match  $Ac(1-c)$  and  $P(x)$  at  $c = 0.5$ ;  $A = 1.596$ . It can be seen that  $Ac(1-c)$  gives an extremely good approximation of  $P$  in  $c$  space, which accounts for its success in modeling mean combustion rates. The points labeled  $1\sigma$ ,  $2\sigma$  and  $3\sigma$  in the figure indicate  $c$  values associated with points 1, 2 and  $3\sigma$  (rms) away from the center of the flame brush in physical space.

Table 3 shows the moments of the derivative of the flamelet position signal. Notable features are the rms values again increasing with both axial distance and equivalence ratio.

The spectra of the flamelet position signal and the spectra of its derivative are plotted in Figures 7 and 8. The flamelet position spectra for  $\phi = 0.8$  and  $\phi = 1.0$  are very similar, adding further support to the assertion [18] that for the same inlet turbulence conditions an increase in equivalence ratio increases only the amplitude of the flamelet motion, while the spectral characteristics are unchanged. Comparison of the spectra for the time derivative of flamelet position shows that they, too, remain quite similar as the equivalence ratio increases. This is to be expected since these spectra can be derived from the corresponding flamelet position spectra. A comment on the shape of these spectra is in order. It is well

Table 3  
Moments of the Derivative of the  
Flamelet Position Signal

	rms (m/sec)	skew	kurtosis
$\phi = 0.8$ :			
$x = 5.5$ cm	2.44	0.21	3.57
$x = 6.0$ cm	2.54	0.29	4.11
$x = 6.5$ cm	2.63	0.32	4.37
$x = 7.0$ cm	2.67	0.37	4.78
$\phi = 1.0$ :			
$x = 5.5$ cm	2.78	-0.36	5.23
$x = 6.0$ cm	3.45	-0.50	5.38
$x = 6.5$ cm	3.51	-0.77	6.17
$x = 7.0$ cm	4.31	-0.91	6.80

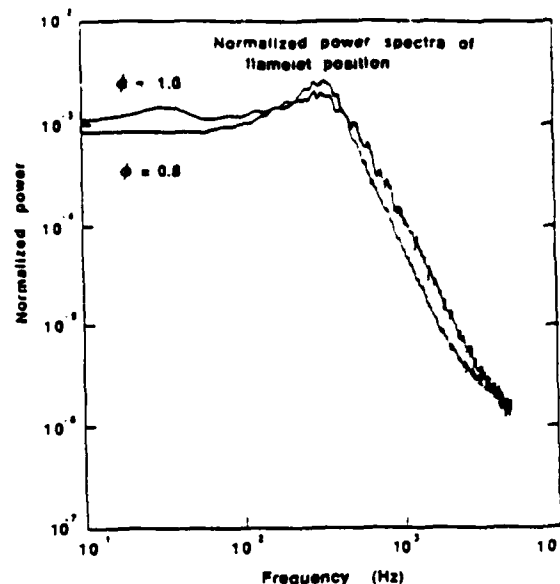


Figure 7. Comparison of Spectra of Flamelet Position for  $\phi = 0.8$  and  $\phi = 1.0$ .

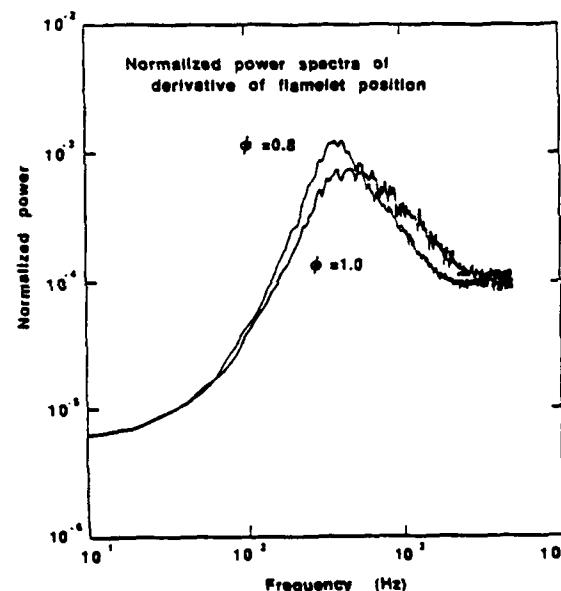


Figure 8. Comparison of Spectra for the Derivative of Flamelet Position;  $\phi = 0.8$  and  $\phi = 1.0$ .

known [16] that the value of a one-dimensional frequency spectra of some physical process at zero frequency is proportional to the integral time scale of that process. Since the flamelet position is a statistically stationary process, the integral scale of its derivative must vanish. This is borne out by the shape of the spectra for the derivative of flamelet position.

In Figure 9 the spectrum for the derivative of flamelet position is compared with the one-dimensional v-component velocity spectra. The velocity spectra is obtained by LDV measurements at a mean data rate of 10 kHz, and can therefore be expected to be accurate up to frequencies of 2 or 3 kHz, at which point the discrete nature of the counter's analog output signal causes distortion. As can be seen, the spectra are nearly identical between frequencies of about 500 to 1500 Hz. This type of comparison has also been reported by Shepherd et al. [18], though a coincidental region between 100 and 1000 Hz was reported. The discrepancy can probably be explained by the different inlet turbulence characteristics, and it appears reasonable to assert that within this spectral region the flamelet movement is controlled by the turbulence field. Moreover, at low frequencies the velocity spectra is affected by aliasing; the energy of high frequency components whose velocity vector is not aligned with the direction of measurement is aliased to low frequencies. Thus, although the spectra diverge at low frequencies, it is quite plausible that flamelet motion in this spectral region is also turbulence controlled.

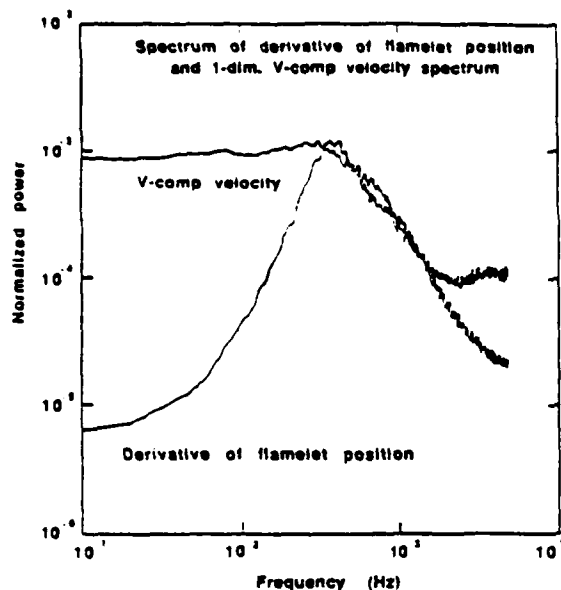


Figure 9. Comparison of Spectra for the Derivative of Flamelet Position and One-dimensional V-component Velocity Spectra.  $\phi = 0.8$ .

Figures 10a and 10b show the conditioned rms velocities,  $u'$  and  $v'$ , plotted against distance from the instantaneous flame front, while Table 4 demonstrates how the higher order moments of velocity evolve with distance from the flame front. The conditioned velocity statistics were computed only if 1024 or more data points were within the limits used to segregate the data. Note that, in general, the turbulent intensities of both velocity components show a slight decreasing trend as the flamelet is approached. The two v-component intensities at  $x = 5.5$  and  $6.0$  cm are the exception; this may be due to an interaction with the wake of the flame stabilizer rod. This decreasing trend is similar to that reported by Cheng [10], though his measurements are conditioned only on being within the reactants or products, and suggests that reported increases in unconditioned turbulent intensities within the flame brush are due to higher intensities within the products and the effects of measuring intermittently within the products or the reactants.

#### IV SUMMARY AND CONCLUSIONS

Flamelet position along a line, its derivative, and reactant gas velocity have been simultaneously measured with Laser Doppler Velocimetry and a variation of Laser Tomography. Reactant flow is seeded with a silicon oil mist which provides LDV scattering particles. On passage through the flame front these particles burn and evaporate; this property is exploited to provide a measure

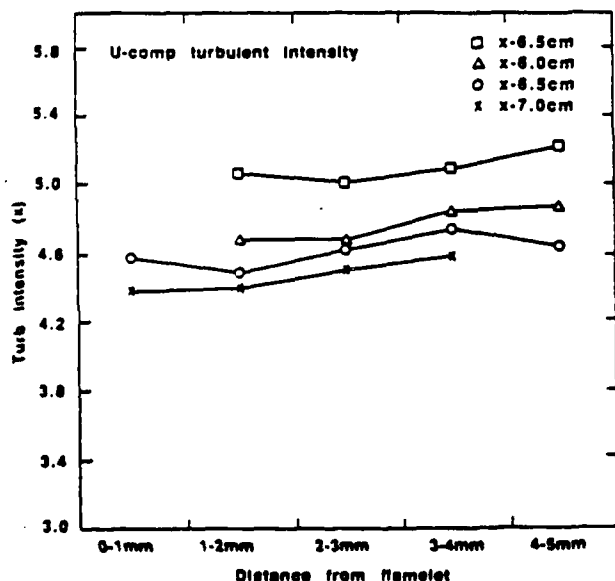


Figure 10a. Conditioned U-component Turbulent Intensities vs. Distance from Flamelet.  $\phi = 0.8$ .

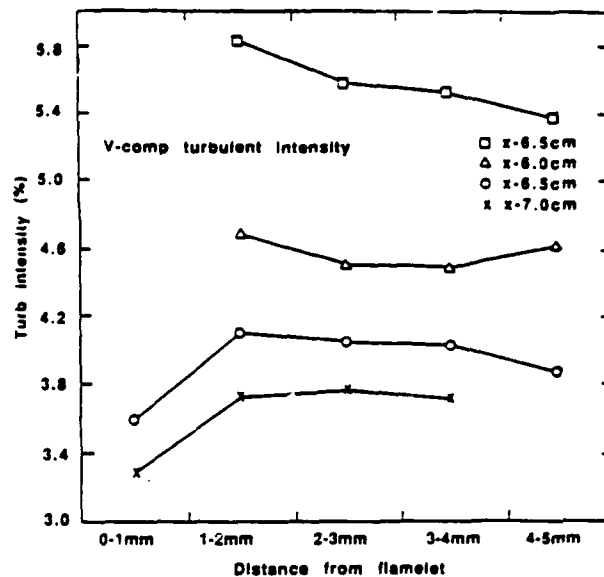


Figure 10b. Conditioned V-component Turbulent Intensities vs. Distance from Flamelet.  $\phi = 0.8$ .

of instantaneous flamelet position within a measurement volume formed by the image of a laser beam on the entrance slit of a photomultiplier tube. The flamelet position signal is differentiated, thus providing information on the flamelet motion in space.

The preliminary results reported here provide insight into the mechanisms and dynamics of turbulent, V-shaped flames. In particular, it was found that the pdf of flamelet position is substantially Gaussian and that the rms fluctuations increase very nearly linearly with axial distance. Furthermore, though an increase in equivalence ratio increases these rms fluctuations, the spectral characteristics of flamelet motion remain unchanged. Spectra for the derivative of flamelet position and the v-component velocity field are compared, and demonstrate that between approximately 500 and 1500 Hz the flamelet motion is controlled by the turbulent velocity field.

Statistics of the velocity field conditioned on distance from the flamelet are also reported. These show the true effect of the flamelet on the turbulent velocity field. It is found that fluctuating turbulent intensities remain relatively constant as the flamelet is approached, perhaps decreasing slightly.

Further application of this technique is in progress. In particular, flamelet position pdfs at greater and more numerous axial locations must be measured,

Table 4a

Moments of Conditional Velocities,  $\phi = 0.8$ .

U-components		$U = 3.8 \text{ m/sec}$				
Axial Position		Distance from instantaneous flamelet position (mm)				
5.5 cm		0-1	1-2	2-3	3-4	4-5
rms (m/sec)			0.192	0.190	0.194	0.198
skew			-0.08	-0.01	-0.05	-0.04
kurt			3.14	3.17	3.14	3.25
6.0 cm						
rms (m/sec)			0.178	0.178	0.184	0.186
skew			-0.19	-0.08	-0.04	-0.07
kurt			3.53	3.33	3.21	3.29
6.5 cm						
rms (m/sec)		0.174	0.170	0.176	0.181	0.176
skew		-0.23	-0.19	-0.14	-0.12	-0.04
kurt		3.62	3.62	3.60	3.36	3.68
7.0 cm						
rms (m/sec)		0.166	0.167	0.171	0.174	
skew		-0.37	-0.33	-0.21	-0.16	
kurt		3.88	3.88	3.45	3.58	

Table 4b

Moments of Conditional Velocities,  $\phi = 0.8$ .

V-components		$U = 1.8 \text{ m/sec}$				
Axial Position		Distance from instantaneous flamelet position (mm)				
5.5 cm		0-1	1-2	2-3	3-4	4-5
rms (m/sec)			0.222	0.212	0.210	0.204
skew			0.65	0.52	0.59	0.54
kurt			5.14	4.22	4.61	4.17
6.0 cm						
rms (m/sec)			0.178	0.171	0.171	0.176
skew			0.22	0.16	0.25	0.24
kurt			3.15	3.16	3.58	4.02
6.5 cm						
rms (m/sec)		0.136	0.156	0.154	0.153	0.147
skew		0.32	0.19	0.12	0.09	0.13
kurt		3.44	3.01	2.97	3.07	3.12
7.0 cm						
rms (m/sec)		0.125	0.141	0.143	0.141	
skew		0.32	0.20	0.16	0.08	
kurt		3.40	3.14	3.14	3.33	

and the effect of equivalence ratio on flamelet motion must be investigated further. Conditional velocity statistics over a wider range of axial and lateral locations must also be determined, and the technique should be modified to enable conditioned velocity measurements within the products as well. In this manner the interaction between the flamelet and the velocity field can be fully investigated.

## ACKNOWLEDGMENT

Support for this work from the United States Army Research Office (contract number DAAG29-82-K-0187) is gratefully acknowledged.

## REFERENCES

1. Rajan, S., Smith, J. R. and Rambach, G. D., *Combustion and Flame* 57, 95-107, 1984.
2. Libby, P. A. and Bray, K. N. C., *Combustion and Flame* 39, 33-41, 1980.
3. Boyer, L., *Combustion and Flame* 39, 321-323, 1980.
4. Borghi, R., University of Rouen, France, personal communication, December 1985.
5. Boyer, L., Cavin, P. and Sabathier, F., 18th Symposium (International) on Combustion, pp. 1041-1049, 1981.
6. Suzuki, T. and Hirano, T., 20th Symposium (International) on Combustion, pp. 437-444, 1984.
7. Gouldin, F. C. and Dandekar, K. V., *AIAA J.* 20, 655-663, 1984.
8. Gouldin, F. C. and Halthore, R. N., *Experiments in Fluids* 4, 269-278.
9. Horowitz, P. and Hill, W., *The Art of Electronics*, Cambridge University Press, p. 122, 1980.
10. Cheng, R. K., *Combustion Science and Technology* 41, 109, 1984.
11. Durst, F., Melling, A. and Whitelaw, J. H., *Principle and Practice of Laser Doppler Anemometry*, Academic Press, London, 1976.
12. Law, C. K., *Prog. Energy Combust. Sci.*, Vol. 8, 171-201, 1982.
13. Becker, H. A., pp. 45-139 in *Studies in Convection*, Vol. 2, B. E. Launder, ed., Academic Press, 1977.
14. Cheng, R. K., Talbot, L. and Robben, F., 20th Symposium (International) on Combustion, pp. 453-461, 1984.
15. Shepherd, I. G. and Moss, J. B., *AIAA J.* 20, 566, 1982.
16. Tennekes, H. and Lumley, J. L., *A First Course in Turbulence*, M.I.T Press, 1972.
17. Dandekar, K. V., 1982, Velocity and Density Measurements in Premixed Turbulent Flames. Ph.D. Thesis, Cornell University, Ithaca, New York.
18. Shephard, I. G., Hubbard, G. L. and Talbot, L., 21st Symposium (International) on Combustion, to appear.
19. Namazian, M., Talbot, L., and Robben, F., 20th Symposium (International) on Combustion, pp. 411-419, 1984.
20. Namazian, M., Shepherd, I. G., and Talbot, L., *Combustion and Flame*, Vol. 64, pp. 299-308, 1986.
21. Bray, K. N. C., Libby, P. A., and Moss, J. B., *Combustion Science and Technology*, Vol. 41, pp. 143-172, 1984.

## **APPENDIX D                      Personnel Working on Project**

F. Gouldin-                      principal investigator

R. Shaw -                      Graduate research assistant

P. Miles -                      graduate research assistant  
Master of Science, August 1987 (tentative)

S. Hilton -                      Master of Engineering, August 1987 (tentative)

T. Lamb -                      Master of Engineering, August 1987 (tentative)

## **APPENDIX E                      Publications, reports and presentations**

### **Publications --**

Gouldin, F.C. and Halthore, R.N.: Rayleigh scattering for density measurements in premixed flames, **Exp. Fluids** 4, 269-278, 1986

Gouldin, F.C.: An application of fractals to modeling premixed turbulent flames, **Comb. Flame** 68, 249-266, 1987

Gouldin, F.C.: An interpretation of jet mixing using fractals, submitted to **AIAA J.**

Gouldin, F.C., Bray, K.N.C. and Chen, J-Y: Chemical closure model for fractal flamelets, in preparation

### **Reports / Meeting Presentations --**

Miles, P. and Gouldin, F.C.: "Simultaneous measurements of flamelet position and gas velocity in premixed turbulent flames", College of Engineering, Energy Report E-86-03, Cornell University, Ithaca, NY, 1986. Presented at the 2nd ASME-JSME Thermal Engineering Conference, Honolulu, Hawaii, March 1987.

Gouldin, F.C.: "An interpretation of jet mixing and jet flame length data using fractals, College of Engineering, Energy Report E-86-02, Cornell University, Ithaca, NY 1986. Presented at the Fall Technical Meeting of the Eastern Section, the Combustion Institute, San Juan Puerto Rico, December 1986

END

10-87

DTIC